# **ETH** zürich

# Research Collection



# **Doctoral Thesis**

# Power requirements in cotton and worsted ring spinning

#### Author(s):

Soliman, Hosny Ali

# **Publication Date:**

1963

# **Permanent Link:**

https://doi.org/10.3929/ethz-a-000093974 →

# Rights / License:

In Copyright - Non-Commercial Use Permitted →

This page was generated automatically upon download from the <u>ETH Zurich Research Collection</u>. For more information please consult the <u>Terms of use</u>.

# Power Requirements in Cotton and Worsted Ring Spinning

#### THESIS

#### PRESENTED TO

THE SWISS FEDERAL INSTITUTE OF TECHNOLOGY, ZURICH

FOR THE DEGREE OF

DOCTOR OF TECHNICAL SCIENCES

 $\mathbf{BY}$ 

# Hosny Ali Soliman

B. Sc. Mech. Eng.
Citizen of the U.A.R. (Egypt)

Accepted on the recommendation of Prof. Dr. E. Honegger and Prof. A. Dutoit

> Zürich 1963 Dissertationsdruckerei Leemann AG

# Erscheint als Nr. 8 der Mitteilungen aus dem Institut für Textilmaschinenbau und Textilindustrie an der Eidgenössischen Technischen Hochschule in Zürich

# Contents

1.	Introduction	9
2.	Previous Related Work	9
3.	Components of the Total Power	10
4.	Air Friction of Tapes	l
5.	Bending Resistance of Tapes	9
6.	Spindle Power	28
7.	Power Absorbed by Tension Rollers	ŧ0
8.	Air Resistance of Tin Rollers	ŀ 1
9.	Package Power	!4
10.	Air Resistance of the Spinning Balloon	52
11.	Traveller Friction	32
12.	Power Absorbed by the Driving Head	30
13.	Power Absorbed by Drafting Systems	32
14.	Power Absorbed by Tin Roller Bearings and other Losses	34
15.	Measurements in Industry	86
16.	Approximate Estimation of the Power Consumption	)1
١7.	Modern Trends in Ring Spinning	)3
18.	Power Requirements of Frames with Special Spindle Drive	)4
9.	Acknowledgements	. 2
00	Deferences	า

Leer - Vide - Empty

# Zusammenfassung

Die vorliegende Arbeit befasst sich mit der Untersuchung des Leistungsbedarfes von Baumwoll- und Kammgarnringspinnmaschinen. Dieser wurde in seine einzelnen Bestandteile aufgeteilt, welche einzeln experimentell und theoretisch untersucht wurden. Besonders eingehend kamen die Läuferreibung, die Luftreibung von Spulen und Ballon, sowie der Biegewiderstand der Spindelbänder zur Behandlung, die zusammen einen grossen Teil der Antriebsleistung absorbieren.

Verschiedene Band-, Spindel- und Streckwerktypen wurden in die Untersuchung einbezogen. Die Versuchsergebnisse liessen sich in mathematischen Formeln darstellen, deren Genauigkeit zudem durch eine Reihe von Messungen in der Industrie bestätigt wurde. Die Messungen umfassen Maschinen von Ringdurchmessern bis zu 75 mm, Spindeltouren bis zu ca.  $14\,000\,U/Min$ . und Baumwoll-Garnnummern von  $Ne\,3\,(\sim\!200\,tex)$  bis zu ca.  $Ne\,80\,(\sim\!7.5\,tex)$ .

Eine daraus entwickelte Methode, die für praktische Zwecke genügt, erlaubt den totalen Leistungsbedarf aus drei Formeln zu berechnen oder aus drei Tafeln direkt abzulesen.

Am Schluss der Arbeit wurden noch Maschinen mit speziellen Spindelantrieben untersucht.

# **Symbols**

```
total tape surface area subjected to air friction.
A_i
\boldsymbol{B}
     bending resistance of tapes.
B_{\circ}
     length of spinning tube.
     coefficient of air friction.
C_{f}
\vec{D}
     2 \times radius of curvature of the tape.
D_r
     ring diameter.
D_1
     equals d_w + t.
D_{\circ}
     equals d_r + t.
D_{\mathbf{a}}
     equals d_t + t.
     equals d_n + t.
D_{\scriptscriptstyle A}
Dui internal diameter of tubes at lower ends.
d
     bobbin diameter.
     diameter of spindle bearing.
d_h
     diameter of driving pulley of the spindle testing stand.
d_d
     diameter of driving pulleys.
d_n
     diameter of tension rollers.
d_r
     diameter of tin rollers.
d_{t}
     wharve diameter.
d_w
     tensile stress in the tape.
ŧ
G
     traveller weight.
     gauge.
g
H
     balloon height.
h
     lift.
L
     spindle length measured from spindle rail.
L_{t}
     total length of tin rollers.
     tape length.
(l)
     lower position of ring rail.
l_{\it eff}
     effective length of tape.
     mass per unit length of yarn.
m
    yarn count (cotton).
N_{e}
```

 $N_m$  metric count.  $N_n$  no load power.

 $N_n$  package power.

 $N_s$  spinning power.

 $N_{sec}$  secondary power.

 $N_t$  total power required to drive the frame (motor output).

 $N_1$  power absorbed by air friction of tapes.

 $N_2$  power required to overcome the bending resistance of the tapes.

 $N_3$  spindle power.

 $N_4$  power absorbed by tension roller.

 $N_5$  power absorbed by air friction of the tin rollers.

 $N_6$  package power  $(=N_p)$ .

 $N_7$  power absorbed by balloon air drag.

 $N_8$  power absorbed by traveller friction.

 $N_9$  power absorbed by driving head.

 $N_{10}$  power absorbed by drafting systems.

 $N_{11}$  power absorbed by tin rollers.

 $N_{12}$  power loss due to the driving belts or V-belts of most frames with movable spindle rails.

n spindle speed.

 $n_d$  r. p. m. of driving pulleys.

 $n_t$  r. p. m. of the front cylinders of drafting systems.

 $n_l$  r. p. m. of the traveller.

 $n_m$  motor speed.

 $n_r$  r. p. m. of tension rollers.

 $n_t$  r. p. m. of tin rollers.

P radial load on spindle bearings.

 $p = \text{equals } \sqrt{\frac{m \omega^2}{T_x}}.$ 

R air friction of tape.

r radius of bottom circle of balloon.

 $r_0$  internal ring radius.

S equals  $(Dui^2 L d_b^2)$ .

 $T_x$  component of the balloon thread tension along the x-axis (spindle axis).

t thickness of tape.

(u) upper position of ring rail.

v tape velocity.

 $v_d$  speed of delivery.

 $v_l$  traveller speed.

W width of tape.

X equals  $(G^{0.87} D_r^{1.7} n_l^{2.4})$ .

 $X^*$  equals  $(G^{0.75} D_r^{1.5} n_l^{2.2})$ .

z number of spindles per frame.

- $\alpha$  the angle by which the traveller leads the balloon thread.
- $\beta$  the angle by which the thread between bobbin and traveller leads the traveller.
- $\gamma$  an air drag constant.
- ν kinematic viscosity of air.
- $\rho$  density of air.
- $\rho'$  balloon radius.
- $\rho_m'$  maximum balloon radius.
- $\omega$  angular velocity of balloon.

#### 1. Introduction

The power consumption of ring spinning frames represents the major part of the total power requirements of a spinning mill. In the case of fine spinning mills, it can attain more than  $80\%^1$  of the total mill power requirement. Thus, the cost of the power required to drive the spinning frame is in most instances an appreciable component of the cost of producing spun yarns.

The question of this power consumption is becoming more and more important owing to the modern trend towards higher spindle speeds and larger packages. The rate of increase of power cost is even greater than that of other spinning costs. When in the course of modernisation the optimum spinning conditions (spindle speed and package size) are to be determined for a certain yarn count, it will be found that the increasing power consumption has to be balanced by the reduction of handling and other costs, which results from larger packages and higher spindle speeds. However, the spindle speed is also limited by other factors, such as the traveller speed, number of yarn breakages per spindle hour and yarn quality.

Accurate prediction, not only of the maximum power consumption which determines the size of the driving motor, but also of the components of the total power requirements under any proposed spinning conditions is therefore necessary for studying the economic aspects of ring spinning.

#### 2. Previous related work

The importance of predicting the power requirements in ring spinning has increased with the introduction of the individual drive in spinning mills.

Stiel [1], in 1929, found an empirical formula for the calculation of the total power consumption of cotton spinning frames. This formula was formerly used and may have given satisfactory results. Nowadays, however, it provides

<sup>1)</sup> According to the "Dokumentation über Spinnerei- und Zwirnereimaschinen" (p. XXXIX) of Messrs. Maschinenfabrik Rieter & Co., Winterthur.

no useful indication of the power requirements of modern frames with larger packages, higher spindle speeds and roller spindle-bearings. The difference between the power consumption with empty and full bobbins, which is mainly due to the air friction of the bobbins, is given by Stiel as 5% and 15% of the mean power for weft and warp frames respectively. Corresponding figures for modern frames can attain 40% (see fig. 77).

In a paper by Catling and  $De\ Barr$  [2], tables were published for the determination of the power requirements of cotton ring spinning frames. These tables may be sufficient for a rough estimation of the power consumption. Only a part of the power was considered and was assumed in all cases to be about 40% of the total power. This corresponds with the tabulated values. Neither theoretical considerations nor a complete separation of the power components were attempted.

Some observations of the power consumption of ring frames were made by *Nakamura* [3], *Johannsen* [4] and *Marzoli* [5].

A detailed theoretical and experimental study of this problem seemed therefore to be necessary.

# 3. Components of the total power

Referring to figure 1, the total power consumption of a ring frame can be considered under two main headings:

- 1. Main power.
- 2. Ancillary power.

The main power is the power transmitted through the tin rollers to drive the spindles. This is in turn divided into two parts:

- a) The primary power, which is the power required to overcome the spindle load, namely, the air resistance of the packages (package power) and the resistance due to the winding tension (spinning power), (changing with increasing package).
- b) The secondary power, which is the power required to drive the spindles, tension rollers, tapes and tin rollers, at no load (approx. constant).

The ancillary power is the power absorbed by the drafting systems and the driving head. This power is relatively small because of the slow speeds of the drafting cylinders (constant).

The eleven elements of the total power (fig. 1) will be studied separately in the following chapters.

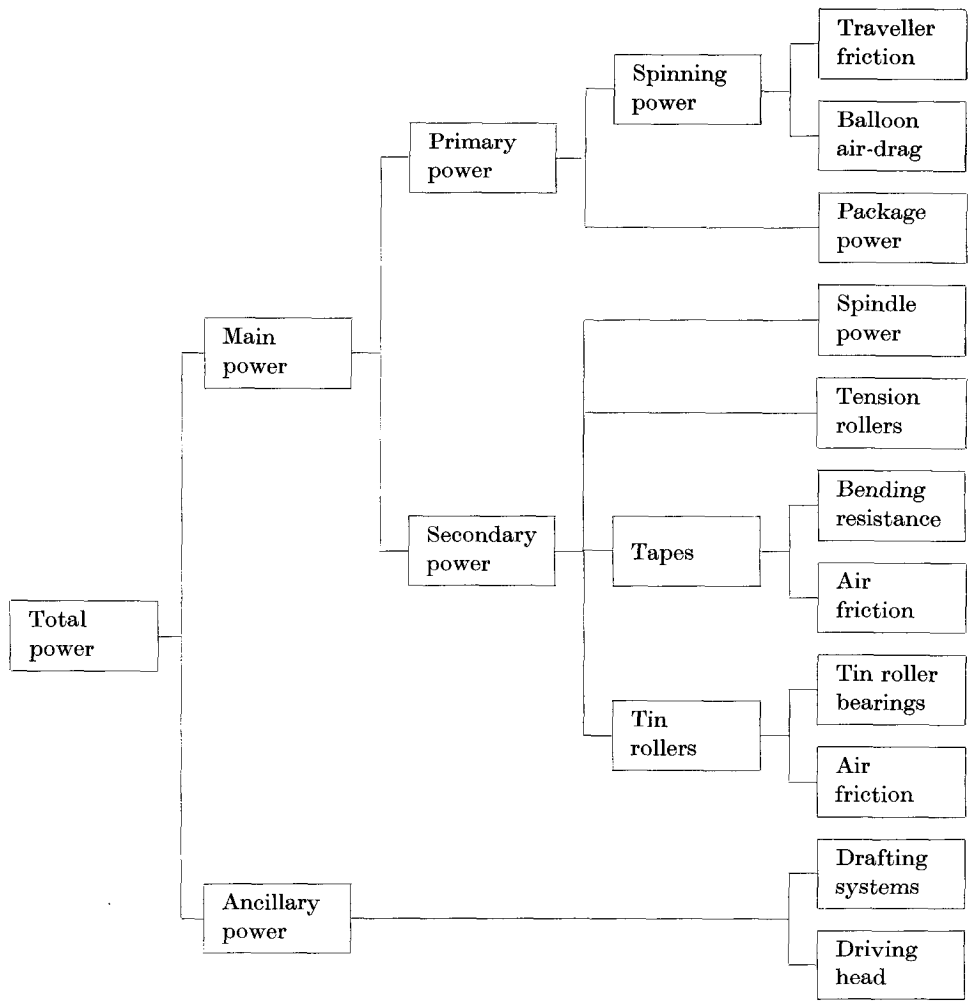


Fig. 1. Components of the total power.

# 4. Air friction of tapes

#### 1. General considerations

Owing to the complicated air motion caused by the tin rollers, tapes and yarn packages of a conventional ring spinning frame, it is very difficult to calculate the exact air friction of the tapes. The straight parts of these tapes, having lengths l varying from the gauge up to about 90 cm, cause the major part of the air friction.

The air friction on a plane surface moving in its own plane can be expressed by the aerodynamical equation:

$$R = C_f A_t \frac{\rho v^2}{2},\tag{1}$$

where

R = air friction in kg,

 $C_t = \text{coefficient of air friction},$ 

 $A_t =$  surface area subjected to air friction in  $m^2$ ,

 $ho = air density in kg \cdot m^{-4} \cdot sec^2$ ,

v = relative air velocity in m/s.

The coefficient of air friction  $C_f$  depends on Reynold's number  $\left(Re = \frac{v d}{\nu}\right)$ , if the geometrical similarity is fulfilled. At the beginning of the programme of this work,  $C_f$  was determined experimentally for cotton and nylon tapes with a wind tunnel, using an air speed range of 6 to 40 m/s. The linear term d in Reynold's number is taken as the length l of the tape.

#### 2. Description of the apparatus

Figure 2 illustrates the apparatus used to determine  $C_f$ . Two wind tunnels (8) with internal diameters of 31.7 mm ( $1^1/_4$ ") and 45 mm were used alternately for testing narrow (11 and 12 mm) and wide tapes (16 mm) respectively.

The air entered the tunnel through a nozzle (5) fitted at its upper end. The nozzle was connected at the two ends of one of its throat diameters to a water manometer (6). Thus the mean velocity of air through the tunnel could be found. A ventilator (9) driven by a variable speed motor was connected to the lower end of the tunnel. The air friction on the tape (7) was measured by a balance (1).

In order to prevent the tape from lateral vibrations, or at least to damp them, it was stretched by a weight (10). Precautions were also taken to prevent it from rotating about its vertical axis by connecting it with two fine threads (4) at each end to the two wires (3). The upper wire was prevented from rotating by the axis of the balance to which it was attached and the rotation of the lower one was retarded by the moment of inertia of the hanging weight (10). To avoid eddy current formation at the ends of the tape, smooth rounded tape ends were made (fig. 2a). The axis of the tunnel was adjusted to coincide with the vertical axis of the tape so that the surface area of the tape was parallel to the stream lines of the air motion.

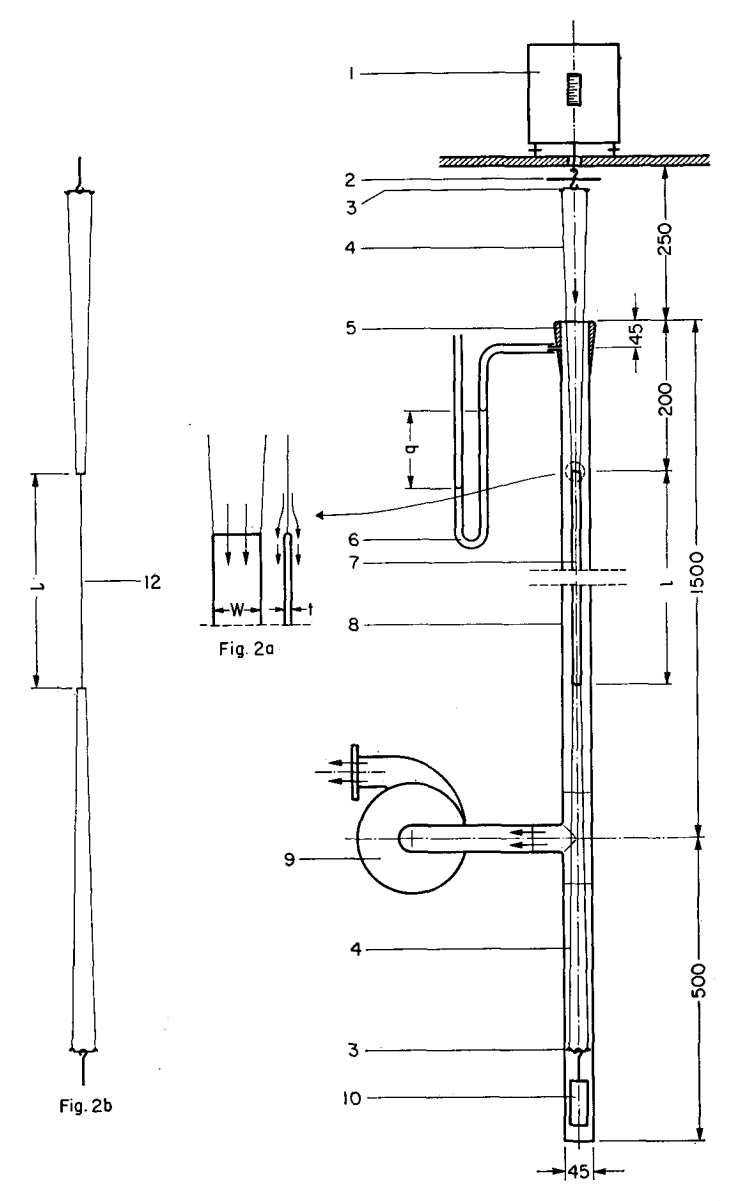


Fig. 2. Diagrammatic representation of the apparatus used to determine the coefficient of air friction  $C_f$  of the tapes (dims. in mm).

# 3. Experiments and results

All the experiments were made in standard air condition of textile testing  $(20\pm2^{\circ}\mathrm{C}, 65\pm2\%)$  relative humidity) under atmospheric pressure of 730 mm Hg. The data of the tapes tested are given in table 1.

Table 1

Tape no.	material	width (mm)	thickness (mm)	weight/unit length (g/m)
1	cotton	12	1.2	6.8
2	nylon	11	0.6	4.25
3	cotton	16	1.2	10.0
4	nylon	16	0.6	6.4

Each tape was tested in lengths of 25, 50, 75 and 100 cm. The difference between the balance readings with and without air stream gives the air friction of both tape and threads (4). Owing to the inclination of these threads to the direction of air motion, they showed a considerable air resistance which could not be neglected. This resistance was determined separately by using fine threads (12, fig. 2b) in place of the tape, and with the same lengths l. The air friction R on the tapes was found by subtracting the values of the air resistance of threads (4) from the total air resistance as indicated by the balance. Because of the small cross-sectional area and the smooth rounded ends of the tapes, their form resistance was assumed to negligible.

Substituting the values of R, A = 2 (W+t)l, where W, t and l are width, thickness and the length of the tape respectively],  $\rho (=0.117 \text{ kg} \cdot \text{m}^{-4} \cdot \text{sec}^2)$  and v in equation (1),  $C_f$  was calculated. Figures 3, 4, 5 and 6 show the values of  $C_f$  for tapes number 1, 2, 3 and 4 respectively, plotted logarithmically against Reynold's number Re. From these figures, it can be seen that Reynold's law of similarity is not fulfilled. This is to be expected, bearing in mind that the validity of Reynold's law is restricted to geometrically similar bodies, which is not the case for tapes. Two pieces of the same tape having different

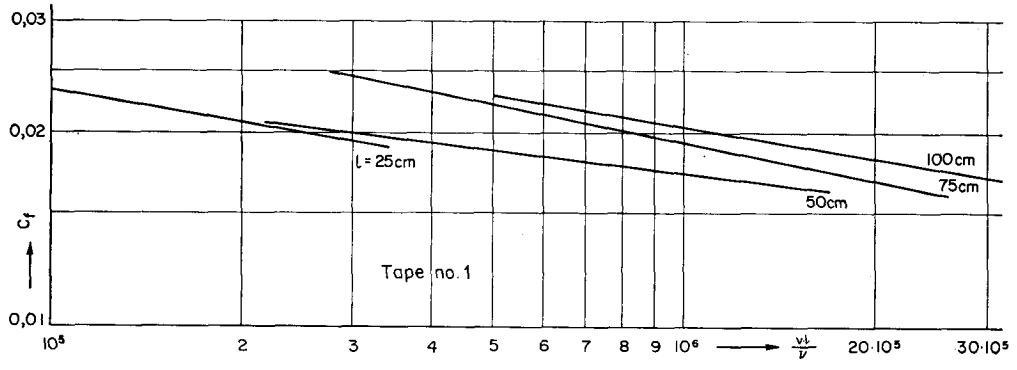
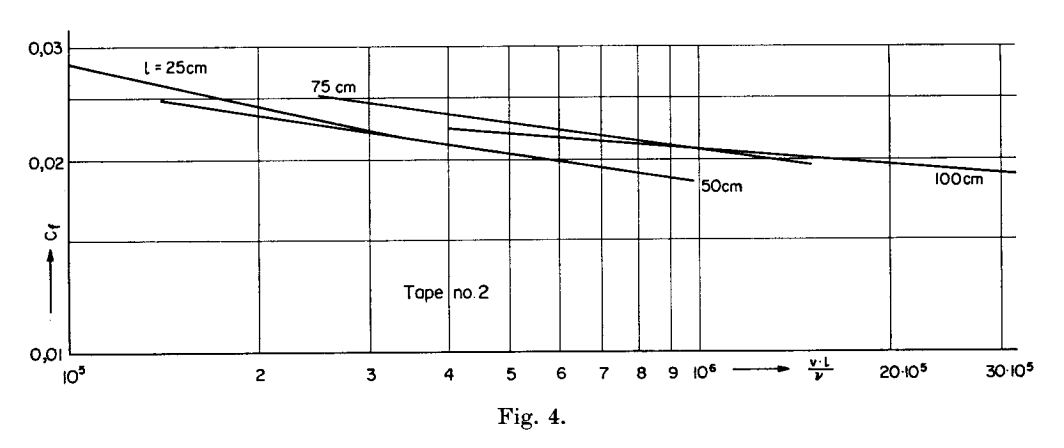
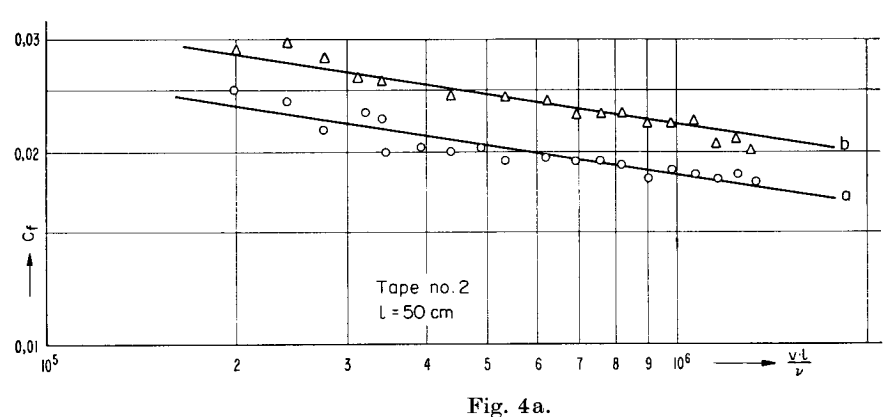
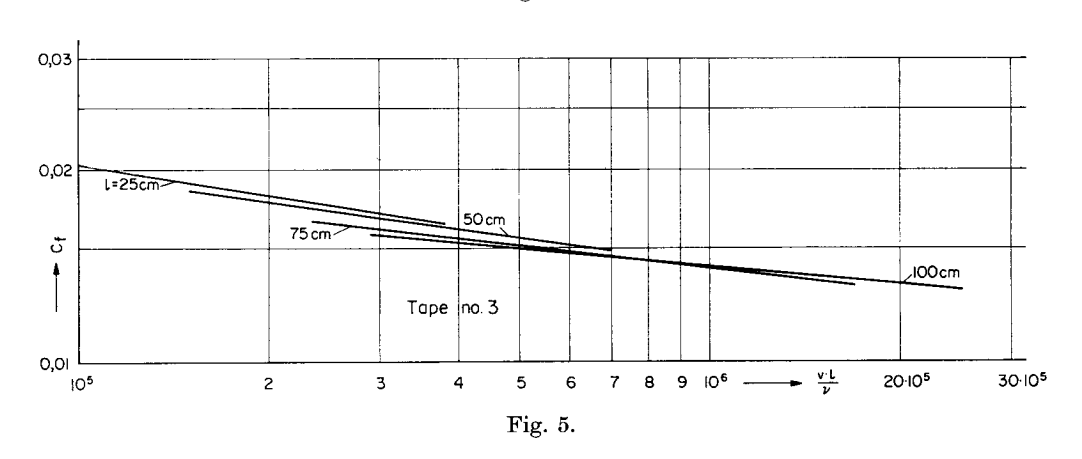


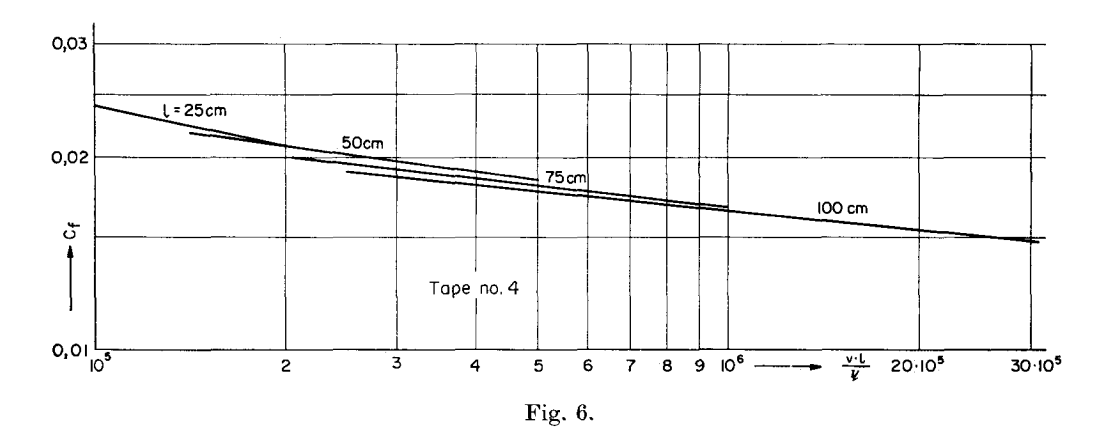
Fig. 3. The coefficient of air friction  $C_f$  against  $\frac{v l}{v}$  for tape no. 1.

lengths will have the same surface roughness but different relative roughness. The shorter piece will be relatively rougher than the other. That is why the values of  $C_t$  for short tape lengths are somewhat higher than those for the

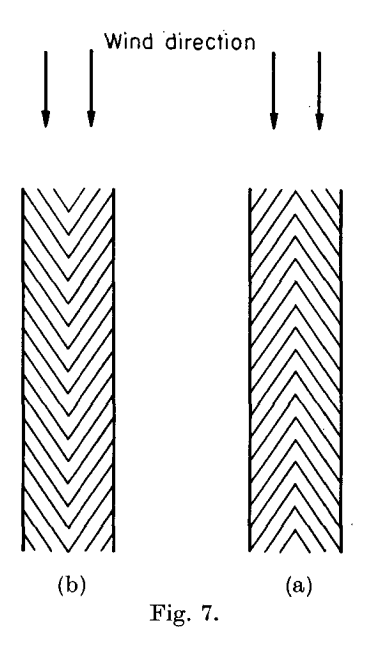








long ones (figs. 5 and 6). The reason why the contrary can be observed in figures 3 and 4 for narrow tapes is the fact that during the tests the lower ends of the long pieces of this tapes were distorted (up to  $180^{\circ}$  for l=100 cm) relative to the upper ends. This caused a certain form resistance which could not be avoided.



Furthermore, for the same tape material it is noticed that the narrow tapes have values of  $C_f$  about 17% higher than the wide ones. Comparing two tapes of the same material, length and thickness, but of different widths, it is clear that the narrow one has a higher relative roughness than the other, and hence higher values of  $C_f$ .

Tests were made in the Göttingen Institute of Aerodynamics [6] to determine  $C_f$  for plates covered with fabrics that had been finished by different treatments. These tests were made for surface lengths of 0.5, 1.0, 1.5 and 2 m with the same width of 1 m in all cases. The values of  $C_f$  obtained for plates covered with raw fabrics were lower (about 30%) than those given by our own tests (fig. 5). This is due to the difference between the width (1 m) of the surfaces used and that of the tapes (11—16 mm). It may also be due to a difference between the surface roughness of the raw fabrics used and that of the tapes.

Referring to figures 5 and 6, it can be seen that nylon tapes have a higher air friction than cotton ones (about 18%) owing to their higher surface roughness. The nylon tapes having a herry-bone twill (fig. 7) were tested with the wind direction as indicated in figure 7a. Reversing the wind direction relative to the tape as shown by figure 7b, the air friction increased by about 20%. These results are given in figure 4a. The straight lines (a) and (b) correspond to the wind directions shown in figures 7a and 7b respectively.

#### 4. Calculation of the power required to overcome air friction of tapes

The air friction R of the straight parts of the tape can be written as

$$R = R_1 + R_2 + R_3 + \dots$$

where  $R_1, R_2, R_3, \ldots$  are the air friction on the straight parts of lengths  $l_1, l_2, l_3, \ldots$  respectively (fig. 8). Therefore,

$$R = C_{f1} A_1 \frac{\rho v^2}{2} + C_{f2} A_2 \frac{\rho v^2}{2} + \cdots$$

$$= C_{f1} l_1 \left[ 2 (W + t) \frac{\rho v^2}{2} \right] + C_{f2} l_2 \left[ 2 (W + t) \frac{\rho v^2}{2} \right] + \cdots$$

$$= \frac{C_{f1} l_1 + C_{f2} l_2 + \cdots}{l_1 + l_2 + \cdots} A \frac{\rho v^2}{2} = C'_f A \frac{\rho v^2}{2}, \qquad (2)$$

$$C'_f = \frac{\sum C_{fi} l_i}{\sum l_i}, \qquad A = 2 (W + t) l,$$

$$l = l_1 + l_2 + l_3 + \cdots = \sum l_i.$$

where

The values of  $C'_f$  corresponding to a tape speed of 15 m/sec for the tapes tested are given in table 2.

The lengths  $l_1, l_2, l_3, \ldots$  may vary slightly from one frame to another. The effect of this variation on  $C'_f$  is negligible for frames of normal dimensions. Taking the variation of  $C'_f$  with respect to v into consideration, we can write,

$$C_t' = C_1 v^a \tag{3}$$

where a= constant; it was found to be about -0.12 for all tapes tested, taken as the inclination of the straight line representing  $C_r$  logarithmically against  $\frac{v\,l}{\nu}$  and corresponding to mean length of tape, since  $\nu$  and l are constants,

 $C_1$  = constant for each tape, and independent of v.

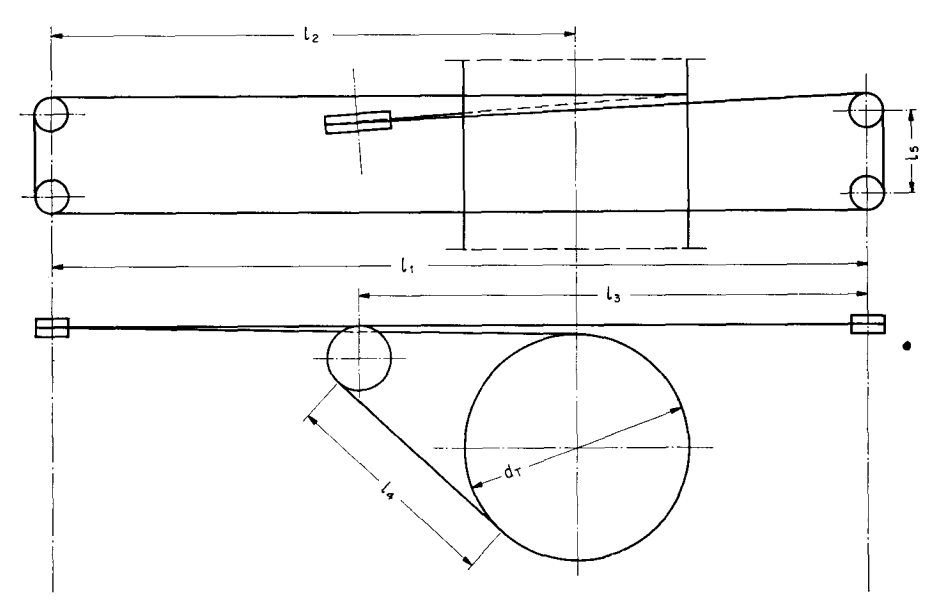


Fig. 8. Diagrammatic sketch of the 4-spindle drive.

Tape no.	I	2	3	4
$C_{1}^{\prime}$ $C_{1}$	$0.017 \\ 0.0235$	$0.02 \\ 0.0277$	0.0145 0.02	0.017 0.0235

Table 2

Substituting the values of  $C_f$  corresponding to  $v = 15 \,\mathrm{m/s}$  in equation (3),  $C_1$  was found to be as given in table 2. Equation (2) can thus be written as follows:

$$R = C_1 A_t \frac{\rho \, v^{1.88}}{2}.\tag{4}$$

The straight lengths of the tape constitute about 80% of its total length. The bent parts with one side in contact with the tin roller, tension roller and

spindle wharves were assumed to have half the air friction of an equal straight length. Therefore, the effective lenth  $l_{eff}$  of the tape will be equal to  $0.9 \times$  the total length l. Accordingly, we can write,

$$N_1 = 9.8 C_1 A_t \frac{\rho v^{2.88}}{2} \frac{z}{4} \cdot 10^{-3}, \tag{5}$$

where  $N_1$  = the power required to overcome the air friction of the tapes in kW.

 $C_1 = \text{constant depending on } C_t \text{ of the tapes and is given in table 2},$ 

 $A_t$  = the effective surface area in  $m^2 = 2(W + t) l_{eff}$ ,

 $l_{eff} = 0.9 \times \text{length of tape},$ 

 $\rho = \text{air density in kg} \cdot \text{m}^{-4} \cdot \text{sec}^2,$ 

v = tape speed in m/sec,

z = number of spindles of the frame.

Considering a ring frame having the following data:

number of spindles z=400, corron tapes, W=16 mm, t=1.2 mm, l=3.1 m, tape speed v=15 m/sec,

 $N_1$  was found using equation (4) to be 0.27 kW. From this figure it can be seen that the air friction of the tapes absorbs a small amount of power, which, however, cannot be neglected.

# 5. Bending resistance of tapes

#### 1. General considerations

One of the important factors which affect the power consumption of a ring spinning frame is the bending resistance of the tapes. This is especially true for frames with small wharve diameters.

We now consider a spindle having a resisting moment equal to M. Let  $T_0$  and T be the tape tensions before and after the spindle assuming that the tape is perfectly flexible and thus has no bending resistance (fig. 9a). T' is the actual tension of the tape after the spindle for the same initial tape tension  $T_0$ , taking the bending resistance into consideration (fig. 9b). Due to the non-flexibility of the tape, it will not be exactly tangential to the wharve, but will have displacements  $e_1$  and  $e_2$  which depend not only on the type of the tape, but also on its tension and the wharve diameter. Referring to figure 9, we can write

$$T = \frac{M}{r} + T_0, \qquad T' = \frac{M}{r - e_2} + T_0 \frac{r + e_1}{r - e_2},$$

$$B = T' - T = M \left(\frac{1}{r - e_2} - \frac{1}{r}\right) + T_0 \left(\frac{r + e_1}{r - e_2} - 1\right)$$

$$= \Delta T \left(\frac{r}{r - e_2} - 1\right) + T_0 \left(\frac{r + e_1}{r - e_2} - 1\right), \tag{6}$$

where B = the bending resistance of the tape,

r = the radius of curvature of the tape,

 $\Delta T$  = the increase of tape tension due to the resisting moment M, = M/r.

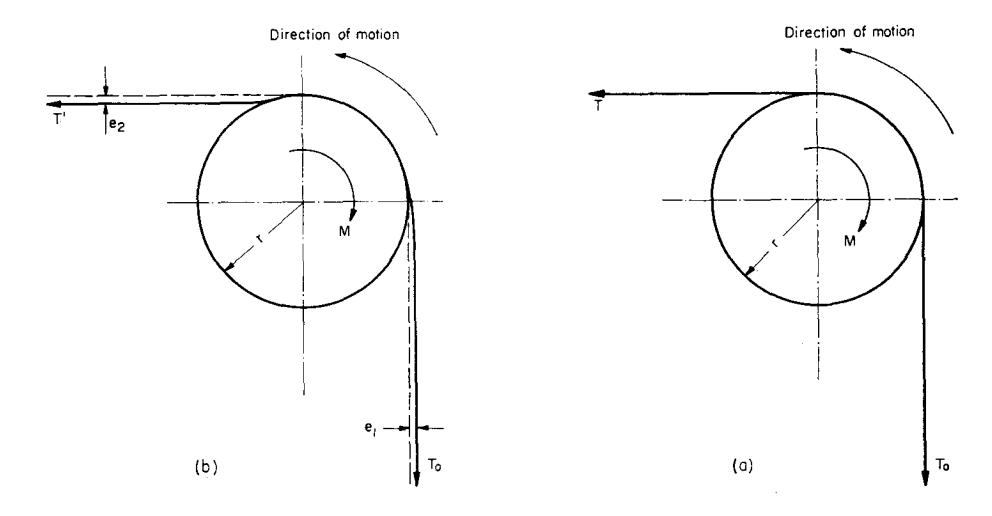


Fig. 9.

The knowledge of T,  $T_0$  and r is not sufficient to calculate B from equation (6), as  $e_1$  and  $e_2$  are unknown and would be difficult to measure with sufficient accuracy.

The bending resistance B depends on:

- the width W of the tape,
- the thickness t of the tape,
- the radius of curvature to which the tape is bent =D/2,
- the mean tensile stress f in the tape,
- material of the tape,
- weave structure (Bindungsart).

It is clear that the bending resistance is proportional to the tape width W. Increasing the tension T of the tape (i.e. increasing f), increases the internal frictional forces between the fibres and hence higher bending resistance can be expected. Higher ratios of t/D also imply higher bending resistances. Therefore, for a certain tape material and weave structure, the bending resistance per unit width of the tape can be written as follows:

$$\frac{B}{W} = C_2 f^b \left(\frac{t}{D}\right)^c,\tag{7}$$

where

B =the bending resistance in grams,

W =width of tape in cm,

f = the tensile stress in the tape in kg/cm<sup>2</sup>,

t =thickness of tape in cm,

 $D = 2 \times$  the radius of curvature of the tape in cm,

 $= d_w + t$ 

 $d_w =$ wharve diameter in cm,

 $C_2$ , b and c are constants depending on the tape material and weave structure.

Equation (7) was also used by  $M\ddot{u}ller$  [7] to represent the results of his tests which were made on leather and hemp yarn belts. D was taken by him as the diameter of the pulley over which the belt was bent.

Equation (7) assumes that the bending resistance vanishes for zero tension in the tape. Actually, the tapes will have a relatively small bending resistance at f=0 due to the internal forces in the tape arising from the weaving. Under normal working conditions, as the tape tension cannot be less than  $^{1}/_{2}$  kg, equation (7) is accurate enough to represent the bending resistance of the tapes.  $C_{2}$ , b and c were determined experimentally, as described in the following.

#### 2. Description of the apparatus

The tape under test was mounted on a roller as shown in figure 10. The roller was supported by two small ball bearings of negligible friction. The tape tension was veried by varying the two equal masses M attached to both ends of the tape. The bending resistance B, measured as the force required to bend the tape over the wharve and to stretch it again, equals the weight mg which is just required to keep the system in slow motion without any acceleration. The length l of the straight part of the tape on both sides of the roller was kept approximately equal, in order to avoid any error due to the weight of the tape. Furthermore, a small vibrator was connected to the roller axis to minimize the rolling friction of the bearings.

The bending resistance measured in this way (at v=0) may not be exactly equal to the bending resistance under normal working conditions (v=14—20 m/sec). The difference is however assumed to be negligible.

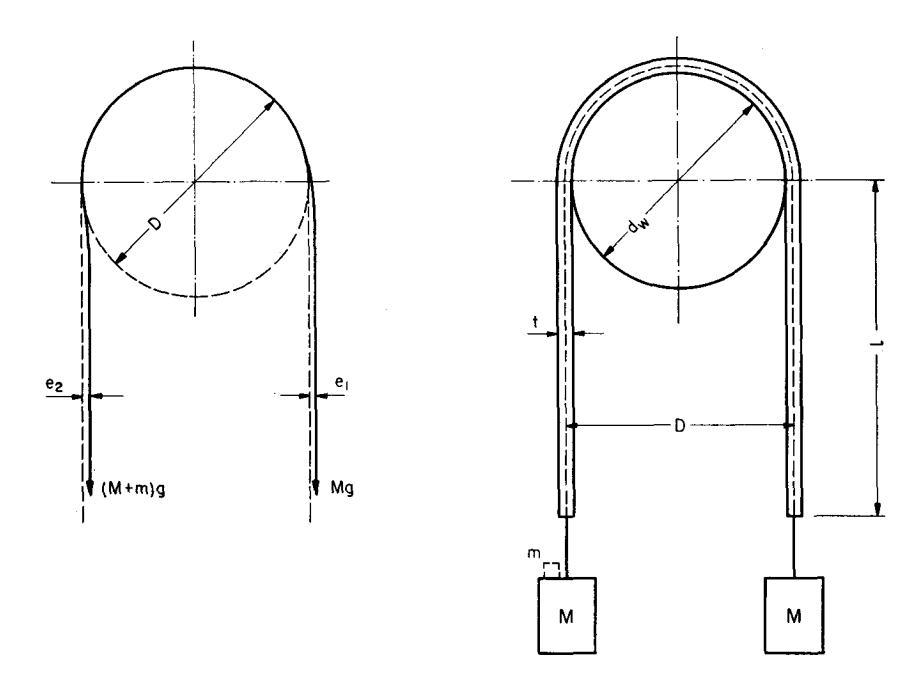
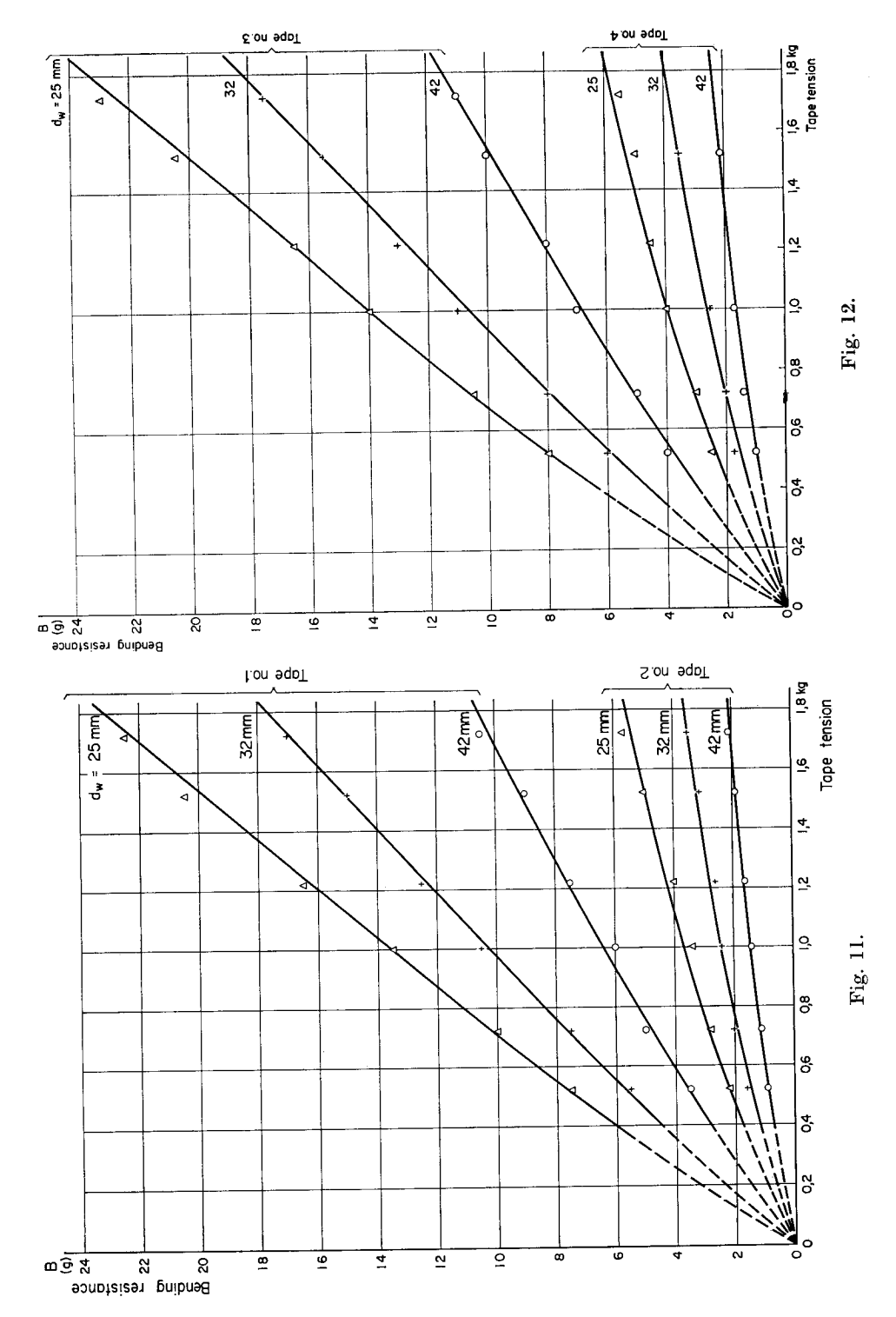
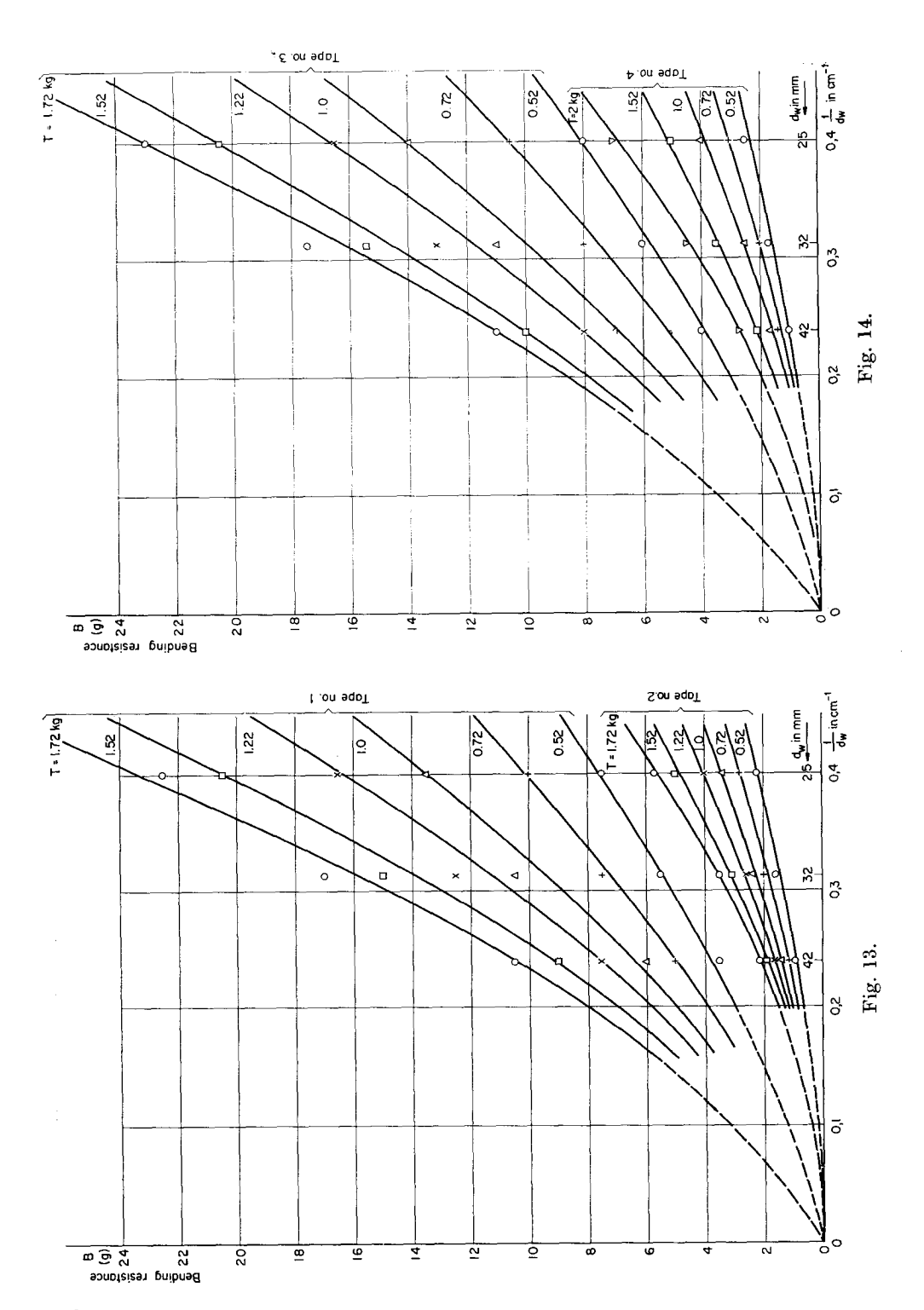


Fig. 10.

#### 3. Experiments and results

The data of the tapes tested are given in table 1. These tapes are commonly used in conventional-type cotton and worsted spinning frames. The bending resistance was measured for tape tensions up to 2 kg. Wharve diameters of 25, 32, and 42 mm were used. Nearly all practical conditions lie in the tested ranges. The results of these tests are given in figures 11 to 16. Figures 11 and 12 represent the bending resistance B in grams for different wharve diameters as a function of the tape tension T in kg. Figures 13 and 14 give B versus  $1/d_w$  in cm<sup>-1</sup> for different tape tensions. From these curves, it can be seen that the bending resistance increases with the tape tension and is also higher for smaller wharve diameters. It can be also seen that the nylon tapes (no. 2 and 4) show much lower values of bending resistance than the others. This is mainly due to their smaller thickness. It might also be traced to the different weave structure, which of course affects the internal friction between the fibres.





To express the results by equation (7), the measured points were plotted in logarithmic charts from which the constants  $C_2$ , b and c were found. Figure 15 gives the bending resistance per unit width of the tapes B/W in g/cm against the tensile stress f in the tape in kg/cm<sup>2</sup>, for different values of t/D. The points corresponding to the same tape material and weave structure lie on a straight

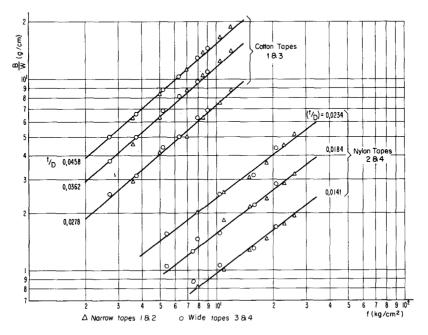


Fig. 15. The bending resistance B/W in gram per cm width of tapes no. 1, 2, 3 and 4 against the tensile stress t for different values of t/D.

line, the slope of which gives the value of b. From this figure and for a certain value of the tensile stress f (12 kg/cm<sup>2</sup>), B/W was found for different values of t/D. These values were plotted logarithmically in figure 16, from which c was found.  $C_2$  was determinded by substituting the values of B/W taken from figure 16, corresponding to certain values of f and f0, in equation (7). The tape constants  $C_2$ , f0 and f0 are given in table 3.

Table 3

Tape no.	$C_{2}$	b	c
1 and 3	$\frac{225}{367}$	0.85	1.5
2 and 4		0.75	1.8

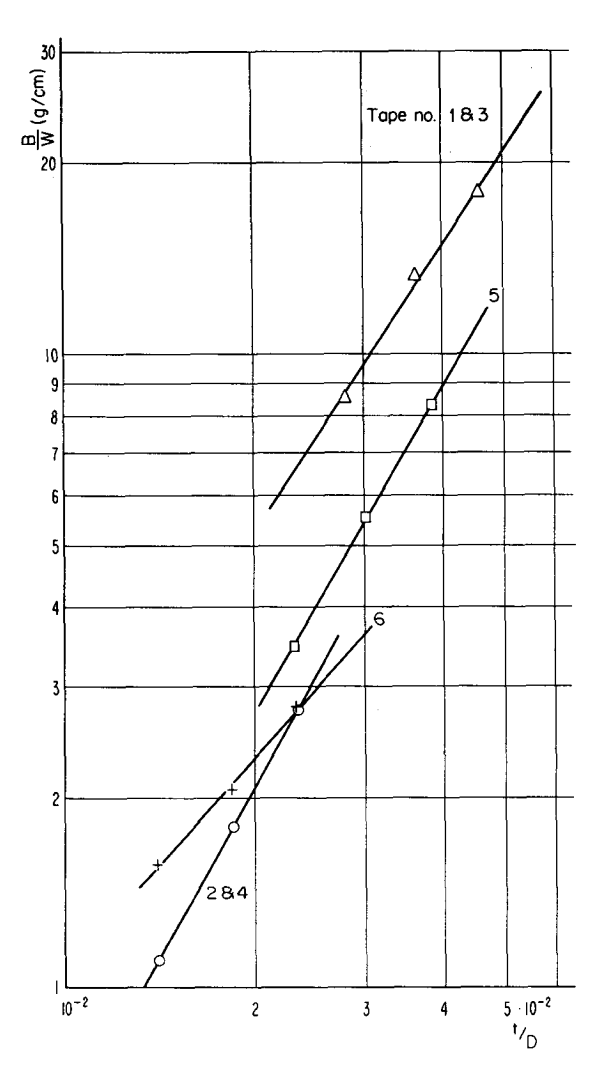


Fig. 16. The bending resistance B/W in gram per cm width of the tapes tested versus t/D for  $f=12 \text{ kg/cm}^2$ .

Tapes 1 and 3 have the same thickness, material and weave structure, therefore they have equal bending resistance per unit width and thus the same tape constants. The same characteristics hold for tapes 2 and 4.

Using equation (7) to calculate the power required to overcome the dending resistance of the tapes of a conventional frame, we can write.

$$N_2 = 9.8 \, C_2 \, W \, v \, z \, f^b \left[ \left( \frac{t}{D_1} \right)^c + \frac{1}{4} \left( \frac{t}{D_2} \right)^c + \frac{1}{4} \left( \frac{t}{D_3} \right)^c \right] \cdot 10^{-6} \,, \tag{8}$$

where  $N_2$  = the power required to overcome the bending resistance of tapes in kW,

W =width of tape in cm,

t =thickness of tape in cm.

v = tape speed in m/sec,

z = number of spindles of the frame

 $D_1 = d_w + t$ ,  $d_w =$ wharve diameter in cm,

 $D_2 = d_r + t$ ,  $d_r = \text{diameter of the tension rollers in cm}$ ,

 $D_3 = d_t + t$ ,  $d_t = \text{diameter of the tin rollers in cm}$ ,

 $C_2$ , b and c are to be taken from table (3).

Neglecting the bending resistance caused by the tin rollers due to their large diameter, equation (8) can be written as follows:

$$N_2 = 9.8 \, C_2 \, W \, v \, z \, f^b \left[ \left( \frac{t}{D_1} \right)^c + \frac{1}{4} \left( \frac{t}{D_2} \right)^c \right] \cdot 10^{-6} \, . \tag{9}$$

As a numerical example,  $N_2$  was calculated from equation (9) for two frames. The necessary data and the results are tabulated in table 4. For each frame,

Frame no. 1 2 number of spindles z 400 400 spindle speed n (r. p. m.) 12,000 7.000 wharve diameter  $d_w$  (mm) 25 42 diam. of tension rollers  $d_r$  (mm) 70 70 mean tape tension T (kg) 0.7 1.4 tape number 1  $\mathbf{2}$ 3 4 tape speed v (m/s) 16.5 16.1 15.8 15.4  $N_2$  (kW) 0.69 0.18 0.63 0.14 $\Delta N_2$ \*) (kW) 0.51 0.49 $\Delta N_2$  % of  $N_t$  \*\*) approx. 10 4.7

Table 4

two suitable tapes were considered. From this table, it can be seen that the power  $N_2$  represents a measurable part of the total power requirements of the frame. It can be also seen that the nylon tapes require less power than the cotton ones. The saving in power consumption obtained by unsing nylon tapes is about 10% in the case of frame no. 1 having  $d_w = 25$  mm, and only about 5% in that of frame no. 2 with  $d_w = 42$  mm. From these figures, the use of nylon tapes would appear to be favourable for frames with small wharves. A thorough study of the economic aspects is, however, necessary in each

<sup>\*)</sup>  $\Delta N_2 \cong$  the saving in power consumption obtained by using nylon tapes.

<sup>\*\*)</sup>  $N_t$  = the total power required to drive the frame.

particular case. These economic considerations must be carried out with the help of equation (9) and the knowledge of the energy cost, motor efficiency, initial cost of tapes and their average life (working hours).

It is obvious that the above comparison deals only with the power consumption, without taking into consideration other factors which may play an important rôle. It has been observed in various spinning mills that the nylon tapes run with a thin layer of fibres on them. This may be due to an electrostatic charging of the tapes, which attract fluff that forms this layer of fibres. It may also be due to the hairy surface of the nylon tapes which helps to trap fluff touching it. With this layer of fibres, more slip may be expected. Reducing this slip by increasing the tape tension will again increase the bending resistance of the tape and the normal pressure on the spindle bearings. This will increase their wear and also increase the spindle power, but only to a small extent for spindles with roller bearings.

As the nylon tapes show a higher air resistance than that of the cotton ones, which plays a secondary rôle, the saving in power consumption when using nylon tapes is somewhat less than that given in table 4.

# 6. Spindle power

#### 1. General considerations

The spindle power is that power which is required to overcome the friction in the spindle bearings and the air resistance of the upper part of the spindle when running with an empty tube. The latter part is very small because of the small diameter of the empty tube and its relatively smooth surface. The spindle power depends on the following:

- spindle speed,
- spindle size,
- radial load on spindle bearing,
- quantity of lubricating oil in spindle casing,
- viscosity of lubricating oil,
- design of the damping system of the spindle.

The normal quantity of lubricating oil and its viscosity are specified by each manufacturer for every spindle size and construction. In this study, normal working conditions of the spindles were assumed. The effect on the spindle power of the variation of the radial load in the case of roller spindle

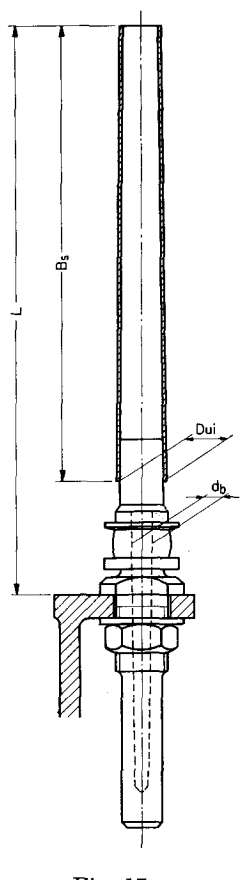


Fig. 17.

bearings is relatively small, as will shown in this chapter. Such bearings are now commonly used in modern spinning frames. On the other hand, the spindle power depends to a great extent on its size, which can be considered as follows:

- the weight of the rotating part of the spindle (for a given material, this weight will be approximately proportional to  $(Dui)^2$ . L see fig. 17);
- the diameter of the spindle bearing  $(d_b)$ .

For a certain spindle construction, assuming the spindle power to be proportional to the weight of the upper part of the spindle and dependent on the speed n and the bearing diameter  $d_h$ , we may write

$$N_3 = C_3 (Dui)^2 L (d_b)^a n^b \tag{10}$$

where

 $N_3$  = the spindle power in watts,

Dui = internal diameter of the tube at its lower end in cm.

L = the length of the spindle in cm, measured from the spindle rail,

 $d_b$  = diameter of the spindle bearing in cm,

n =spindle speed in thousands of r. p. m.,

 $C_3$ , a and b are constants which are determined experimentally.

#### 2. Description of the apparatus

The spindle power was measured by using the testing stand of the textile institute of the S.F.I.T. Figure 18 gives a diagrammatic sketch of the testing stand, which was made by Messrs. Alfred J. Amsler & Co., Schaffhausen (Switzerland). The spindle (1) under test was driven by the tape (2), which was driven in turn by a 180 mm diameter pulley (3). The latter was attached through a torsionmeter (4), to a D.C. motor (5), supported in such a way that it could be translated with its axis vertically, while the driving pulley (3) remained in its horizontal plane. The radial load on the spindle bearing could be changed by changing the weight (6), which was attached to the motor by a rope over a roller (7). Different adjustments could be made to suit different spindle types and sizes. The motor (5), having a speed range from 0 to 3,000 r. p. m., was controlled by a rheostat. The speed could be directly read off on

a speedometer (8) connected to the motor axis. To measure the driving torque a torsionmeter (4) was used, consisting of two torsion springs with opposite coil directions. By this means, the angular deflection of the springs due to the centrifugal forces could be compensated. The deflection of the torsionmeter was determined stroboscopically.

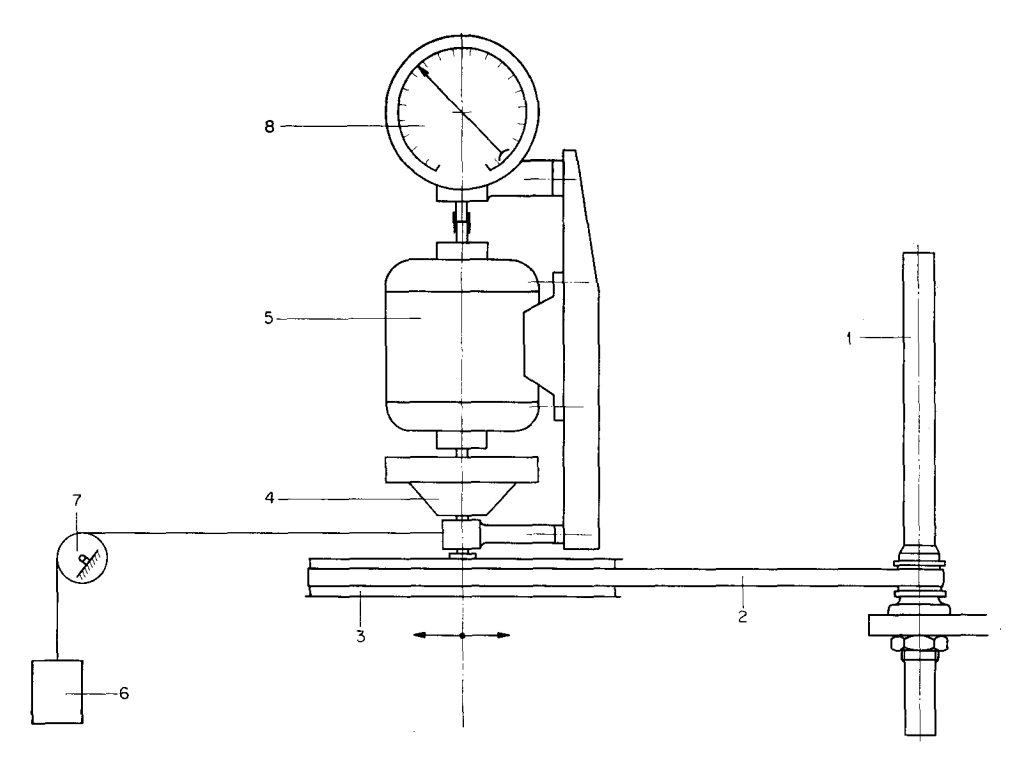


Fig. 18. The spindle testing stand.

# 3. Experiments and results

The torsion meter was calibrated under running conditions covering a wide range of the driving torque for different motor speeds. For the tape tensions used in these tests, the slip was assumed to be negligible owing to the large angle of wrap (more than  $\pi/2$ ) and the small resisting moment of the spindle with empty tube and without spinning balloon. Taking only the tape thickness into consideration, the spindle speed was calculated by the following formula:

$$n = n_m \frac{d_d + t}{d_w + t},\tag{11}$$

where

n = spindle speed in r. p. m., $n_m = \text{motor speed in r. p. m.},$ 

 $d_d$  = diameter of driving pulley,

t =thickness of tape,

 $d_w$  = wharve diameter of the spindle under test.

The spindle speeds measured stroboscopically gave the same values as those calculated by equation (11). This confirms the aforementioned assumption.

The power required to drive the spindle was calculated from the two readings of the torsionmeter (4) and the speedometer (8). This power equals the sum of the following:

- the spindle power  $N_3$ ,
- the power required to overcome the air resistance of the driving tape, and
- the power required to overcome its bending resistance.

The last two powers were determined with the help of the results of the last two chapters. These were subtracted from the total calculated power to give the spindle power separately. It should be noticed here that the readings of (4) and (8) were taken after reaching the stationary state, i.e. after the lubricating oil had reached a constant temperature corresponding to the spindle speed and radial load considered.

Spindle speeds up to 18,000 r. p. m. were tested, each spindle according to its size and construction. The spindles tested had tubes of lengths varying from 190 to 300 mm, with Dui from 18 to 30 mm. Their bearing diameters

Spindle no.	$B_s$ (mm) *)	Dui (mm)	L (mm)	$d_b \text{ (mm)}$	P (kg) **)
1	235	22	295	7.8	I
2	250	24	310	8.8	1
3	260	24	370	8.8	1.5
4	270	24	340	10	1.5
5	270	27	340	10	1.5
6	270	30	340	10	1.5
7	300	30	370	12	2.0
8	190	18.25	240	7.8	0.75
9	250	24	310	7.8	1
10	280	27	340	8.8	1.5
11	300	30	370	10	2.0
12	300	30	370	12	2.0

Table 5

<sup>\*)</sup>  $B_s = \text{length of tube.}$  \*\*) P = radial load.

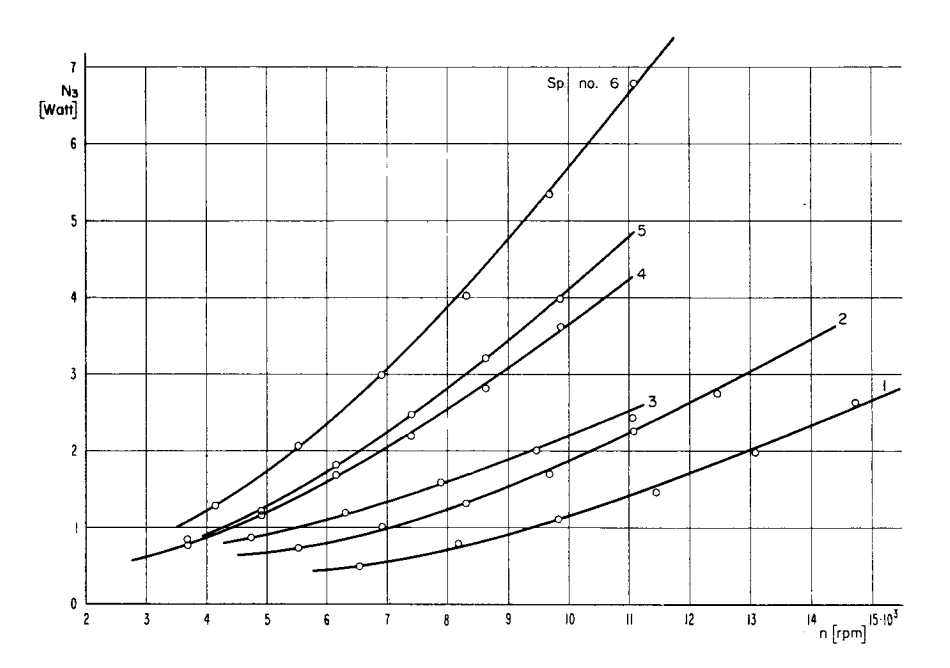


Fig. 19. The spindle power  $N_3$  against n for normal speed spindles.

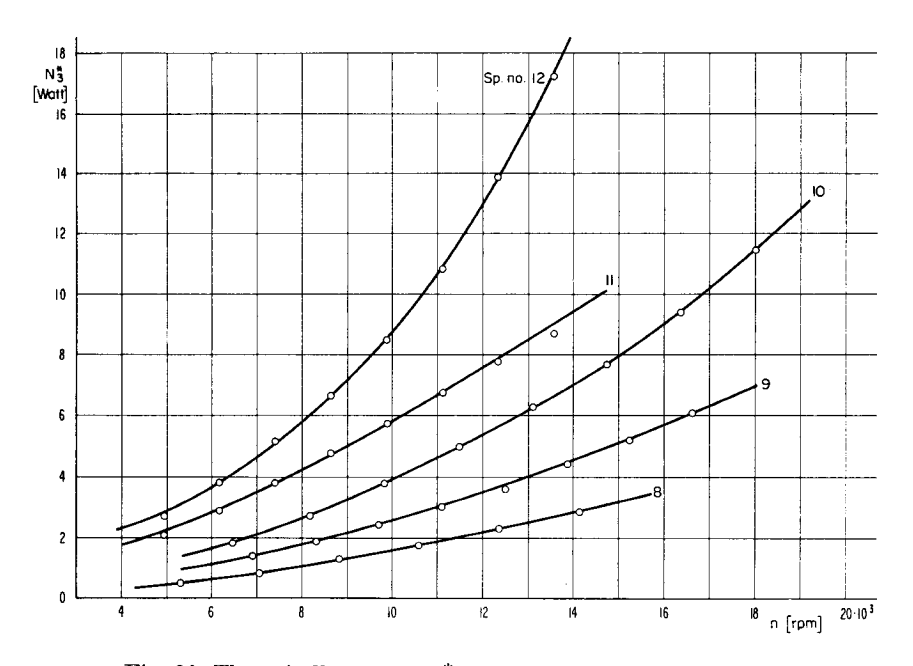


Fig. 20. The spindle power  $N_3^*$  against n for high speed spindles.

were 7.8, 8.8, 10 and 12 mm. Spindles made by four spindle manufacturers in Europe were tested. All of these spindles had roller bearings and were filled with oil of the quantity and viscosity specified by the spindle manufacturers. The specifications of some of these spindles are given in table 5.

Spindles no. (1) to (7) are normal-speed spindles having maximum speeds varying from 8,000 to 15,000 r.p.m. according to their design and size. Spindles no. (8) to (12) are high-speed spindles specially constructed to run at speeds up to 20,000 r.p.m.

The results of the tests are given in figures 19 to 29. Figure 19 shows the spindle power  $N_3$  of the spindles no. (1) to (6) in watts as a function of the spindle speed n in r. p. m. Figure 20 represents  $N_3^*$  versus n for the high-speed spindles no. (8) to (12). Each spindle was tested with the same radial load on its bearing that it would be subjected to under normal working conditions in a spinning mill (P as given in table 5). Figures 21 and 22 show the effect of the radial load P on  $N_3$  using spindles no. (1) and (7) respectively.

From these figures it is obvious that the spindle power rises rapidly with n, depends on the spindle size, and is slightly affected by the variation of the radial load P.

It should be noted that the spindles given in table 5 under no. (1) to (7) are complaratively new ones. Other spindles made by the same manufacturer, having the same size and construction but having run for some years in spinning mills (still in a perfect state), were tested under the same conditions. No appreciable differences could be registered for usual radial loads on the spindle

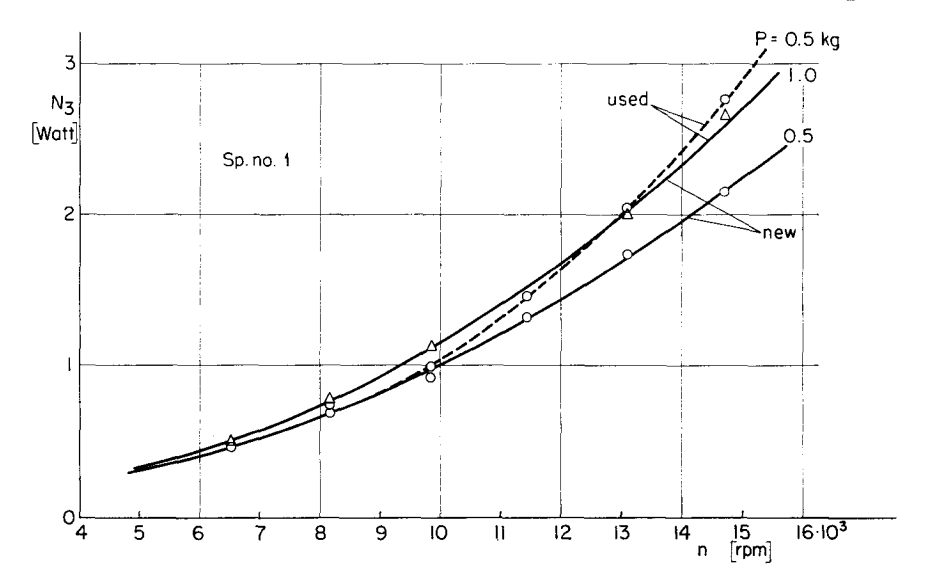


Fig. 21.

bearings, as can be seen in figure 21. Spindles which have run for some years in industry will have more play in their bearings and thus more tendency for their upper parts to vibrate. This may cause a higher spindle power consumption. This is specially true for small radial loads P. A coording to figure 22 no difference could be measured.

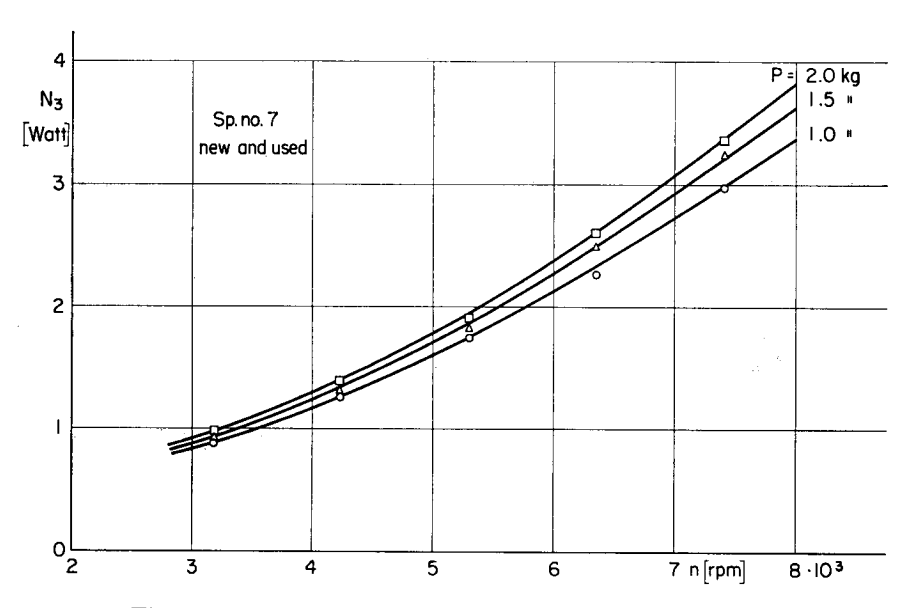


Fig. 22. The effect of bearing pressure on the spindle power.

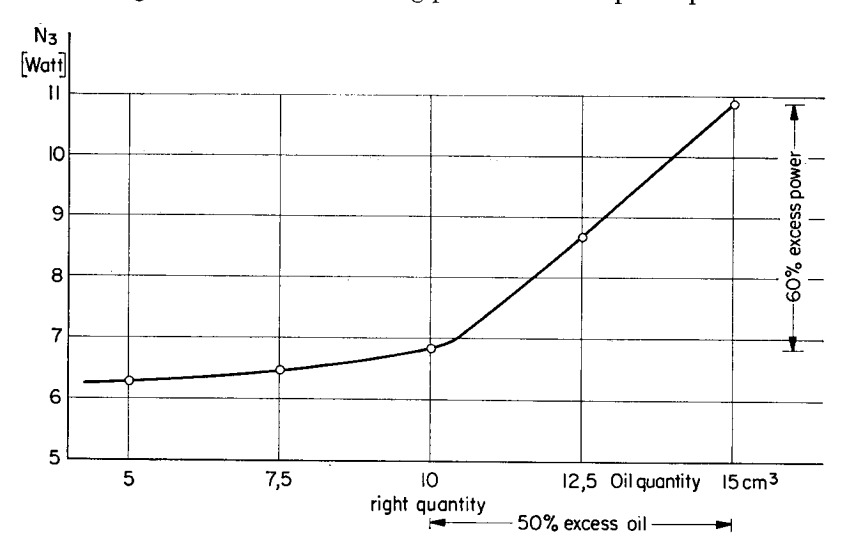


Fig. 23. Effect of the quantity of spindle oil on the spindle power for spindle no. 6. P=1.5 kg, n=11,070 r. p. m. and with empty tube.

It was also observed in this study that spindles of the same size and made by the same manufacturer but with different constructions of their damping systems could show differences of up to 30% in the spindle power.

The effect of changing the quantity of lubricating oil on the spindle power was examined. Spindle no. 6 was tested with different quantities of oil keeping all other testing conditions unchanged (n=11,070 r.p.m., P=1.5 kg). The results of this test are given in figure 23. A slight increase in the spindle power with increasing the oil quantity up to the right amount specified for this spindle ( $10 \text{ cm}^3$ ) can be observed. When the oil quantity was increased beyond that specified, a very rapid increase of the spindle power was found. In this case, the lubricating oil will reach the upper bearing (roller bearing) of the spindle under the action of the forced vortex created by the rotating spindle shaft. After some working hours a great part of the excess oil will be projected by the roller bearing out of the casing. This will again reduce the power consumption of the spindle, but it may still remain higher than its consumption with the specified oil quantity.

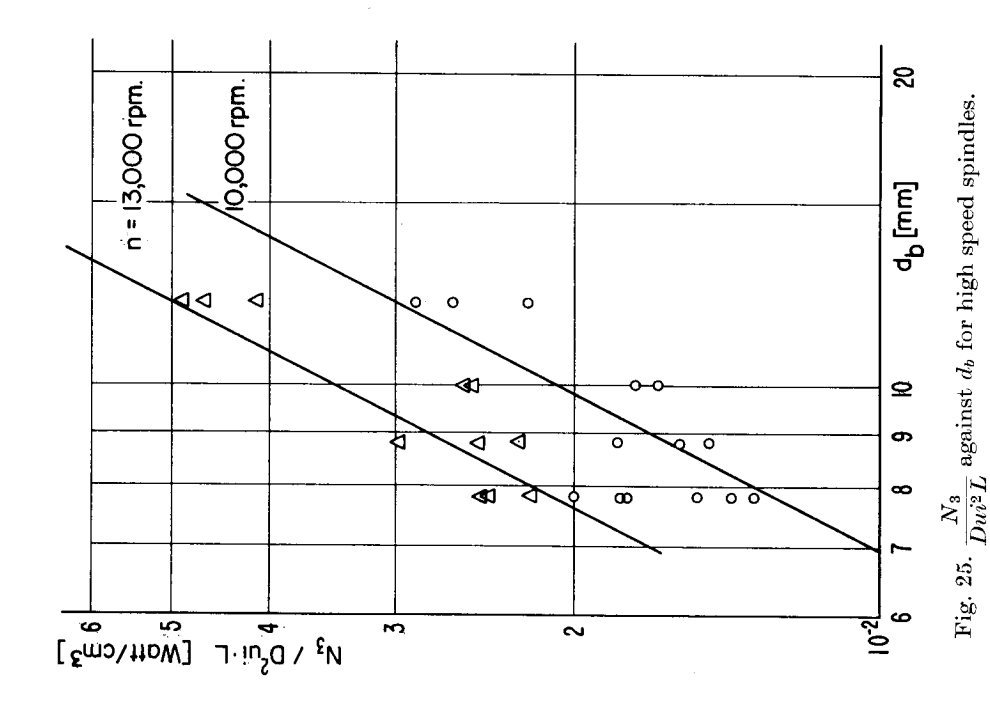
To obtain a formula describing the spindle power, it is not practicable to consider all the factors which affect the spindle power. Only tests under normal running conditions of the spindles (but with empty tubes and without balloon) were considered. Accordingly, the main factors to be considered are the spindle speed, size and construction. It was observed in the results that the high-speed spindles, which have special designs of damping systems, showed characteristics different from those of the normal-speed ones. It was thus necessary to express the results of the two groups of spindles by two different formulas.

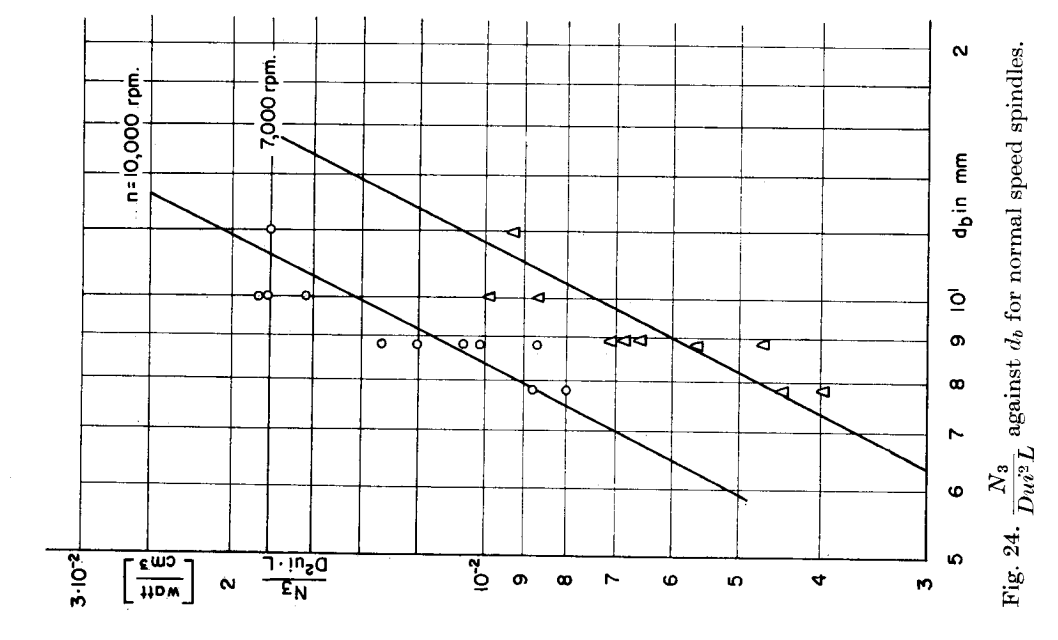
Equation (10) can be written in the form

$$\frac{N_3}{(Dui)^2L} = C_3(d_b)^a \, n^b = K_1(d_b)^a \, ,$$

where  $K_1$  is constant for constant speed n.

Figures 24 and 25 show the values of  $\frac{N_3}{(Dui)^2L}$  plotted against  $d_b$  on logarithmic scales for different speeds n and for the two groups of spindles respectively. From these figures, a was found to be approximately equal to 2. Thus, the spindle power  $N_3$  will be proportional to  $(Dui)^2L(d_b)^2$ , which can be denoted by S. Figure 26 represents the relation between  $N_3$  in watts and S in cm<sup>5</sup> for different speeds n. Figure 27 represents the same relation for the high speed spindles. The direct proportionality of  $N_3$  with the function found for S, representing the spindle size, can be observed. The scatter of the measured points with respect to the straight lines of proportionality is mainly due to the different constructions of the spindles tested. The values of  $N_3$  corresponding to an arbitrary spindle size ( $S=250~\rm cm^5$ ) were taken from figures 26 and 27 for different spindle speeds. These values were plotted logarithmically in





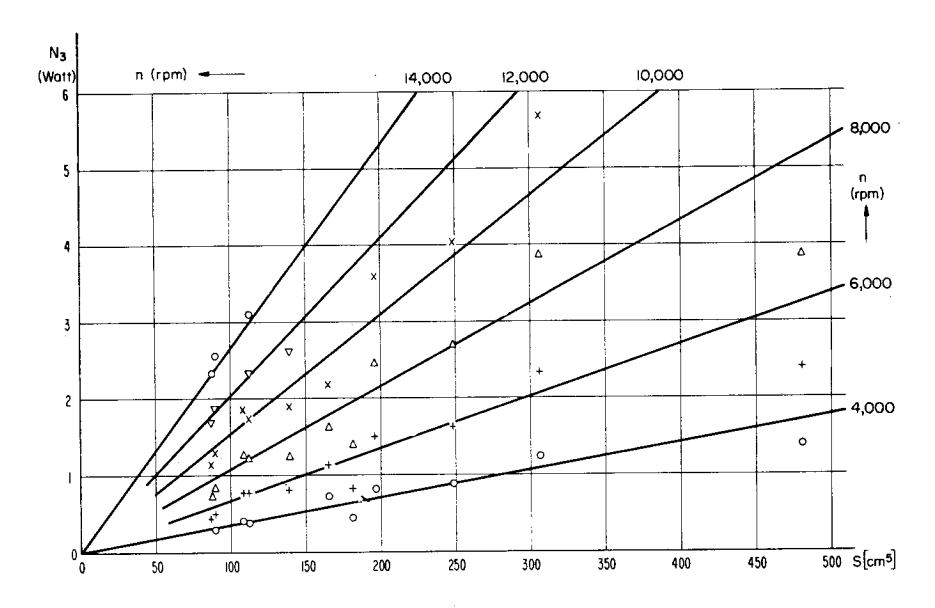


Fig. 26. The spindle power  $N_3$  against S for normal speed spindles.

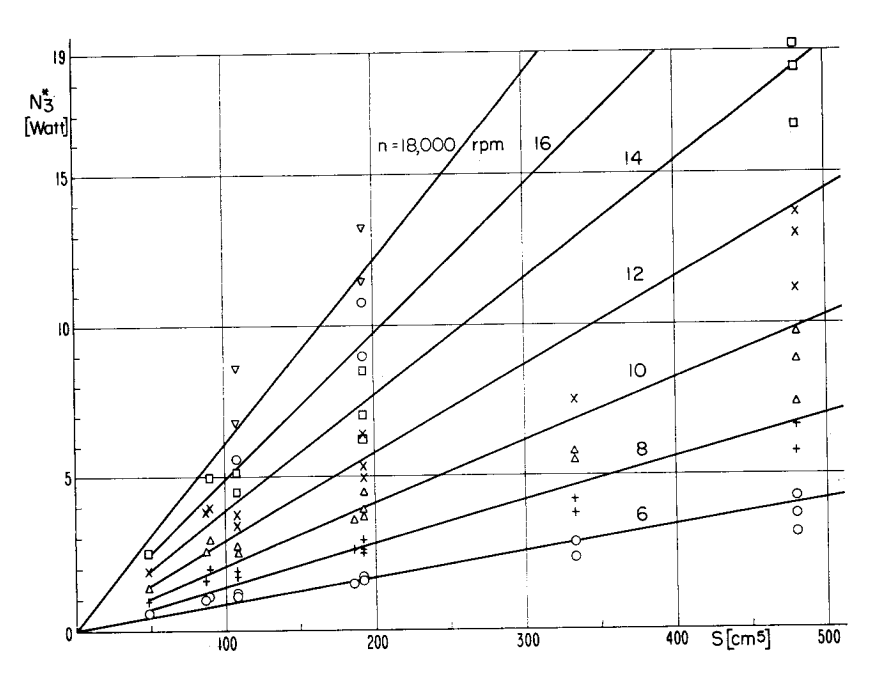


Fig. 27. The spindle power against S for high speed spindles.  $S = (Dui^2 L d_b^2)$ .

figure 28, from which  $C_3$  and b in equation (10) were found for both groups of spindles. The values of  $C_3$ , a and b were substituted in equation (10) to give:

$$N_3 = 3.9 \, S \, n^{1.6} \cdot 10^{-4} \tag{12}$$

$$N_3^* = 3.33 \, S \, n^{1.8} \cdot 10^{-4} \tag{13}$$

where

 $N_3$  = spindle power in watts for a normal-speed spindle,

 $N_3^*$  = spindle power in watts for a high-speed spindle,

S = a function representing the spindle size,

 $= (Dui)^2 L(d_b)^2$  in cm<sup>5</sup> (see fig. 17),

n =spindle speed in thousands of r. p. m.

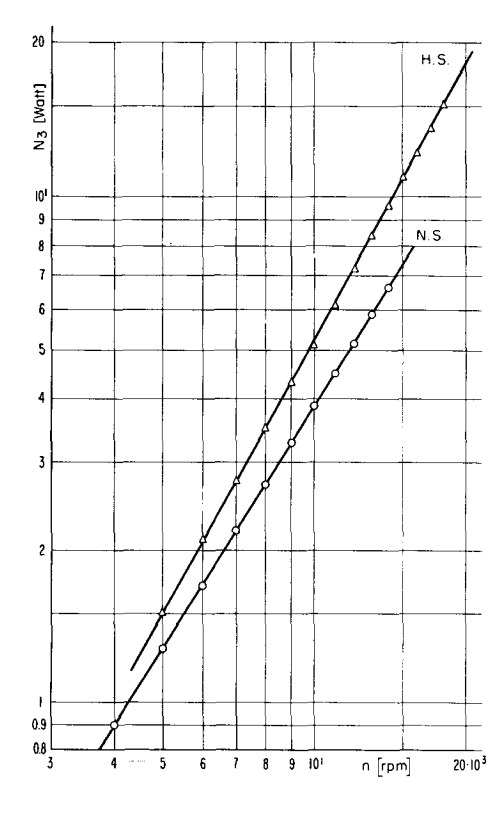


Fig. 28. The spindle power against n for  $S = 250 \text{ cm}^5$ , N.S. normal-speed spindles, H.S. high-speed spindles.

Figure 29 shows a plot of equation (12) in three dimensions.  $N_3$  is given as a function of S and n. It increases linearly with S and parabolically with n (to the power 1.6).

For the whole frame, equations (12) and (13) can be written as follows:

$$N_{3t} = 3.9 \ z \, S \, n^{1.6} \cdot 10^{-7} \tag{14}$$

$$N_{3t}^* = 3.33 z \, S \, n^{1.8} \cdot 10^{-7} \tag{15}$$

where  $N_{3t}$  and  $N_{3t}^*$  are the total spindle power of the frame in kW and z is the number of spindles.

We now consider a spinning frame having the following specifications:

Number of spindles z=400Spindle speed  $n=10{,}000$  r. p. m. Lower internal diameter of tubes Dui=2.4 cm Diameter of the spindle bearings  $d_b=0.88$  cm Spindle length measured from

spindle rail L = 31 cm

The total spindle power  $N_{3t}$  of this frame, calculated with the help of equation (14), was found to be 0.86 kW.

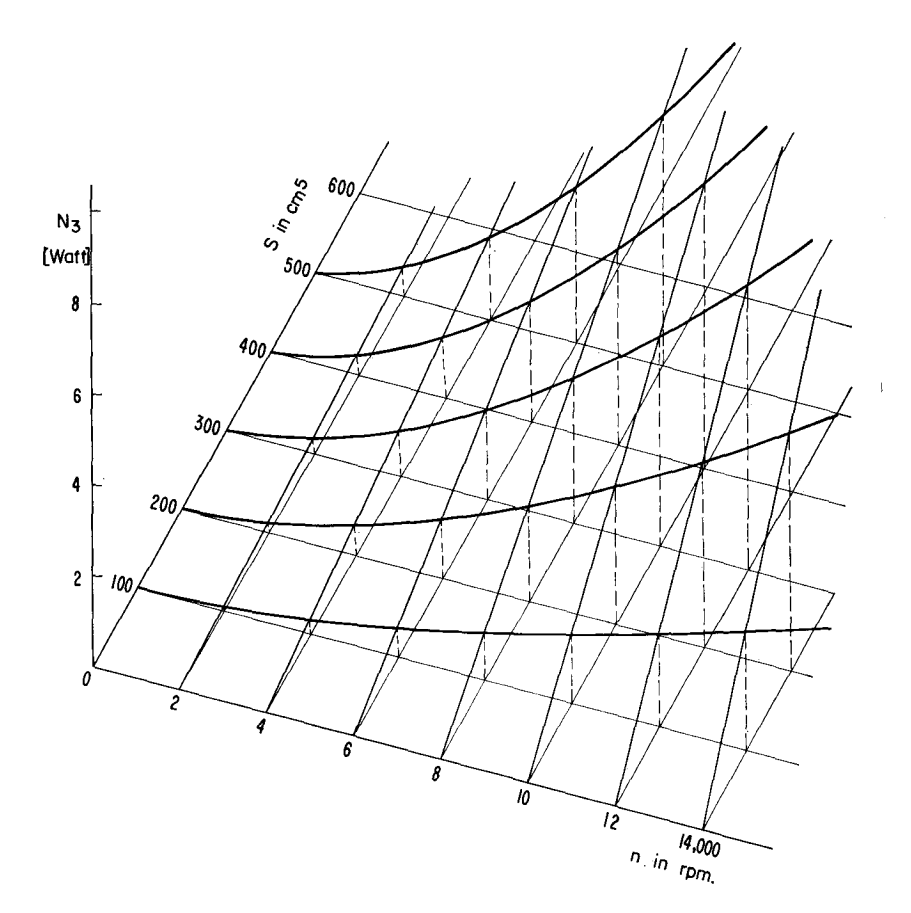


Fig. 29. The spindle power  $N_3$  as a function of the spindle speed n and  $S = (Dui^2 L d_b^2)$ .

# 7. Power absorbed by tension rollers

#### 1. General considerations

The tension rollers of a conventional frame having diameters ( $d_r = 70$  to 90 mm) which are larger than the wharves of the spindles turn with much lower speeds than the spindles. The number of these rollers in a frame is z/4. Therefore, the part of the power which is required to overcome their bearing friction is relatively small. This is not true for frames with single spindle drive: these frames have for each spindle two rollers of the same diameter as the wharve, thus running at the same speed n as the spindles.

The power consumption of the tension rollers, which generally have doublerow ball-bearings, depends on their speed  $n_r$ , the radial load  $P_r$  on their bearings, and the kind of grease used for lubrication. However, the last two factors have only a secondary effect. Thus, the power  $N_4$  could be expressed as follows:

$$N_4 = C_4 n_r^a \tag{16}$$

where  $N_4$  = the power in watts required to overcome the bearing friction of the tension roller,

 $n_r$  = the speed of the roller in thousands of r. p. m.,

 $C_4$  and a are constants which are determined experimentally.

#### 2. Experiments and results

The tests were made using the testing stand described in the last chapter. The power  $N_4$  was measured in the same way as  $N_3$ . The power required to overcome both the air and the bending resistances of the driving tape was also here subtracted from the total power calculated from the readings of (4) and (8) in figure 18.

Different types of new and used rollers were tested. The results of all rollers tested — having different diameters  $d_r$  — lie in the ranges given in figure 30. In this figure,  $N_4$  in watts is plotted against the speed  $n_r$  in r.p.m. of the roller for a radial load  $P_r = 1.0$  kg. The values of  $N_4$  for  $P_r = 1.5$  kg were found to be about 15% higher than those given in figure 30.

It can be seen from this figure that the used rollers consume only about 50 to 70% of the power consumed by the new ones. This may be due to the smaller amount of grease staying on the bearing rails after many working hours.

Some differences in the power consumption of the various types of rollers were observed. But with regard to the small value of this power, only the average — plotted as a full line in figure 30 — was taken into consideration.

From the above results, the values of  $C_4$  and a in equation (16) were found to be as tabulated below:

Table 6

$P_r$ (kg)	1.0	1.5
$egin{array}{c} C_4 \ a \end{array}$	0.09 1.6	$0.1\\1.6$

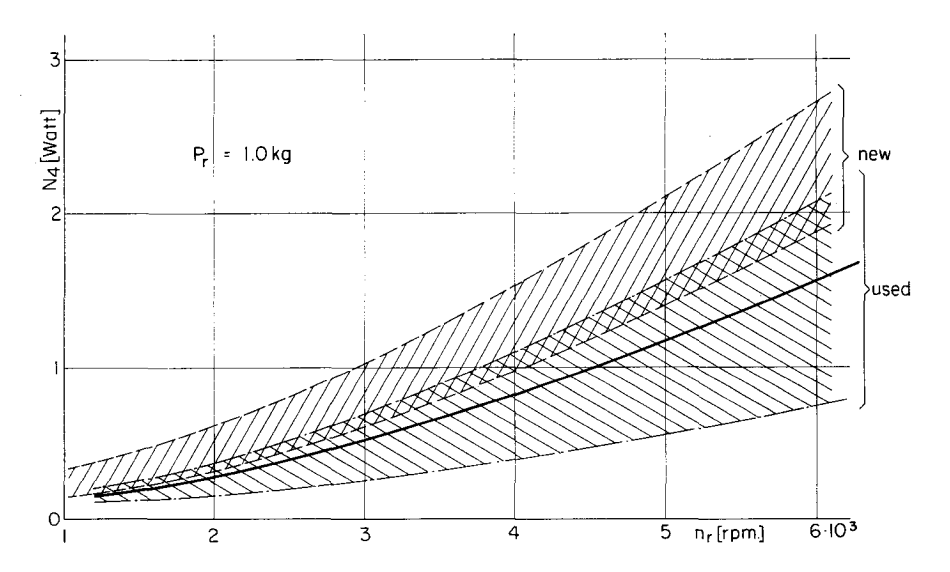


Fig. 30. The power absorbed by tension rollers against roller speed  $n_r$ .

## 8. Air resistance of tin rollers

A very small part of the total power consumption of a conventional ring frame is required to overcome the air resistance of its tin rollers.

The air resistance on the cylindrical surface of the tin rollers can be written as follows:

$$R = C_f A \frac{\rho v^2}{2},$$

The power required to overcome this resistance is thus

$$N_5 = C_f A \frac{\rho \ v^3}{2} \qquad \text{in kg m/sec.}$$

The coefficient of air friction  $C_f$  depends on Reynold's number Re, specially for relatively smooth surfaces. Tests were made by Ackeret [8] to study the effect of blowing a radial stream of air on  $C_f$  of a rotating cylinder. The values of  $C_f$  corresponding to zero radial blowing speed are plotted against Re in figure 31, from which the relation between  $C_f$  and Re can be expressed as follows:

$$C_f = \frac{0.2}{(Re)^{0.3}}. (17)$$

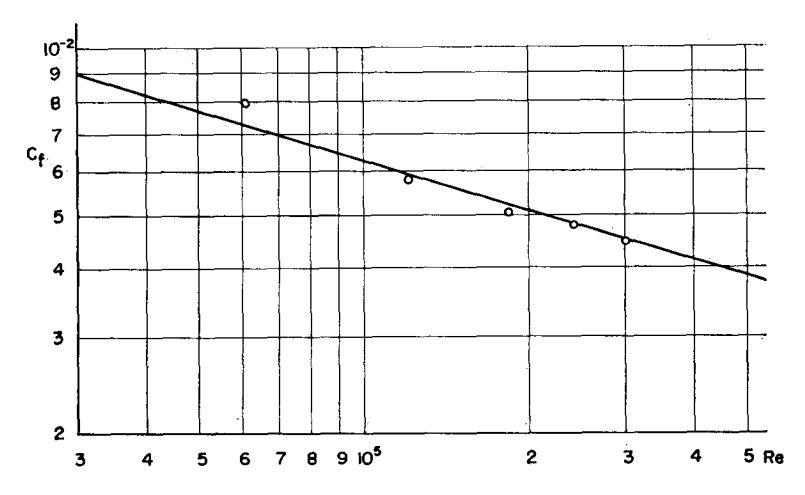


Fig. 31. The coefficient of air friction  $C_f$  of a smooth rotating cylinder against Reynolds no. Re.

In these tests, a smooth metallic cylinder of 100 mm diameter was used. As the tin rollers have diameters of 230 mm (9") and 254 mm (10"), and also a higher surface roughness, they could be assumed to have approximately the same relative roughness as the cylinder tested. Moreover, the range of Reynold's number tested covers the practical running conditions of the tin rollers. The values of  $C_f$  given by equation (17) are therefore suitable for calculating  $N_5$ , which can be written as follows:

$$N_5 = \frac{0.2}{(Re)^{0.3}} \, A \, \frac{\rho \, v^3}{2} \qquad \mbox{ kg m/sec.}$$

Substituting  $Re = \frac{v d_t}{v}$ 

$$A = \pi d_t L_t, \qquad \qquad v = rac{\pi d_t 1000 \, n_t}{60}, \ 
ho = 0.12 \, \mathrm{kg} \, m^{-4} \, \mathrm{sec^2}. \, , \qquad 
u = 0.15 \cdot 10^{-4} \, \mathrm{m^2/sec.},$$

in the above equation, we get:

$$N_5 = 0.58 L_t d_t^{3.4} n_t^{2.7} (18)$$

where

 $N_5$  = the power in kW required to overcome the air friction of the tin rollers,

 $d_t = \text{diameter of tin rollers in m},$ 

 $L_t$  = total length of tin rollers in m,

 $n_t$  = speed of tin rollers in thousands of r. p. m.

Tin rollers, which generally have diameters of 9" and 10", show a negligible difference in their relative roughness. Equation (18) was thus used to calculate  $N_5$  for both diameters. Figure 32 shows the relation between the power  $N_5$  per meter length of the tin rollers  $(N_5/L_t)$  and  $n_t$  in r. p. m. for diameters of 9" and 10".

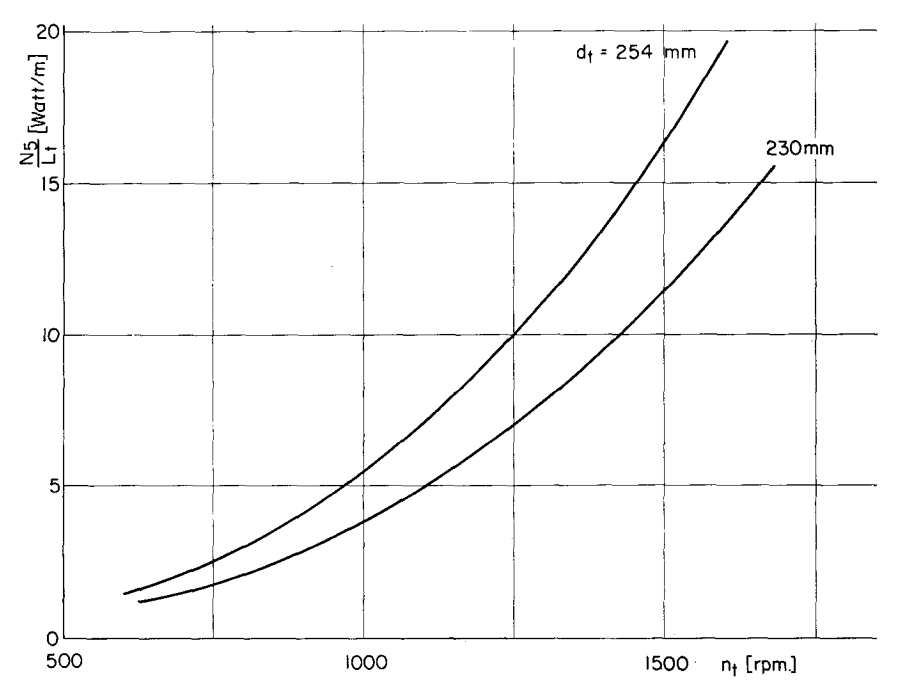


Fig. 32. Power absorbed by air friction of tin rollers per meter length against speed of tin rollers.

# 9. Package power

#### 1. General considerations

A great part of the power consumption of a spinning frame is used to overcome the air resistance of the rotating yarn packages<sup>2</sup>). However, this fact has recently attained a greater importance owing to the modern tendency towards higher spindle speeds and larger packages.

The package power can be defined as the power required to overcome the air drag on the package surface and the additional spindle-bearing friction caused by the weight and possible unbalance of the package. The latter part is evidently small. The problem can thus be considered as a purely aerodynamical one.

Consider a cylindrical package, having a diameter d, height h' and a high ratio of h'/d. Let this package rotate about its axis with a speed n r. p. m. The air resistance R on its cylindrical surface can be expressed as follows:

$$R = C_f A \frac{\rho \, v^2}{2}.$$

The power required to drive the package against this resistance

$$N_6 = C_f A \frac{\rho \, v^3}{2}.$$

Substituting  $A = \pi dh'$  and  $v = \frac{\pi dn}{60}$ , we get

$$N_6 = C_f \frac{\pi^4 \rho}{2 (60)^3} d^4 h' \, n^3.$$

The coefficient  $C_f$  depends generally on the Reynold's number, as stated previously. But for complete turbulence and rough cylinders — which is the case for spinning packages —  $C_f$  is slightly dependent on Re. Considering it to be constant, we may write

$$N_6 = \operatorname{constant} d^4 h' n^3. \tag{19}$$

The above discussion is applicable to cylindrical packages with a high ratio of h'/d. Let h' be the equivalent height of that cylindrical package which has the same diameter and air drag as a normal spinning package with conical ends (fig. 33). As the spinning packages are more or less geometrically similar — without regarding the variation of the relative roughness — h' can be considered proportional to the lift h. Moreover, as the above equation is valid for

<sup>2)</sup> In this work, package denots the tube with yarn wound on it in the usual way.

geometrically similar cylinders (relative roughness  $\epsilon/d$  = constant) with negligible end effects, which is not exactly the case for spinning packages,  $N_6$  should be expressed in the general form as:

$$N_6 = C_6 d^a h n^b \tag{20}$$

where

 $N_6$  = the package power in watts of a full bobbin,

d = package diameter in cm,

h = lift in cm,

n = spindle speed in thousands of r. p. m.

 $C_6$ , a and b are constants, determined experimentally.

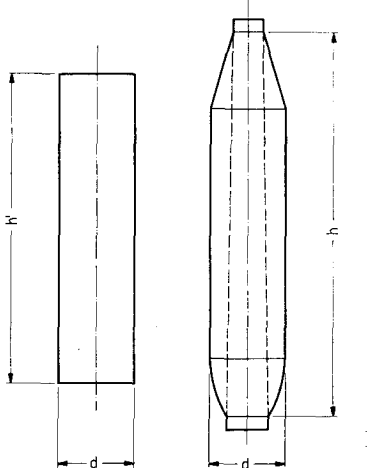


Fig. 33.

It can be seen from equation (20) that the function  $S_p$  for the size of the package is expressed as  $S_p = d^a h$ . In this equation, the complicated air motions which take place in a spinning frame, due to eddy currents caused by the neighbouring packages, tapes, tin rollers and balloons, are not considered. The effect of these eddy currents will be studied later on in this chapter.

Equation (20) describes the package power at the end of a doffing. It is clear that the package power increases as the building of the bobbin proceeds. This was also studied for a cop-build which is commonly used in spinning frames.

## 2. Experiments and results

The measurements of the package power were made on the testing stand described in chapter 6. Spindles were tested with empty and full tubes respectively, from which the package power  $N_6$  was found.

Full cotton bobbins having various sizes (d = 35 to 82 mm and h = 180 to

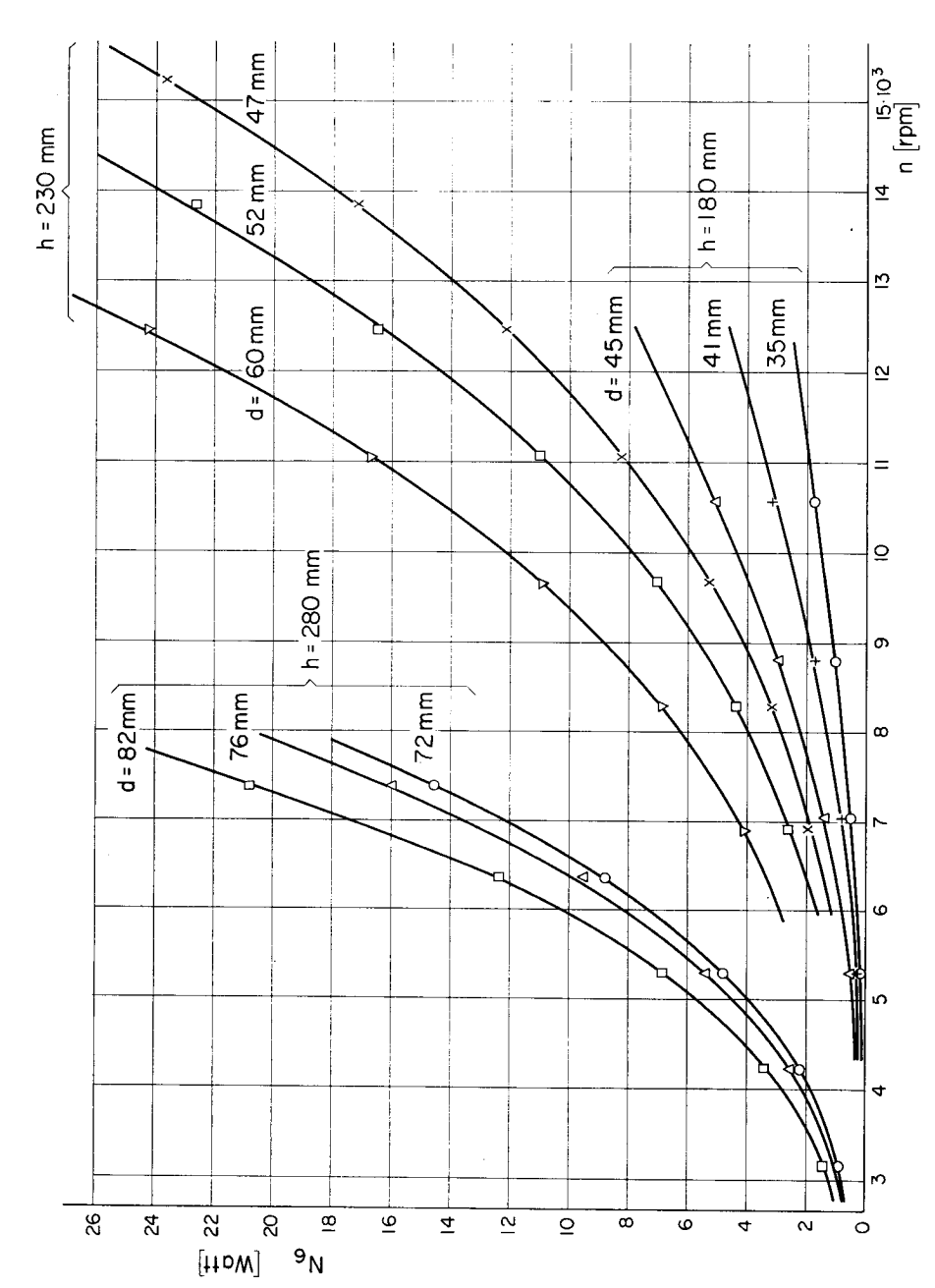


Fig. 34. The package power against spindle speed for different package sizes.

280 mm) were tested at speeds up to 17,000 r.p.m. The results of a few of these tests are given in figure 34.

To find the values of  $C_6$ , a and b in equation (20), it can be written in the form

$$N_6/h = C_6 d^a n^b = K_2 d^a$$

where  $K_2$  is constant for a constant speed n. The package power per unit height of bobbin  $N_6/h$  in watts per cm is plotted against the package diameter d on a logarithmic chart (fig. 35) for n=7,000 and 10,000 r. p. m. From this figure,

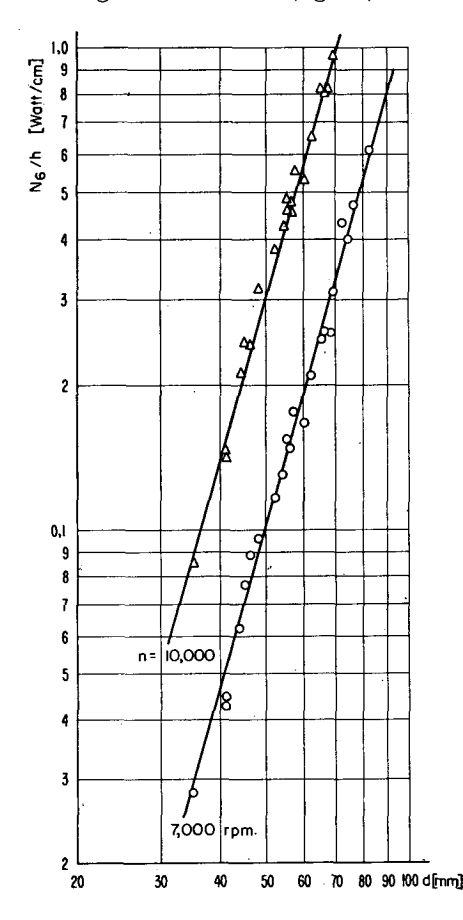


Fig. 35. Package power per cm lift versus package diameter.

a was found to be equal to 3.5. The function representing the package size can therefore be given as  $S_p = d^{3.5}h$ . The power  $N_6$  in watts of all the packages tested, is plotted in figure 36 versus  $S_p$  in cm<sup>4.5</sup> for different speeds n. From this figure, the direct proportionality of  $N_6$  to  $S_p$  can be observed.  $N_6$  of an arbitrary package size ( $S_p = 15{,}000~\rm{cm^{4.5}}$ ) was taken from figure 36 for different speeds n. These values of  $N_6$ , were plotted versus n logarithmically in figure 37,

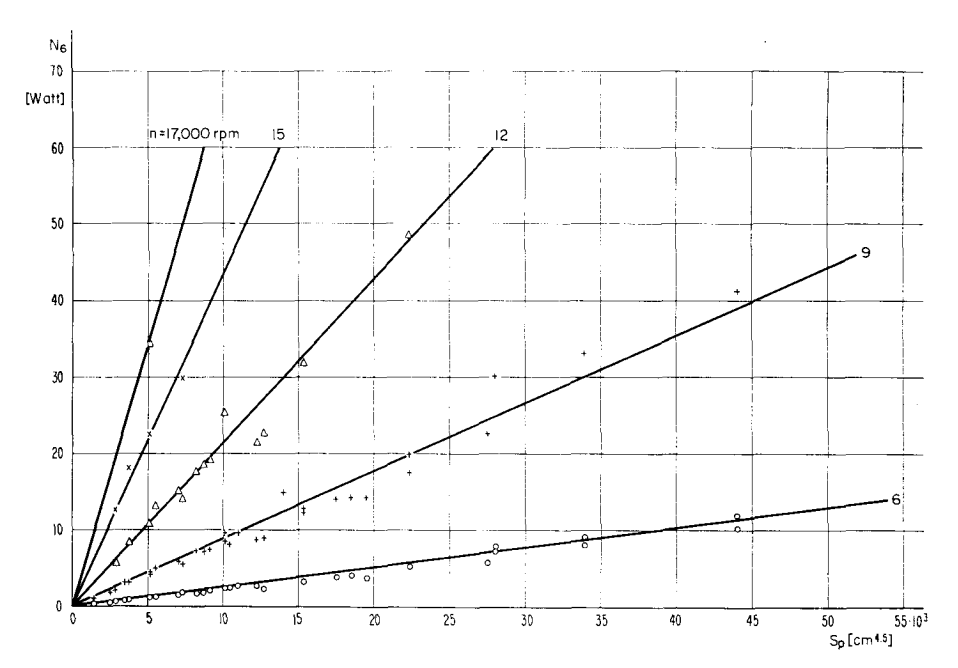
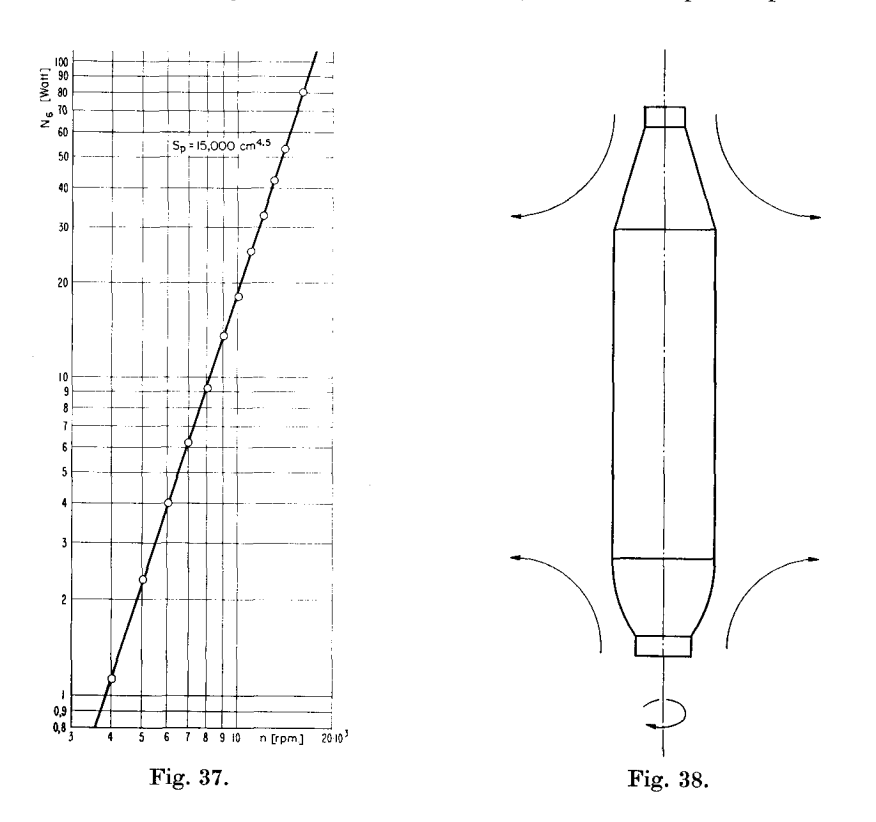


Fig. 36. The package power versus  $S_p = (d^{3.5}h)$  for different spindle speeds.



from which  $C_6 = 1 \cdot 10^{-6}$  and b = 3.1 was found. Equation (20) can thus be written as follows:

$$N_6 = d^{3.5} h \, n^{3.1} \cdot 10^{-6}. \tag{21}$$

It should be stated here that we are dealing with turbulent flow ( $Re \gg 4,000$ ). The power of n (=3.1) in equation (21) is slightly higher than that of n in the theoretical equation (19). This could be considered due to the excessive turbulence caused by the end effects of the packages (fig. 38). On the other hand, the power of d was found to be 3.5 instead of 4. This may be explained by the difference in relative roughness of packages with different diameters. Assuming the yarn packages to have the same surface roughness, the packages with larger diameters will be relatively less rough than the others.

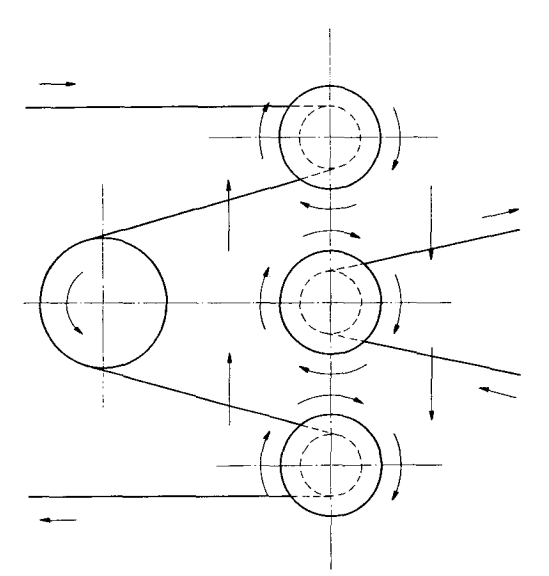


Fig. 39. The arrangement used to find the effect of the adjacent bobbins on the package power.

The package power as measured on the testing stand, with the air surrounding the package free to rotate without any disturbance, may not represent exactly the package power of the spinning frame. In the full-size frame there are more complicated air streams which are mainly due to the adjacent packages. To study this effect, three spindles with full bobbins of the same size (fig. 39) were driven with the same speed and direction. The middle one was driven separately by the driving pulley of the testing stand, and the others by a variable-speed motor. The package power of the middle spindle was measured with and without the effect of the other ones for various speeds, package sizes and corresponding suitable gauges. In all cases, no effect of the neighbouring packages on the package power could be measured. This can be explained as follows. In the region between the packages, a contra-flow of air

will occur at running conditions, which causes an increase in the package power. On the other hand, a parallel flow of air will exist parallel to the plane containing the axes of the spindles and on both sides of them. This decreases the air friction of the bobbins. The two effects apparently compensate each other, and hence, equation (21) can be used to calculate the package power of a full-size frame<sup>3</sup>).

The increase of the package power during the building of the bobbin (cop build) was studied as follows. Several packages of different sizes were tested with partial yarn fillings (1/4, 2/4, 3/4 and 4/4) at various speeds. The results of these tests lie in the range given in figure 40. The mean package power  $\overline{N}_6$  during a cop build was found to be 50 to 56% of the maximum power  $N_6$  of a full bobbin.

Figure 41 shows a three dimensional plot to illustrate equation (21), where  $S_p = d^{3.5}h$  in cm<sup>4.5</sup>.  $N_6$  increases linearly with  $S_p$  and parabolically with n to the 3.1 power.

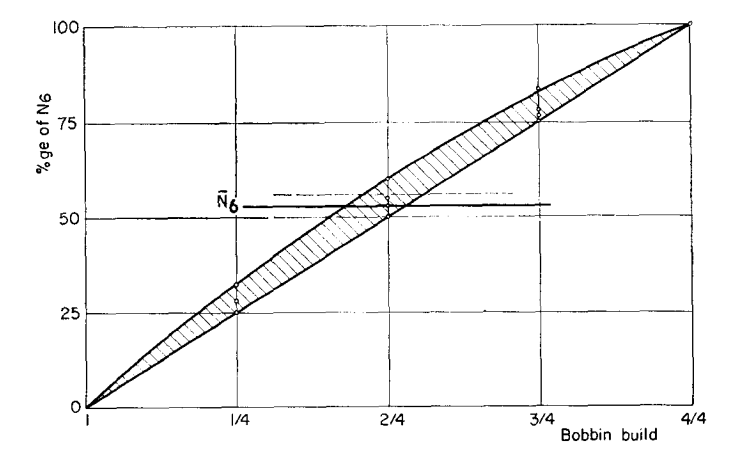


Fig. 40. Increase of the package power during the build up of the bobbin.

<sup>3)</sup> Catling and De Barr [2] found from their measurements that the package power was proportional to the (package diameter)<sup>2.75</sup> and the (spindle speed)<sup>2.5</sup>, but this was not treated theoretically. Obviously, these results cannot agree with equation (19).

<sup>4)</sup> The corresponding value given by Catling and De Barr [2] is 76.4%. This great difference is mainly attributed to the fact that the package power given by them for empty tubes was more than 20% of its value with full bobbins. No explanation was given in their article. The power required to overcome the air friction of the empty tube — having a diameter of about  $\frac{1}{2}$  that of the package — is much less than  $(\frac{1}{2})^{3.5}$  of the package power of the full bobbin because of its relatively smooth surface. Thus, this power, which is considered in this work to be a part of the spindle power (see p. 28), cannot reach 20% of  $N_6$ .

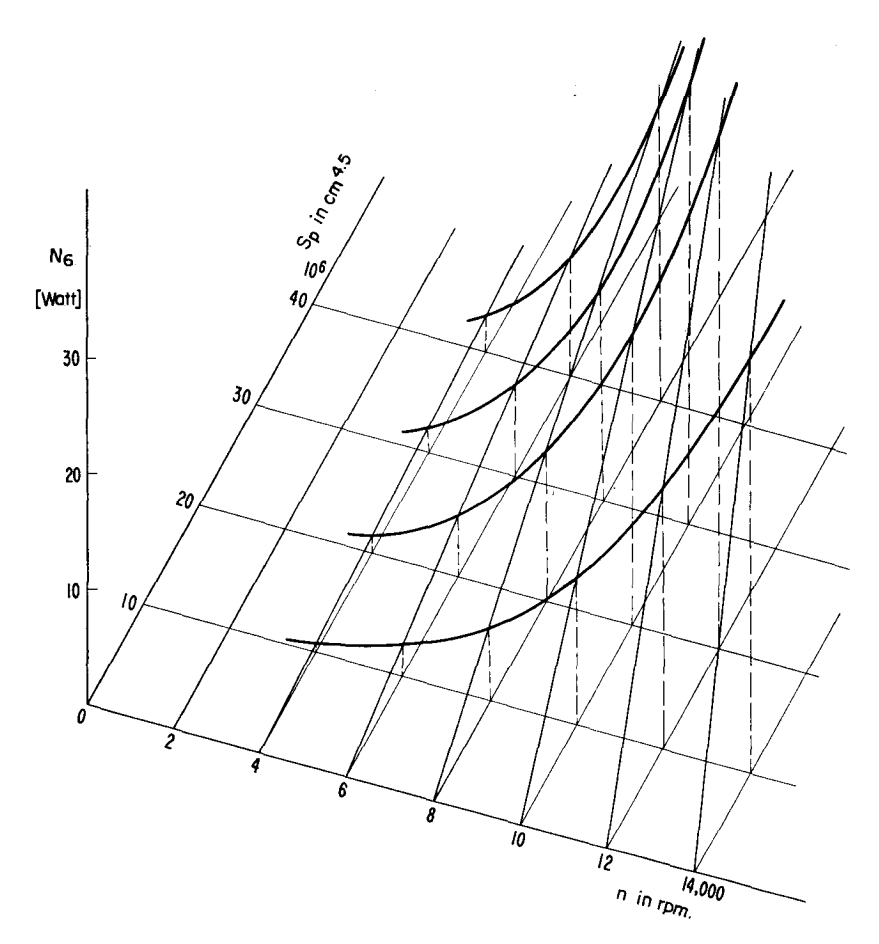


Fig. 41. The package power  $N_6$  as a function of the spindle speed n and  $S_p = (d^{3.5}h)$ .

Wool bobbins (worsted), having generally rougher surfaces than the cotton ones, show a higher coefficient of air friction  $C_f$ . Tests made on wool bobbins show a power consumption which is 25% greater than that given by equation (21) for cotton bobbins. The package power  $N_6^*$  of wool bobbins can therefore be written as follows:

$$N_6^* = 1.25 d^{3.5} h n^{3.1} \cdot 10^{-6}.$$
 (22)

The total package power  $N_{6t}$  and  $N_{6t}^*$  in kW for cotton and wool (worsted) spinning frames with full bobbins can be written as

$$N_{6t} = d^{3.5} h \, n^{3.1} z \cdot 10^{-9} \,, \tag{23}$$

$$N_{6t}^* = 1.25 \, d^{3.5} \, h \, n^{3.1} \, z \cdot 10^{-9} \,. \tag{24}$$

As an example, consider a cotton spinning frame having the following data:

number of spindles z=400ring diameter  $D_r=50.8 \text{ mm}$ lift h=23.0 cmpackage diameter d=48.0 mmspindle speed n=10 thousand of r. p. m.

Using equation (23),  $N_{6t}$  was found to be equal to 2.77 kW. The mean package power for a cop build  $(\overline{N}_{6t} = 0.53 N_{6t})$  equals 1.47 kW.

The percentage of the package power to the total power requirements of the frame can vary over a very wide range depending on the spindle speed, package size and yarn count. The latter affects mainly the spinning power and hence the total power.

# 10. Air resistance of the spinning balloon

#### 1. Theoretical considerations

To calculate the power required to overcome the air friction of the spinning balloon, it is necessary to use the equations of the balloon thread. These have been derived by several authors making different assumptions to simplify the problem. The balloon characteristics can be precisely specified by:

- the balloon height H,
- ring diameter  $D_r = 2 r_0$ ,
- maximum balloon diameter  $2 \rho'_m$ ,
- yarn count  $N_e$ ,
- traveller speed  $n_{I}$ .

Capello [9] found an approximate solution of the equations of the spinning balloon by making simplifications suggested by experimental results.

Consider three Cartesian axes with the origin at the apex of the balloon (fig. 42) and rotating with a constant velocity  $\omega$  (angular velocity of the traveller) around the x-axis (axis of the spindle). It was found by Capello, that in every case it is possible to find a plane containing the spindle axis (x-axis) on which the projection of the thread shape is very nearly a straight line. The angle  $\alpha$  between this line and the x-axis is that by which the traveller leads the yarn. Taking as a projection plane the one normal to the plane defined by the balloon apex, the point of maximum radius and the lowest point of the thread in the balloon (just before the traveller), the projection on this plane for balloons of height H = 20-22 em did not depart from a straight line by

more than 1 mm, when  $\rho'_m/r_0 > 2$ , or more than few tenths of a millimetre, when  $1.6 < \rho'_m/r_0 < 2$ . For balloons of smaller diameters, which are the normal spinning ones, the departures were found to be even smaller.

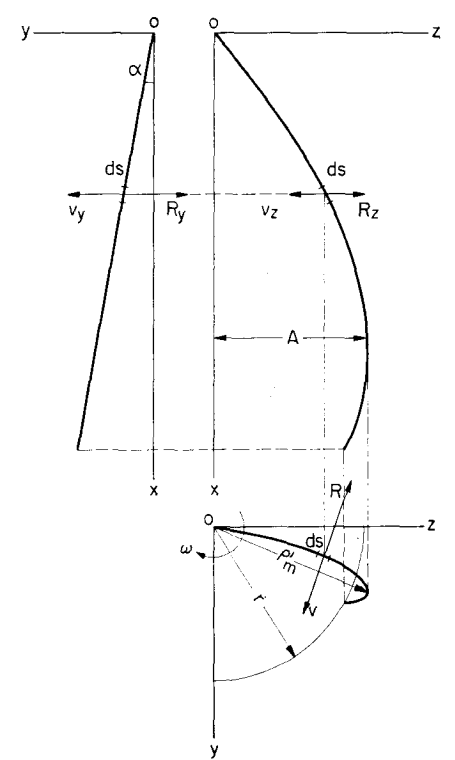


Fig. 42.

Moreover, the air drag per unit length of the balloon thread R was assumed to be proportional to  $v^2$ , i.e.,  $R = K v^2$  and thus R was expressed as follows:  $(v = \omega \rho')$ 

$$R = \gamma \sqrt{m} \,\omega^2 \rho'^2 \tag{25}^5$$

where

R =the air drag per unit length of yarn in g/cm,

 $\gamma=$  constant assumed to be equal to  $3.16\cdot 10^{-5}$  g<sup>1/2</sup>·cm<sup>-2</sup>·sec., with which very good results were obtained for cotton threads,

m = the mass per unit length of yarn,

 $=\,\frac{1}{9.81\,Nm}\cdot 10^{-4}\quad {\rm g}\cdot {\rm cm}^{-2}\cdot {\rm sec}^2,$ 

 $\omega$  = the angular velocity of the traveller,

 $\rho'$  = the balloon radius in cm.

<sup>&</sup>lt;sup>5</sup>) Equations (25) to (28) were derived by Capello [9].

Accordingly, the balloon thread equations were given as follows:

$$y = \alpha x, z = A \sin p x.$$
 (26)<sup>5</sup>)

And the components of the air drag per unit length of thread on the xy and xz planes are

$$R_{y} = -\gamma \sqrt{m} \omega^{2} A^{2} \sin^{2} p x, \text{ and }$$

$$R_{z} = \gamma \sqrt{m} \omega^{2} A \sin p x \alpha x$$

$$(27)^{5}$$

where x, y and z are the Cartesian co-ordinates of any point on the balloon thread,

 $R_y$  and  $R_z$  are the components of the air drag per unit lenth on the xy and xz planes respectively,

A= arbitrary constant, which was found from the boundary conditions to be equal to  $\frac{\sqrt{r^2-\alpha^2H^2}}{\sin p\,H}$ ,

$$p = \sqrt[4]{\frac{m\,\omega^2}{T_x}},$$

 $T_x$  = the component of the thread tension along the x-axis. It can be found by solving the following two equations graphically to get p and  $\alpha$ :

$$\left(\frac{\alpha H}{r_0}\right)^2 + \frac{\sqrt{m}}{r_0 \gamma} \frac{2 p H \sin^2 p H}{2 p H - \sin 2 p H} \left(\frac{\alpha H}{r_0}\right) - \left(\frac{r}{r_0}\right)^2 = 0, 
\left(\frac{\rho'_m}{r_0}\right)^2 = \frac{1}{\sin^2 p H} \left[\left(\frac{r}{r_0}\right)^2 - \left(\frac{\alpha H}{r_0}\right)^2\right] + \frac{\pi^2}{4 p^2 H^2} \left(\frac{\alpha H}{r_0}\right)^2.$$
(28)<sup>5</sup>)

 $\alpha$  = the angle by which the traveller leads the yarn,

r= the radius of the bottom circle of the balloon. It was found to be equal to  $r_0+k$ , where k=0—0.17 cm,

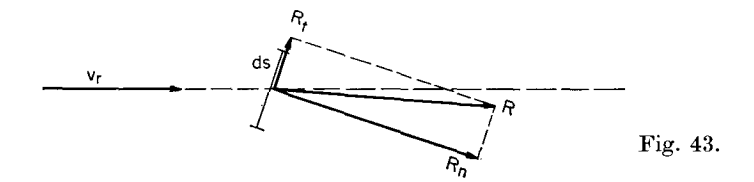
 $r_0$  = the radius of the ring in cm.

The air drag factor  $\gamma$ , assumed to be constant, varies actually with the relative velocity of the air  $v_r$ , yarn count, twist and hairiness. Accordingly, it varies not only from one spinning condition to another, but also along the same balloon thread from the apex to the traveller. For our purpose, however, such an assumption cannot lead to any considerable error. Similar assumption was made also by *Grishin* [10].

Consider a balloon thread element of length ds. The air resistance acting on this element is equal to  $\overline{R} ds$ . The power  $dN_7$  required to drive this element with a velocity  $\overline{v}$  against the air resistance  $\overline{R} ds$  is equal to  $\overline{R} \overline{v} ds$  (scalar product). Therefore, we can write

$$dN_7 = \bar{R}\bar{v}ds$$
  
=  $(R_xv_x + R_yv_y + R_zv_z)ds$ .

The component of the air resistance in the x-direction  $R_x$  can be neglected, considering the air resistance  $\overline{R}$  to be in the direction of the relative velocity of air. In fact, it lies, as shown in figure 43, between the normal resistance



 $R_n$  and the relative velocity  $v_r$ , but very near to the latter and in the plane determined by ds and  $v_r$ . It takes the direction of  $v_r$  if ds were normal to  $v_r$ . In this case the tangential air resistance  $R_t$  will vanish. Moreover, the axial component of the speed of delivery  $v_x$  is also negligible.

Accordingly,  $R_x v_x \cong 0$ , and

$$dN_7 = (R_y v_y + R_z v_z) ds$$

$$= (R_y v_y + R_z v_z) \frac{ds}{dx} dx.$$
(29)

For normal spinning balloons  $\frac{ds}{dx} \cong 1$ . The velocity components  $v_y$  and  $v_z$  can be written as follows:

$$v_y = \omega z = \omega A \sin p x, v_z = -\omega y = -\omega \alpha x.$$
 (30)

Substituting the values of  $R_y$ ,  $R_z$ ,  $v_y$  and  $v_z$  given by equations (27) and (30) in equation (29), we get:

$$dN_7 = -\gamma \sqrt{m} \omega^3 A (A^2 \sin^3 p x + \alpha^2 x^2 \sin p x) dx.$$

Integrating the above equation over the whole length of the balloon, we get:

$$\begin{split} N_7 &= \int\limits_0^H d\,N_7 = -\gamma\,\sqrt{m}\,\omega^3\,A\,\big[A^2\int\limits_0^H (\sin^3p\,x)\,dx + \alpha^2\int\limits_0^H (x^2\sin p\,x)\,dx\big] \\ &= -\gamma\,\sqrt{m}\,\omega^3\,A\,\bigg[\frac{A^2}{3\,p}\{\cos^3p\,H - 3\cos p\,H + 2\} \\ &\quad + \frac{\alpha^2}{p^3}\{2\,p\,H\sin p\,H + (2-p^2\,H^2)\cos p\,H - 2\}\bigg] \end{split} \tag{31}$$

The negative sign in the above equation is clearly because the air friction R is in the opposite direction to the thread velocity v.

The first part of equation (31) gives the power absorbed by the air friction of the balloon thread if it were in the form of a sine curve (with maximum

ordinate = A) lying in a meridian plane. The second part of this equation represents the excess power due to the displacement of the thread from the meridian plane. Dealing with equations (31) and (28) it was found in all cases that the second part of equation (31) is very small compared with the first one.

We now consider *Lindner*'s [11] equation:

$$z = \rho_m' \sin p \, x. \tag{32}$$

This equation is based on the assumption that the balloon thread lies in a meridian plane and neglects the speed of delivery, i.e. it neglects the effect of the air drag and the Coriolis force on the thread shape.

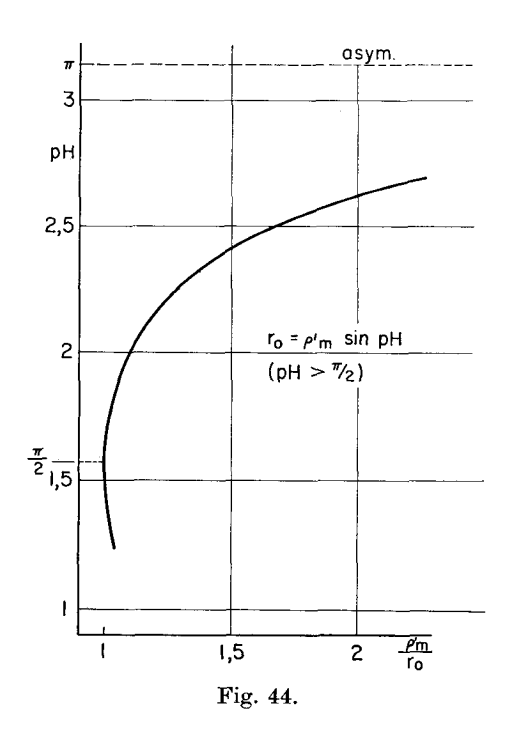
Substituting  $z=r_0$  for x=H (i.e.  $r_0=r$ ) in equation (32), p can be found for balloons with one real maximum diameter from the following equation:

$$pH = \pi - \sin^{-1} \frac{1}{\frac{\rho_m}{r_0}}.$$
 (33)

Figure 44 shows the relation between pH and  $\rho'_m/r_0$ , from which pH can be found for any given value of  $\rho'_m/r_0$ .

In this case, we can write (referring to figure 45):

$$d\,N_7 = -\,R\,v\,ds = -\,K\,v^3\frac{ds}{dx}\,dx = -\,K\,\omega^3\,z^3\,dx\,.$$



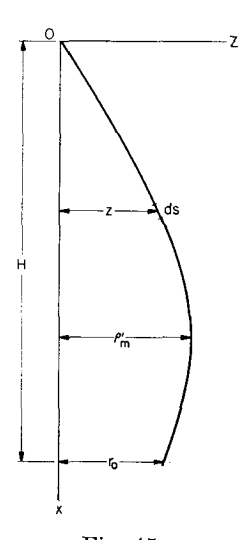


Fig. 45.

Therefore

$$N_7 = -K \,\omega^3 \rho_m^{\prime 3} \int_0^H \sin^3 p \,x \,dx = -K \,\frac{\omega^3 \rho_m^{\prime 3}}{3 \,p} [2 - 3\cos p \,H + \cos^3 p \,H]. \tag{34}$$

From equation (32) (substituting  $z = r_0$  for x = H) we have

$$\cos p H = -\sqrt{1 - \left(\frac{r_0}{\rho_m'}\right)^2}.$$

Therefore, equation (34) can also be written in the following form:

$$N_7 = -K \frac{\omega^3 \rho_m'^3}{3 p} \left\{ 2 + 3 \sqrt{1 - \left(\frac{r_0}{\rho_m'}\right)^2} - \left[1 - \left(\frac{r_0}{\rho_m'}\right)^2\right]^{3/2} \right\}. \tag{35}$$

Comparing equations (31) and (34), it could be seen that equation (34) can be found by neglecting the second part of equation (31) and considering  $A \cong \rho_m'$ . Using both equations to calculate  $N_7$ , a maximum difference of not more than 2% could be found in all cases.

It should therefore be stated here that *Lindner*'s equation (32) is quite sufficient to determine the spinning balloon characteristics for practical purposes.

The factor K in equation (35) has been calculated according to different authors as follows:

a) According to Capello [9]:

$$\begin{split} K &= \gamma \sqrt{m}\,, \\ \gamma &= 3.16 \cdot 10^{-5} & \text{g}^{1/2} \,\text{cm}^{-2} \,\text{sec.}\,, \\ m &= \frac{1}{9.81 \,N_m} \cdot 10^{-4} & \text{g} \,\text{cm}^{-2} \,\text{sec}^2\,, \\ K &= \frac{1.01}{\sqrt{N_m}} \cdot 10^{-7} & \text{g} \,\text{cm}^{-3} \,\text{sec}^2\,. \end{split}$$

b) According to Grishin [10]:

$$\begin{split} R &= 0.8 \cdot 10^{-6} \, d_y \, v^2 & \text{g/cm} \\ K &= 0.8 \cdot 10^{-6} \, d_y \\ d_y &= \text{yarn diameter} \, = \frac{0.125}{\sqrt[]{N_m}} & \text{cm} \\ K &= \frac{1}{\sqrt[]{N_m}} \cdot 10^{-7} & \text{g cm}^{-3} \sec^2. \end{split}$$

where

c) According to Mack and Smart [12]:

$$K = \frac{1}{2} \rho \, d_{eff} \, C_D$$

where  $C_D$  = the coefficient of air drag for a smooth cylinder,

 $d_{eff} =$  the effective air drag diameter of the yarn,

= the diameter of that smooth cylinder which has the same air drag as that of the yarn over the range of practical air speeds,

 $\rho \quad = \text{ air density} = 1.2 \cdot 10^{-6} \quad \text{g} \cdot \text{cm}^{-4} \cdot \text{sec}^2.$ 

 $C_D$  was found experimentally by the N.P.L. (Goldstein [13] p. 15) as a function of the Reynold's Number for smooth cylinders. For practical range of  $Re, C_D$  can be taken equal 1. The effective diameter  $d_{eff}$  was found by Mack and Smart for different counts. It can be expressed in the following form:

$$d_{\it eff} = \frac{0.18 \text{ to } 0.25}{\sqrt[]{N_m}}, \quad \text{with a mean value of} \frac{0.2}{\sqrt[]{N_m}}.$$

Accordingly, 
$$K = \frac{1.2}{\sqrt{N_m}} \cdot 10^{-7}$$
,  $g \, \mathrm{cm}^{-3} \mathrm{sec}^2$ .

The latter value of K is about 20% higher than the others. Substituting  $K = \frac{1.01}{\sqrt{N_m}} \cdot 10^{-7}$  and  $\omega = \frac{\pi \, 1000 \, n_l}{30}$  in equation (34), neglecting its negative sign and expressing the power in watts, we get:

$$N_7 = 3.8 \cdot 10^{-6} \frac{\rho_m'^3 n_l^3}{p \sqrt{N_m}} [2 - 3\cos p H + \cos^3 p H], \qquad (36)$$

where  $N_7$  = the power required to overcome the air drag of the spinning balloon in watts,

 $\rho'_m$  = the maximum balloon radius in em,

 $n_l$  = traveller speed in thousands of r. p. m.,

 $N_m = \text{yarn count (metric)} = \frac{1000}{tex},$ 

H = balloon height in cm,

 $p=\sqrt[4]{rac{m\,\omega^2}{T_x}}$  in cm<sup>-1</sup>, which can be determined by equation (33) or from figure 44.

To confirm equation (36) experimentally, tests were made in the laboratory to measure  $N_7$  for different balloons.

The air drag on a ballooning yarn was measured firstly by *Honegger* [14] in 1935.

### 2. Description of the apparatus

A simple ballooning yarn apparatus similar to that made by Brunnschweiler and Mohamadain [15] was used. Figure 46 shows a diagrammatic sketch of the apparatus, which was mounted on the testing stand described in chapter 6. An aluminium disc (2) was set in rotation by the driving pulley of the testing stand and the tape (1). One end of the yarn under test was attached to one of the small holes in the disc (2), which were at different radii r from the axis of rotation. The other end was fixed to a short spindle which was free to rotate in a miniature ball bearing (4). The housing of the ball bearing was connected at its centre to a spindle (5) of a square crossection. Both could slide almost frictionlessly vertically along the axis of rotation of the disc (2). The spindle (5) and the parts attached to it were supported by a thread (7), which was attached to a scale pan (8) after passing around ball bearing pulleys (6). The balloon height H could be varied by changing the position of the yarn guide (3), while the maximum balloon radius  $\rho_m'$  could be controlled by putting suitable weights in the scale pan (8).  $\rho'_m$  and H were measured accurately using a simple arrangement described by Morris [16] p. 20.

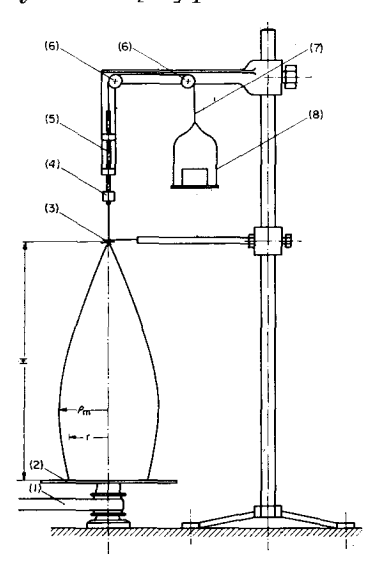


Fig. 46. Simple ballooning yarn apparatus.

#### 3. Experiments and results

It is clear that the balloons produced by the above described apparatus do not represent exactly the ballooning yarn in the spinning process. However, the absence of the speed of delivery, which is very small in spinning process, does not make any considerable difference to the balloon characteristics.

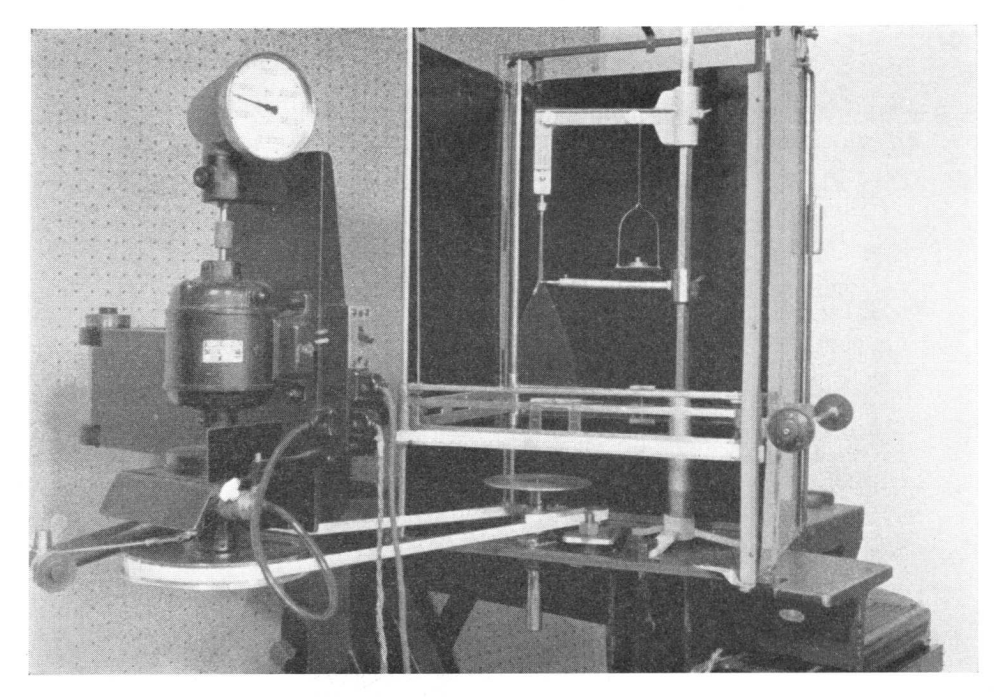


Fig. 46a.

Moreover, the resisting moment of the miniature ball bearing was so small that no perceptible increase of twist could take place in the ballooning threads of low and medium counts.

The power  $N_7$  was measured as the difference between the power consumption with and without the ballooning thread. This was done for balloons with different H,  $r_0$ ,  $\rho'_m$ ,  $N_m$  and  $n_l$ . In all cases the measured  $N_7$  agreed with that calculated by equation (36).

Figure 47 shows the results of some of the balloons tested, the data of which is given in table 7. The curves in this figure represent the values of  $N_7$  given by equation (36).

Table 7

Ne	$2r_0$ (mm)	H (mm)	$2 \rho'_m$ (mm)
5.8	82.5	340	109
16	63.5	280	89
16	63.5	280	75
32	50.8	250	75
32	50.8	250	65
	5.8 16 16 32	5.8 82.5 16 63.5 16 63.5 32 50.8	5.8     82.5     340       16     63.5     280       16     63.5     280       32     50.8     250

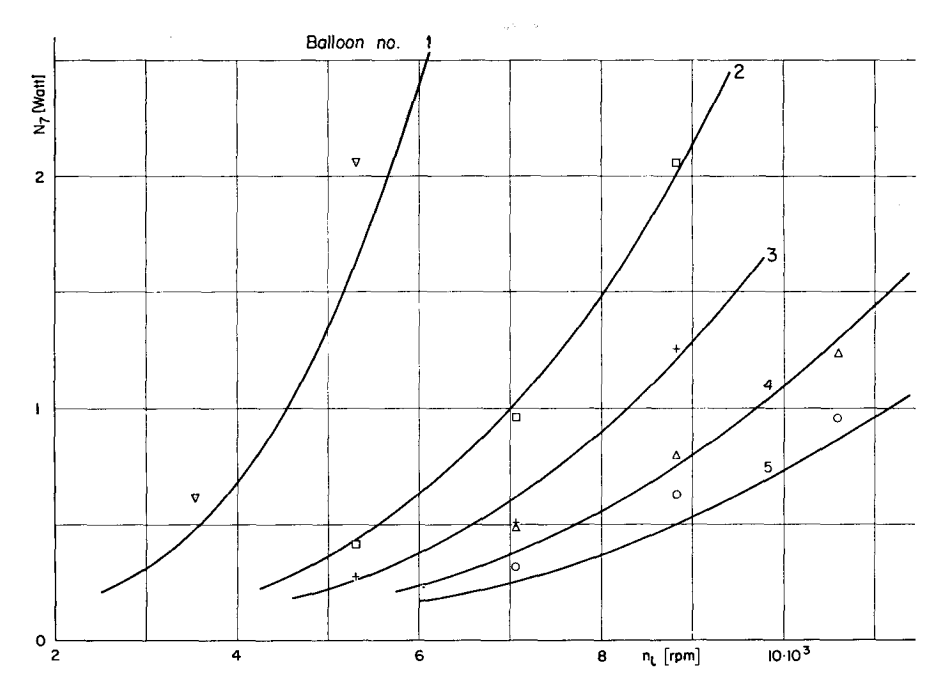


Fig. 47. Power absorbed by balloon air drag against traveller revolutions.

To calculate the power  $N_{7l}$  absorbed by the air drag on the ballooning threads of the whole frame, it should be noticed that  $H, \rho'_m$  and  $n_l$  vary continuously during the spinning process. With regard to the small value of  $N_{7l}$ , this needs to be calculated only for the balloons at half the time of a doffing and for the two extreme positions of the ring rail shown in figure 48.

It was observed for different spinning conditions with properly chosen travellers that (fig. 48)

$$\rho'_{mu} \cong 1.05 r_0$$
 and  $\rho'_{ml} \cong 1.35 r_0$ .

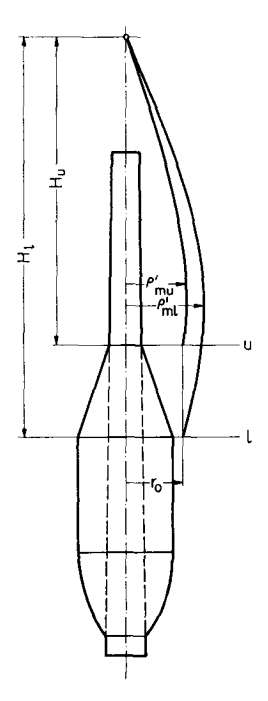


Fig. 48.

# 11. Traveller friction

#### 1. General considerations

The estimation of the traveller friction represents one of the most important items of this work. Early measurements were carried out under normal spinning conditions by *Honegger* in 1935 [14] and 1947 [17] and recently by *Axson* [18].

In this chapter, a simple formula is derived to express the power  $N_8$  required to overcome the traveller friction.

The forces acting on the traveller are shown in figure 49, in which x, y and z are considered to be the tangential, radial and axial directions respectively. These forces are:

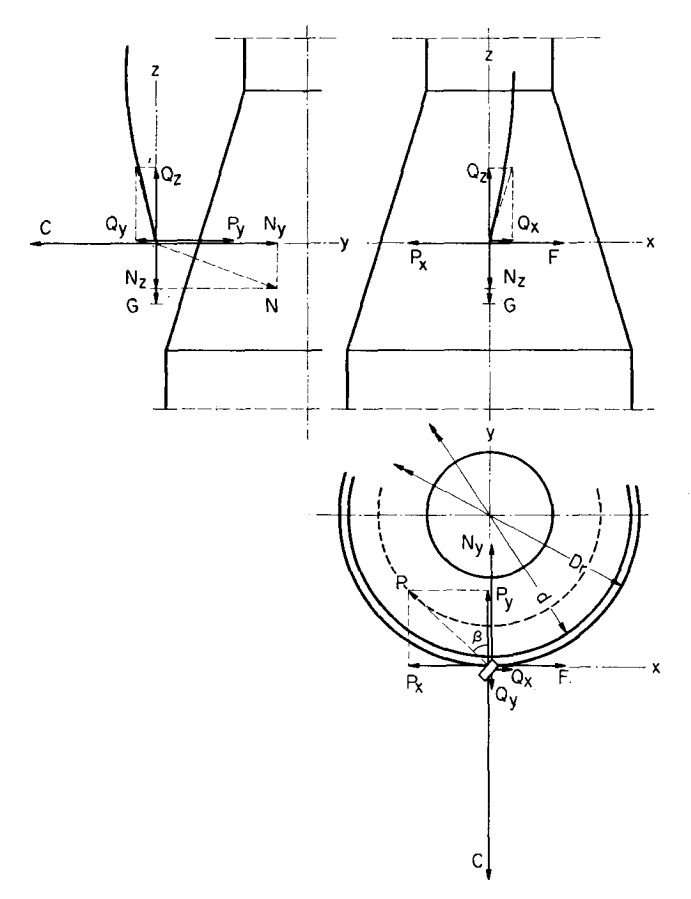


Fig. 49. Forces acting on the traveller.

- The balloon thread tension at its lower end (just before the traveller)  $Q \equiv (Q_x, Q_y, Q_z)$ .
- The winding tension  $P \equiv (P_x, P_y, 0)$ , which is the yarn tension between the traveller and the bobbin  $(P_z \cong 0)$ .
- The centrifugal force C of the traveller in the y-direction.
- The weight G of the traveller in the z-direction.
- The normal reaction between ring and traveller,  $N \equiv (0, N_u, N_z)$ .
- The force of friction F between ring and traveller in the x-direction.

For cop build, all these forces (except G) vary continuously during the spinning process. The variation of the centrifugal force C is slight, due to the small variation of the traveller speed  $n_l$  during one cycle of the periodic movement of the ring rail (assuming constant spindle speed n, i.e. without speed regulation). The thread tensions Q and P just before and after the traveller are maximum at the upper position (u) of the ring rail (fig. 48) and minimum at its lower position (l). On the other hand, the contrary is true for the traveller friction F and the normal reaction N. At the upper position of the ring rail (winding diameter = tube diameter), the thread tension Preaches its maximum value and approaches the radial direction (here the minimum angle of lead  $\beta = 25^{\circ}$  is reached). This minimizes the traveller pressure on the ring and thus N and F reach their minimum values. As a consequence, the instantaneous power consumption due to traveller friction varies during one cycle of the ring rail movement, with a maximum and a minimum at its lower and upper positions respectively. For these positions, the winding diameter  $d_w$  can be written as follows:

> $d_{wu} = \text{mean tube diameter} \cong 0.42 \times \text{ring diameter},$  $d_{wl} = \text{bobbin diameter } d \cong 0.94 \times \text{ring diameter}.$

The variation of the traveller friction over the total time of build of a bobbin was found to be small, as will be seen later on in this chapter.

The balloon thread tension Q at the lower end (just before the traveller) can be calculated accurately for given balloon data, using the spinning balloon equations. The relation between Q and the winding tension P can be written as follows:

$$P = Q e^{\mu_0 \theta}$$

where  $\mu_0$  = the coefficient of friction between yarn and traveller,  $\theta$  = the angle of contact between yarn and traveller.

The values of  $\mu_0$  and  $\theta$  cannot be determined accurately. Apart from some values of P/Q given as a function of the angle of lead  $\beta$  (see fig. 49) by *Honeg-*

ger and Fehr [17], no detailed determination of  $\mu_0$  seems to have been carried out under normal spinning conditions.

The coefficient of friction  $\mu = F/N$  between ring and traveller has been investigated by several authors. In those cases where normal spinning conditions prevailed,  $\mu$  was found to depend on the traveller speed  $v_l$  and the normal reaction N. Thus it varies not only with different spinning conditions, but also with the periodic motion of the ring rail.

Referring to figure 49, we can write:

$$\begin{split} N_y &= C + Q_y - P_y, \\ N_z &= Q_z - G, \\ &= Q_z \quad \text{(neglecting the weight of the traveller $G$),} \\ N &= \sqrt{(C + Q_y - P_y)^2 + Q_z^2} \,. \end{split}$$

Under normal spinning conditions with properly chosen travellers (i.e. for normal shapes of spinning balloons) and at half the time of build of a bobbin, it can be assumed that for a certain angle of lead  $\beta$ , the thread tensions  $(Q_y, P_y)$  and  $(Q_z)$  are proportional to the centrifugal force  $(Q_z)$ . Accordingly, we can write

$$N = \text{constant } G n^2 D'$$

where D' = the diameter of the circle traced by the centre of gravity of the traveller. It was assumed to be proportional to the ring diameter  $D_r$ .

Accordingly, the power  $N_8$  required to overcome the traveller friction for a certain angle of lead  $\beta$  at half the time of build can be written as follows:

$$\begin{split} \boldsymbol{N}_8 &= \mu \, \boldsymbol{N} \, \boldsymbol{v}_l \,, \\ &= \text{constant } \mu \, \boldsymbol{G} \, \boldsymbol{D}_r^2 \, \boldsymbol{n}_l^3 \,. \end{split}$$

The lower values of  $\mu$  correspond to higher traveller speeds  $v_l$  and normal reactions N [14, 18]. Therefore,  $\mu$  varies with G,  $D_r$  and  $n_l$ . Taking this variation into consideration, we can generally write

$$N_8 = C_8 \, G^a \, D_r^b \, n_l^c \tag{37}$$

where  $C_8 = \text{constant}$  for a given angle of lead  $\beta$ , and will be determined experimentally for the two positions (u) and (l) of the ring rail. a, b and c are constants which should be less than 1, 2 and 3 respectively. Their values are determined by experiment.

It should be noticed that the choice of the traveller depends mainly on the yarn count for a given ring diameter  $D_r$ , lift h and spindle speed n. The yarn count is thus taken into account in the above equation by the traveller weight G.

The bobbin density increases with the winding tension. For a given count, ring diameter, lift and spindle speed, higher densities can be achieved by using heavier travellers. It is thus necessary to take the traveller weight G into consideration when estimating the spinning power, as well as the yarn count.

The effect of the balloon control rings on the traveller friction will also be studied in this chapter.

# 2. Description of the apparatus

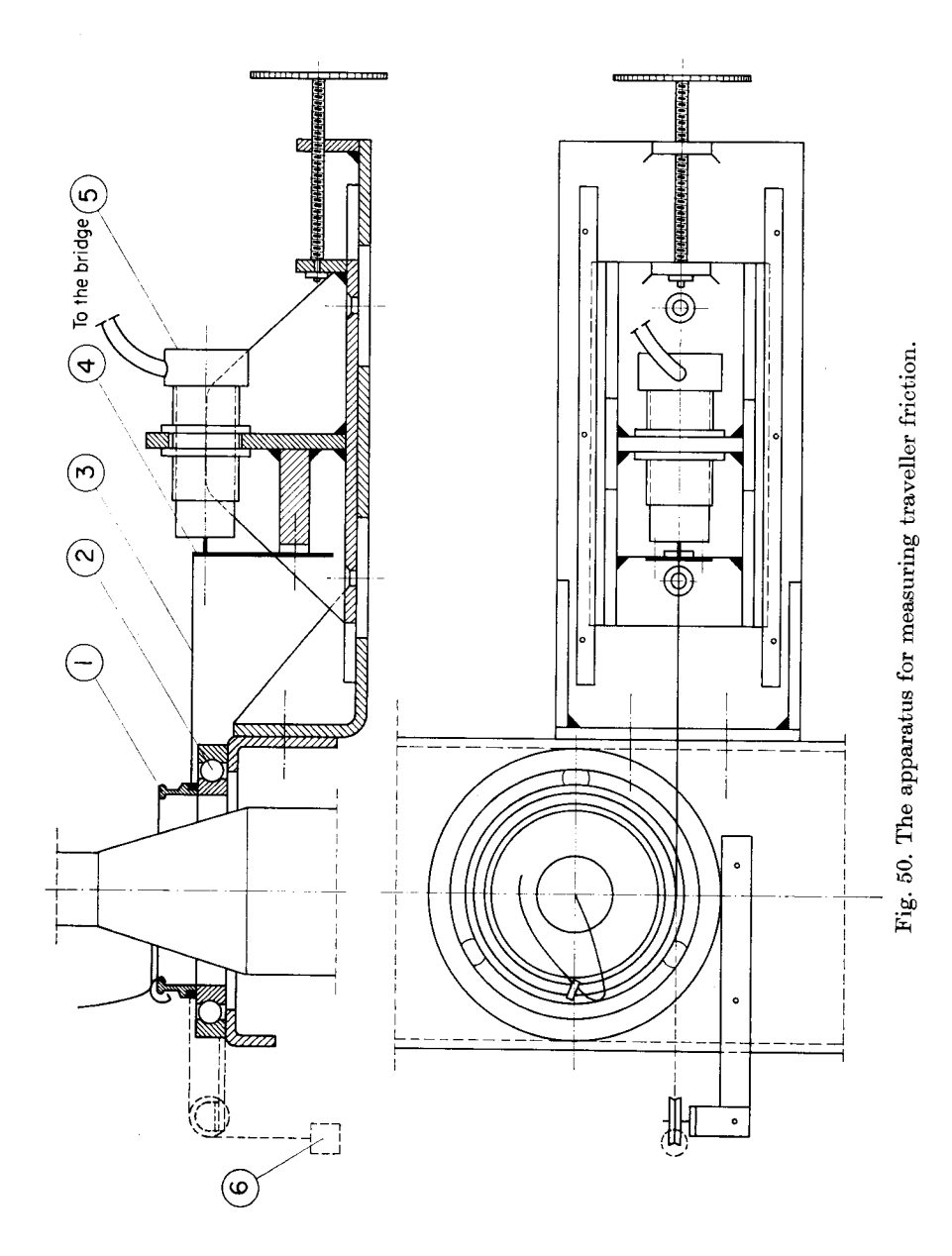
The traveller friction F was measured by an apparatus similar to that used by Honegger and Fehr [17]. However, some modifications were made to measure F electronically instead of with a balance.

Figure 50 shows the assembly of the apparatus diagrammatically. The ring (1) was mounted on the inner race of a special (extra narrow) ball bearing (2). To get sufficiently accurate results, this bearing had to be practically frictionless. This was achieved satisfactorily by unsing only three balls to support the inner race. The traveller friction force was held in equilibrium by a non-extensible flexible thread (3), one end of which was attached tangentially to the ring (1). The other end was fixed to the free end of a cantilever spring (4), whose deflection was picked up by the pin of a Philips inductive displacement pick-up PR 9310 (no. 5, fig. 50), used in connection with a Philips measuring bridge PR 9300. The chief advantages of this pick-up are its high sensitivity and its small mass (about 1 gram). Detailed descriptions of both the pick-up and the measuring bridge, their operating principles and their performance are given in Philips' brochures for these instruments.

As it is not necessary in this work to measure the variations of the traveller friction F of high frequencies (of the order of  $n_l$ ), the built-in meter of the bridge was quite sufficient for measuring the variation of F with the periodic movement of the ring rail.

The hanging weight (6) was used for calibration. The cnatilever spring (4) was made of a strip of spring steel. Its dimensions and method of fixation were made such that no remaining deflection could take place in it after removing a load of 80 grams, i.e. the pointer of the bridge returns back to zero exactly, even when using the most sensitive scale of the bridge (3  $\mu$  scale). The accuracy of the pick-up varies with the pin displacement from its central position with zero deflection of the bridge pointer. It is less than  $\pm 1.5\%$  for displacements up to  $\pm 500 \,\mu$ . The maximum deflection which took place in our tests was about  $100 \,\mu$  and thus an accuracy within 0.3% was achieved.

The special extra narrow ball-bearing (2) had a small moment of inertia



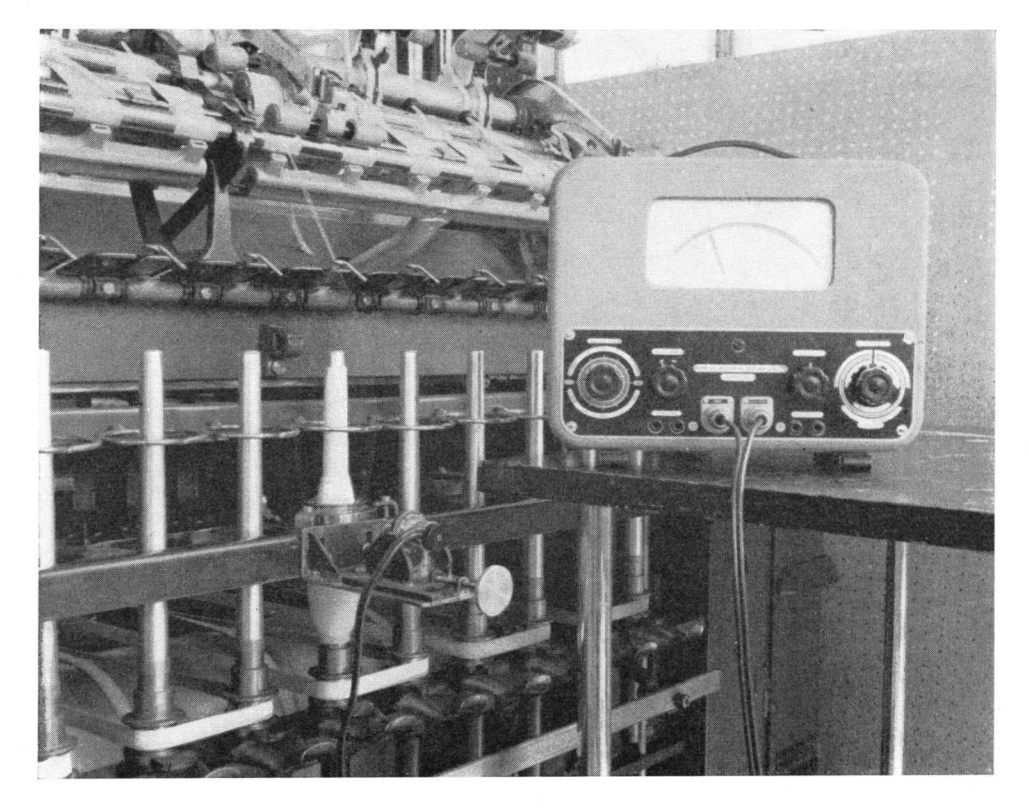


Fig. 50a.

of its inner race and the parts attached to it. However, this moment of inertia had a negligible effect on the accuracy of the measurements because of the very small peripheral displacements (maximum  $0.1~\mathrm{mm}$ ) of the ring and the slow variation of F with the ring rail movement.

Care was taken to keep the ball-bearing in a perfectly clean state during the tests. Various rings of different diameters were tested. Suitable ball bearings and different adjustments of the apparatus were available.

## 3. Experiments and results

Before each test, the instruments were calibrated for all the bridge ranges used. The stability of the calibration was checked and found to be satisfactory. Although the instruments did not exhibit any drift after the warming-up period, which lasted about 30 minutes, to make sure, this was always rechecked during the experiments.

The traveller friction F was measured under normal spinning conditions at half the time of build of a bobbin for the two extreme positions (u) and (l) of the ring rail (fig. 48). These tests covered the following range of conditions:

— yarn counts  $N_e$ : 3 to 80 s (197 to 7.4 tex) (3, 6, 12, 16, 24, 40 and 80 s)

— ring diameters  $D_r$ : 42, 50.8, 56 and 75 mm

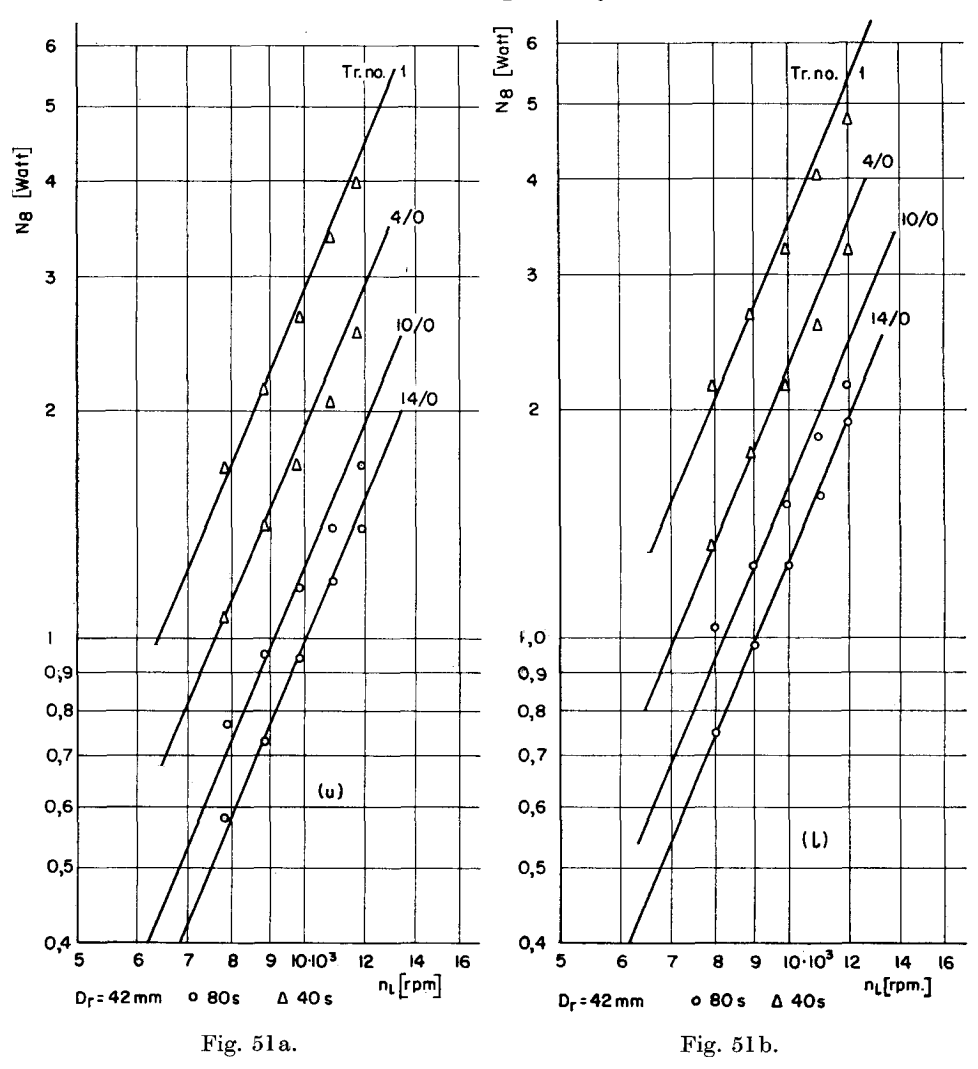
— traveller no. : 14/0 to 65 (G = 15.94 to 920.16 mg)

— spindle speed n: up to 12,000 r. p. m.

— traveller speed  $v_l$ : up to 31 m/s

— lifts  $h:180,\ 220,\ 250$  and 280 mm, according to the ring

diameters respectively.



In all cases, the ratios of the bobbin and tube diameters to the ring diameter were kept as outlined above. The balloon heights were suitably adjusted for every ring diameter and lift. The tests were carried out on two types of frames, manufactured by Messrs. J. J. Rieter & Co., Winterthur (Switzerland), namely model 44 (G 3) with stationary spindle rail and model 46 (G 4) with movable spindle rail. The tests of the 50.8, 56 and 75 mm rings were carried out on frame G 4, with balloon control rings of diameters of about  $1.2 \times$  the ring diameter. The 42 mm ring was tested on frame G 3 with a free balloon. All the rings tested, which had normal flanges (Fl. II), were manufactured by Rieter. They had been used for some years in spinning mills but were still in perfect condition.

The travellers were of the normal spinning C-flat type, made by Messrs. C. Walter Bräcker & Co., Pfäffikon (Zürich).

The spinning material in these tests was middle staple carded American

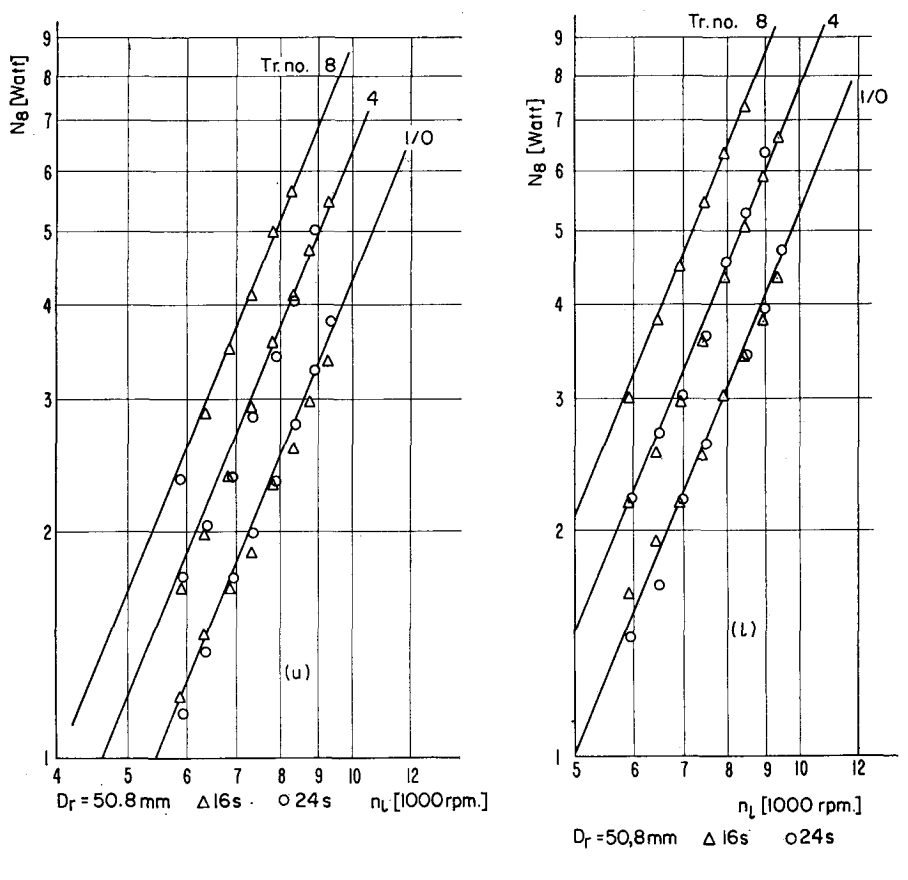


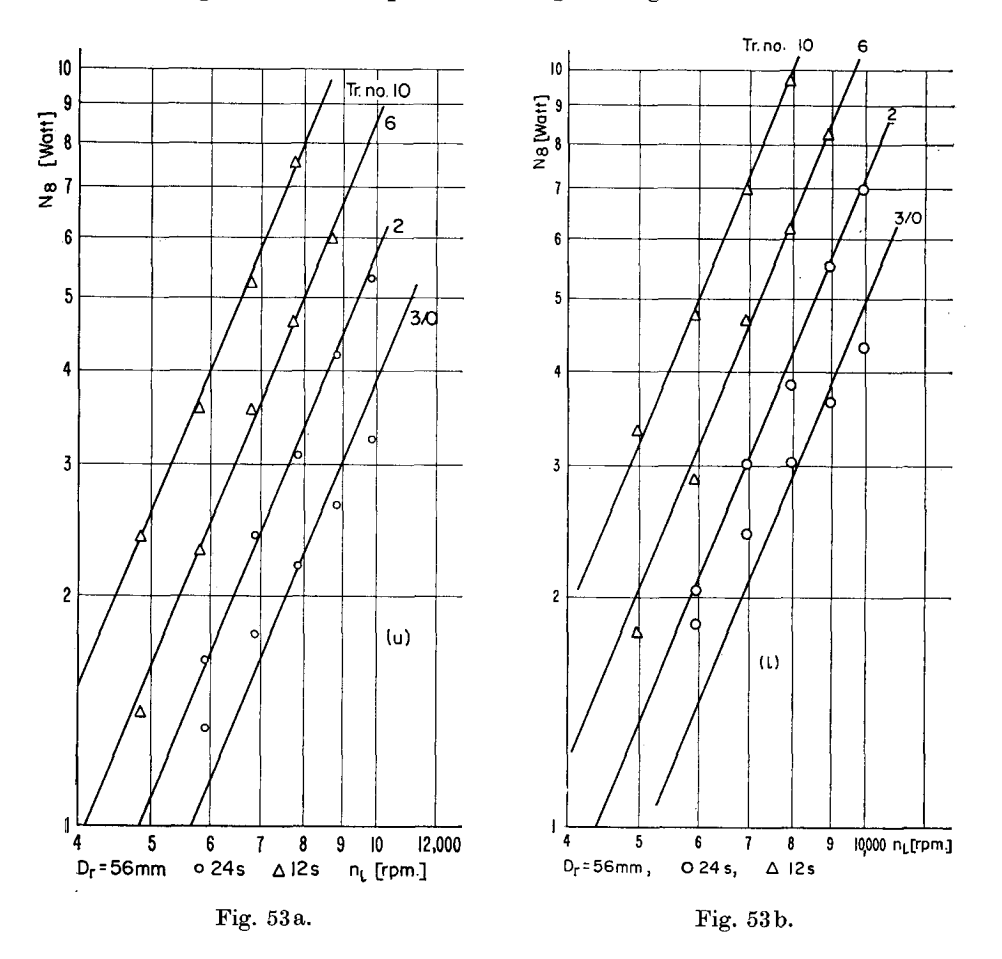
Fig. 52a.

Fig. 52b.

cotton for counts 3, 6, 12, 16, and 24s. For finer counts (40 and 80s), long staple combed Egyptian cotton (Karnac) was used. In each case, a suitable twist was given to the yarn.

Some results of these tests are given in figures 51 to 58. Figures 51 to 54 represent logarithmically the power  $N_8$  in watts absorbed by the traveller friction at both ring rail positions (u) and (l), against the traveller speed  $n_l$  in r. p. m. for different traveller weights and yarn counts. For each count, different traveller sizes were used.

It can be seen from figure 52 that the values of  $N_8$  corresponding to the same traveller weight but to different yarn counts lie on a straight line. This means that, for a given ring diameter  $D_r$ , traveller speed  $n_l$  and balloon height H, the traveller friction F is the same for different yarn counts spun with the same traveller size. This can be explained as follows. The balloon thread tension for a given balloon speed and shape is higher for lower counts. But

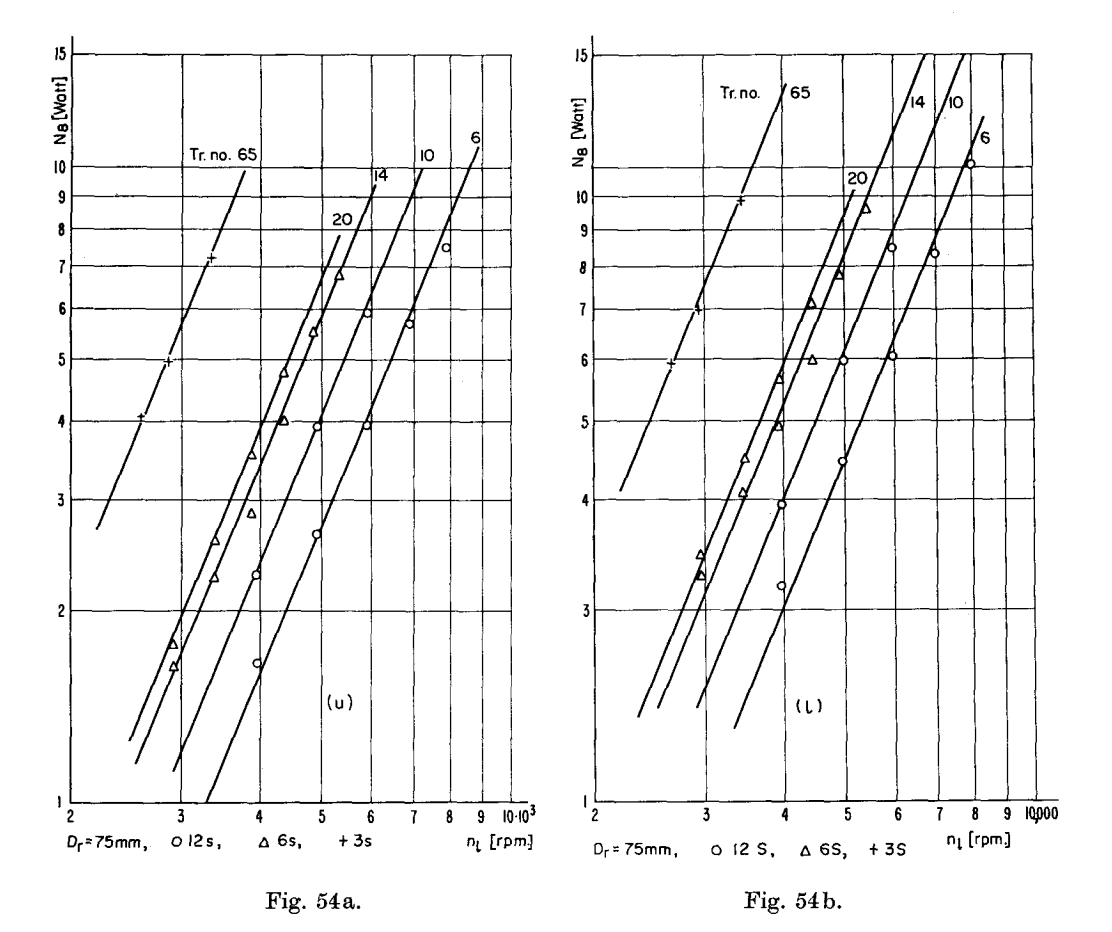


since the maximum balloon diameter is larger for lower counts spun with the same traveller size, the resultant of the thread tensions on the traveller may remain approximately the same in both cases. Accordingly, no variation in F could be measured.

The above discussion is limited to small differences in yarn counts. Naturally, for large differences, it will not be possible to use the same traveller size.

From figures 51 to 54, the value of c in equation (37) was found to be about 2.4 in all cases. The values of  $N_8$  corresponding to an arbitrary traveller speed  $(n_l = 6,000 \text{ and } 10,000 \text{ r.p.m.})$  were found from these figures for different traveller weights G and ring diameters  $D_r$ . These values were plotted logarithmically in figures 55 and 56 against G in mg for the upper and lower positions of the ring rail respectively. These plots yield a value of 0.87 for the constant a in equation (37).

Figure 57 gives the relation between  $N_8$  and  $D_r$ , which was found from



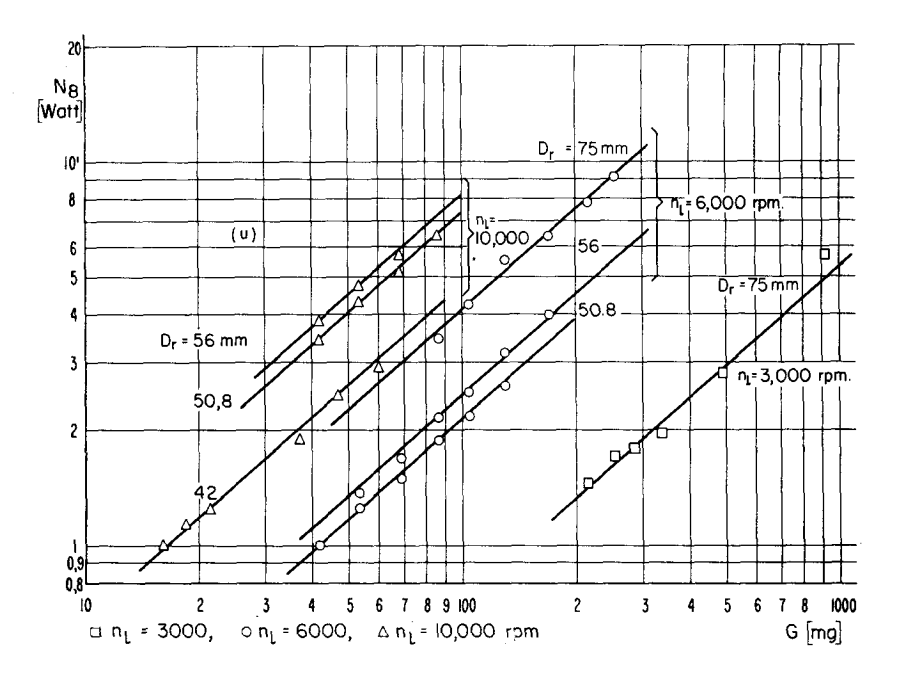


Fig. 55.

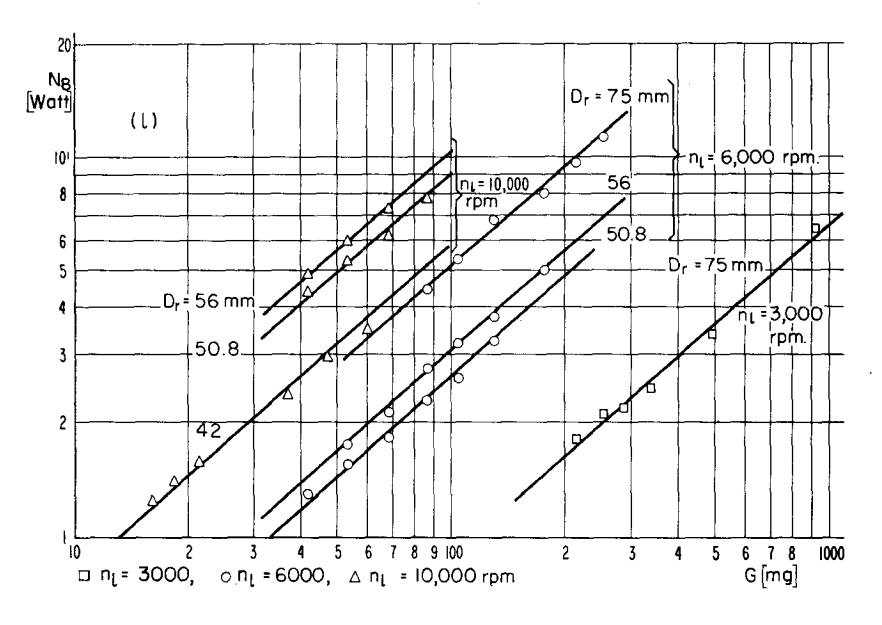


Fig. 56.

figures 55 and 56 for constant traveller speed ( $n_l = 6,000$  and 10,000 r.p.m.) and traveller weight (G = 50 and 100 mg). The power of  $D_r$  in equation (37) was found to be equal to 1.7.

Accordingly, the power  $N_8$  required to overcome the traveller friction is proportional to  $(G^{0.87}D_r^{1.7}n_l^{2.4})$ , which will be denoted by X. Figure 58 gives all the measured values of  $N_8$  in watts versus X, for the positions (u) and (l) of the ring rail (G is in mg,  $D_r$  in cm and  $n_l$  in thousands of r. p. m.). The direct proportionality of  $N_8$  to X can be seen in this figure. Here,  $C_8$  was found to be  $3.3 \cdot 10^{-5}$  for the upper and  $4.05 \cdot 10^{-5}$  for the lower positions of the ring rail. All measured points lie within the range given by  $C_8 \pm 13.5\%$ .

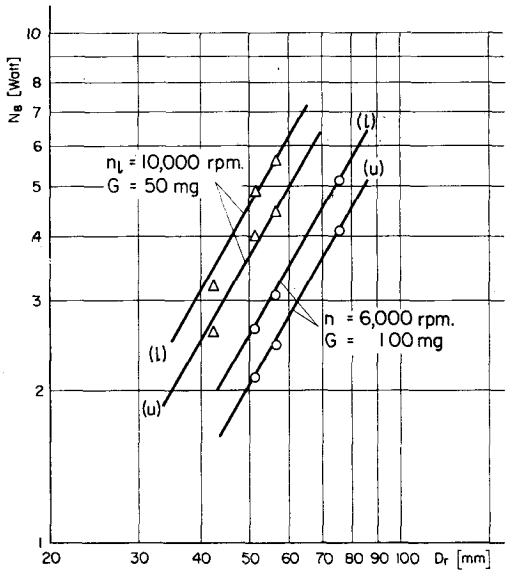


Fig. 57.

For normal spinning rings and travellers, equation (37) can therefore be written as follows:

$$N_8 = C_8 \, G^{0.87} \, D_r^{1.7} \, n_l^{2.4} \tag{38} \label{eq:38}$$

where

 $N_8$  = the power required to overcome the traveller friction in watts per spindle (measured at half the time of build),

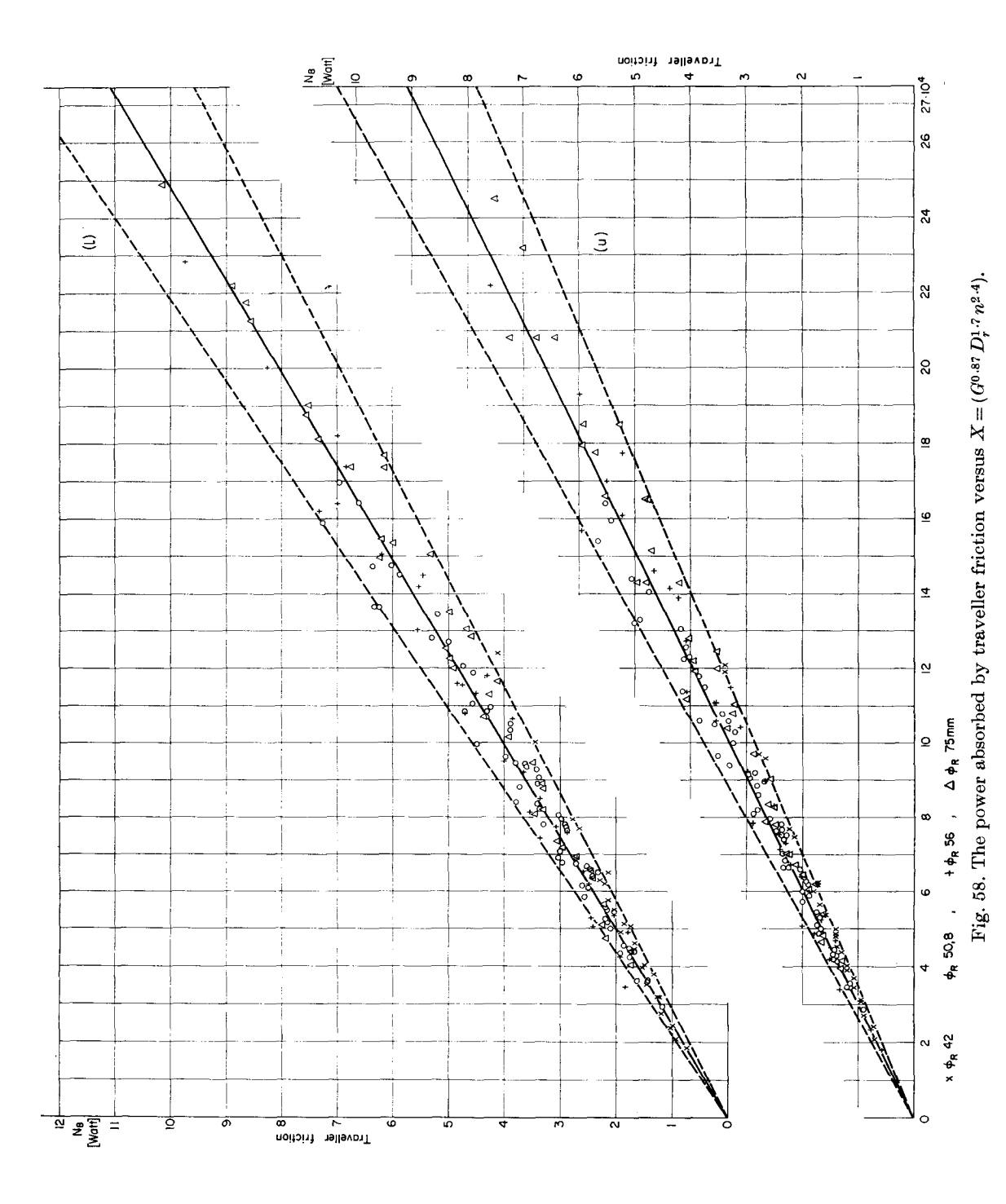
 $C_8 = 3.3 \cdot 10^{-5}$  for the upper position of the ring rail (winding diameter =  $0.42\,D_r$  ), and

=  $4.05 \cdot 10^{-5}$  for the lower position of the ring rail (winding diameter =  $0.94 D_r$ ),

G =traveller weight in mg,

 $D_r$  = internal diameter of ring in cm,

 $n_i$  = traveller speed in thousands of r. p. m.



The power  $N_{8l}$  in kW absorbed by traveller friction can be written for the whole frame as

$$N_{8t} = \frac{3.3}{4.05} z G^{0.87} D_r^{1.7} n_l^{2.4} \cdot 10^{-8}.$$
 (39)

The two constants 3.3 and 4.05 correspond to the two positions (u) and (l) of the ring rail respectively, and z is the number of spindles of the frame.

The effect of the balloon control rings on the traveller friction F will be considered next. F was measured with and without balloon control ring, all the other spinning conditions being unchanged. A maximum increase in F of not more than 6% was observed without the balloon control ring. In most cases, no increase of F could be determined; this holds true especially for the upper position of the ring rail, where the ballooning yarn practically does not touch the control ring. Therefore, it was not necessary to take the two cases of free and controlled balloons into consideration separately.

The traveller friction F was also measured continuously during the total time of build. No appreciable change in the cyclic variation of F with the ring rail movement could be observed after the full bobbin diameter had been reached. This held true for both frames with fixed and movable ring rails. A possible explanation is as follows. The decrease of the balloon height as the build of the bobbin proceeds is always accompanied by a decrease of the maximum balloon diameter  $2\rho'_m$ . Both effects compensate practically each other and thus no change in F could be measured. The variation of  $N_8$  during the total time of build was found to be as sketched in figure 59.

Similar tests were made to measure the traveller friction of a lubricated ring with ear traveller. The ring under test was mounted, with a small oil reservoir, on a special ball bearing as shown in figure 50. The lubricating oil

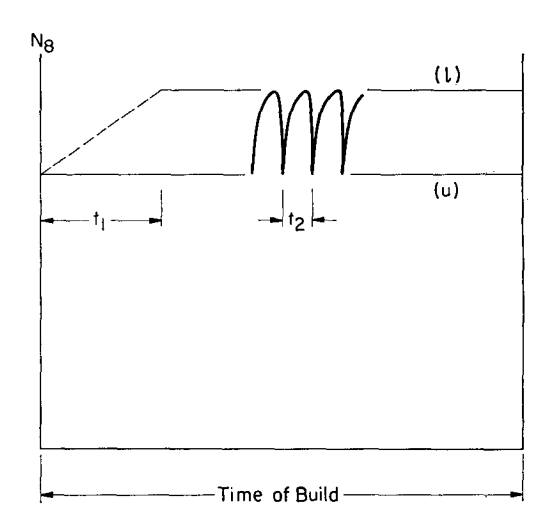


Fig. 59. Variation of the power absorbed by traveller friction during the time of build of a bobbin.

t<sub>1</sub> the time in which the full bobbin diameter is reached,

 $t_2$  the period of the ring rail movement.

used (Durol 262) had a viscosity of 14.7° Engler at 20°C. A Rieter ring of 57 mm diameter and 16.7 mm (21/32") height was tested with round Bräcker ear travellers. This type of ring and traveller is commonly used in worsted spinning. With this traveller form, it is not possible to utilise more than 85% of the ring diameter for the bobbin. The ratios of the bobbin and mean tube diameters to the ring diameter were kept in this case at 0.85 and 0.42 respectively.

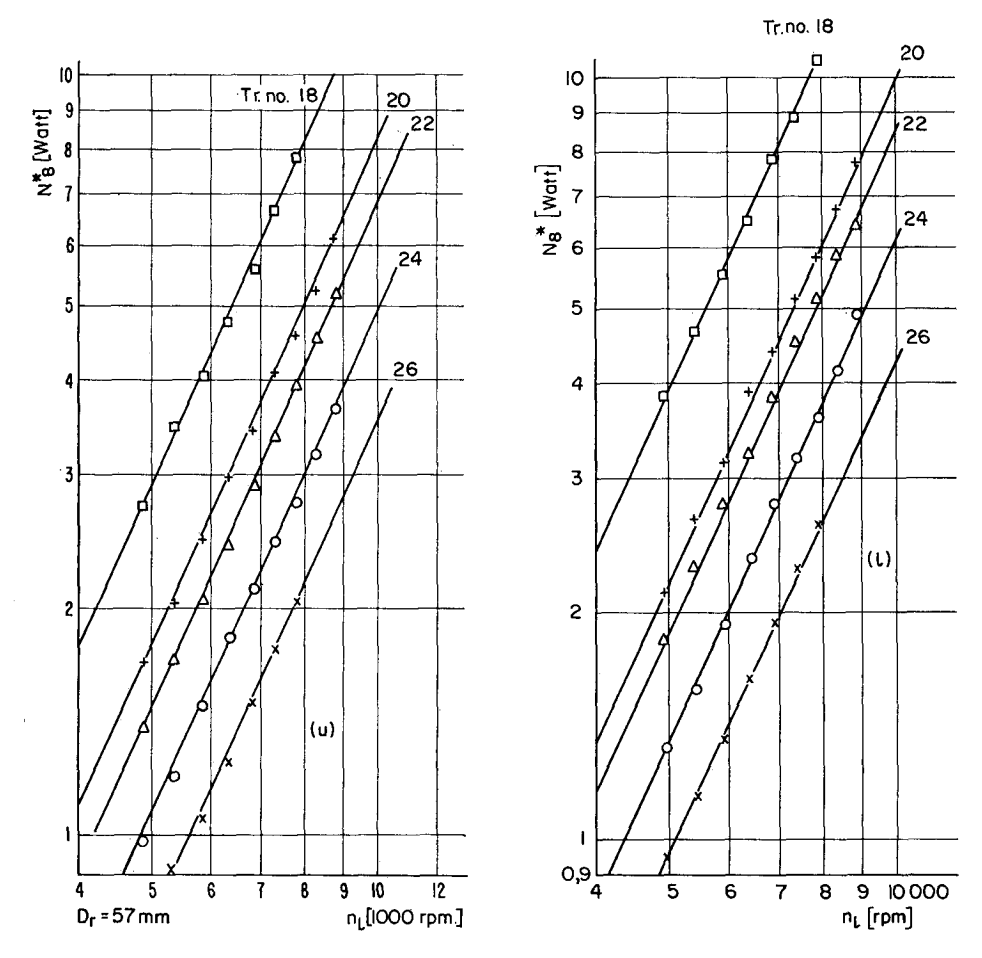


Fig. 60. Results for lubricated ring with ear traveller,  $D_r = 57$  mm.

The results of these tests are given in figures 60 to 62. Figure 60 represents the power  $N_8^*$  absorbed by the traveller friction on the lubricated ring tested versus  $n_l$  for different traveller weights G and yarn counts at both ring rail positions (u) and (l). Figure 61 gives the relation between  $N_8^*$  and G for an

arbitrary traveller speed  $(n_l = 7,000 \text{ r.p.m.})$ . From these figures,  $N_8^*$  was found to increase with  $(n_l)^{2,2}$  and  $(G)^{0.75}$ . The powers of  $n_l$  and G in this case are less than the corresponding values for the non-lubricated normal spinning rings and travellers. Considering the variation of  $N_8^*$  with  $D_r$ , larger ring diameters mean higher traveller speeds  $v_l$  and normal pressures N, i.e. the variation of  $D_r$  has the same nature as that of  $n_l$  and G. It should therefore

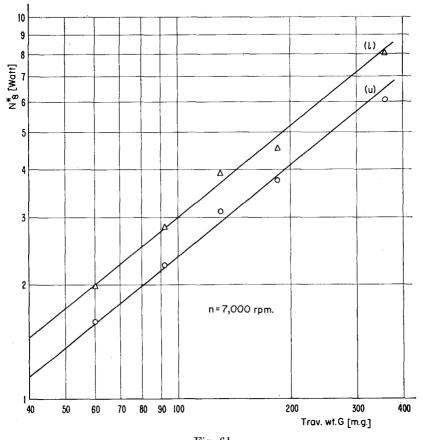


Fig. 61.

be expected here that the power of  $D_r$  will also be less than in the case of non-lubricated rings. Assuming it to be 1.5,  $N_8^*$  will be proportional to  $X^* = (G^{0.75} D_r^{1.5} n_I^{2.2})$ .

Figure 62 gives all the measured values of  $N_8^*$  versus  $X^*$  for both ring rail positions (u) and (l). The values of  $C_8^*$  were found to be  $7.7 \cdot 10^{-5}$  and  $9.8 \cdot 10^{-5}$  for both positions respectively. Thus, we can write

$$N_8^* = C_8^* G^{0.75} D_r^{1.5} n_l^{2.2}$$
 (40)

where  $N_8^*$  = the power in watts required to overcome the traveller friction for lubricated rings (height = 16.7 mm) and ear travellers,

 $C_8^*=7.7\cdot 10^{-5}$  for the upper position of the ring rail (winding diameter = 0.42  $D_r$  ), and

= 9.8  $\cdot$  10<sup>-5</sup> for the lower position of the ring rail (winding diameter = 0.85  $D_r$ ),

G = traveller weight in mg,

 $D_r = \text{ring diameter in cm},$ 

 $n_l$  = traveller speed in thousands of r. p. m.

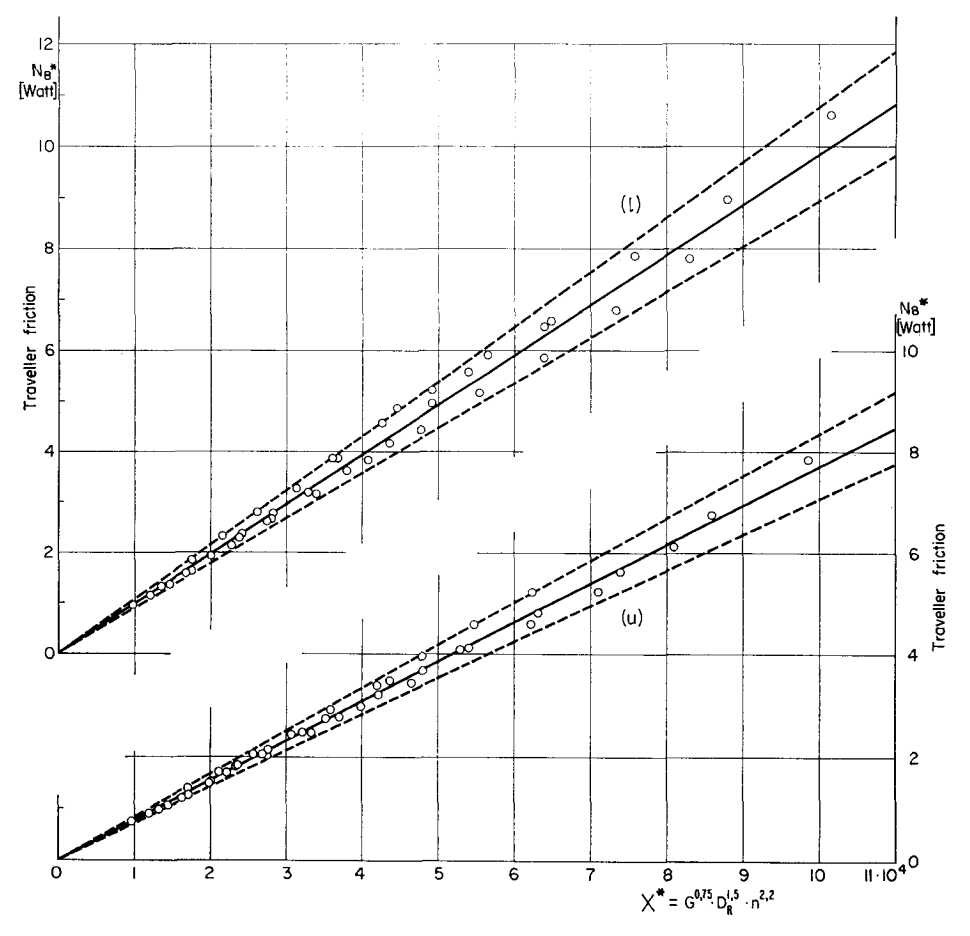


Fig. 62.

For the whole worsted (wool) frame,  $N_{st}^*$  in kW can be written as follows:

$$N_{8t}^* = {7.7 \atop 9.8} z G^{0.75} D_r^{1.5} n_l^{2.2} \cdot 10^{-8}.$$
 (41)

The constant 7.7 corresponds to (u) and 9.8 to (l).

It should be noticed here that equation (41) is only valid for lubricated rings of 16.7 mm height. The traveller friction depends on the area of contact between the ring and the traveller, which is approximately proportional to the height of the ring. This should be taken into consideration when calculating  $N_{8t}^*$  for rings of heights other than 16.7 mm.

The effect of the spinning material on the traveller friction was also studied for the case of lubricated rings. Threads of cotton, wool (worsted) and viscose rayon, all of the same count, were used alternately, all the other test conditions being unchanged. No difference in traveller friction could be observed when using cotton and wool threads, while an increase of about 12—14% was measured in case of rayon filaments. A thin continuous lubricating oil film exists on the ring in all the cases. The lower values of the traveller friction for cotton and wool threads can be explained by a suggestion due to *Honegger* [14]. He postulated that the surface roughness of staple yarns disturbs the traveller motion on the ring, i.e. increases its vibrations of and thus reduces the coefficient of friction between ring and traveller.

As a numerical example for this chapter, the power required to overcome the traveller friction of two frames (cotton and worsted) was calculated using equations (39) and (41). The calculated power and the required data of these frames are given in table 8.

The winding diameters corresponding to (u) and (l) are assumed to be as previously given for each type of frame. The spinning power  $N_s$ , which is approximately equal to  $N_7 + N_8$ , is that power required to drive the spindle against the resisting moment of the winding tension. It varies with the winding diameter, having a maximum at (l) and a minimum at (u). As the traverse velocity of the ring rail decreases for increasing winding diameter, the variation of  $N_s$  with time t will have the form given in figure 63, which can be approximated as a series of half sine curves. The mean value of the spinning power can thus be written as follows:

$$\bar{N}_s = N_{su} + \frac{2}{\pi} (N_{sl} - N_{su}),$$
 (42)

where  $\overline{N}_s$  = the mean spinning power over a cycle of the ring rail movement,  $N_{su}$  and  $N_{sl}$  are the spinning powers  $(N_7 + N_8)$  at (u) and (1) respectively.

<sup>6)</sup> This was also observed by Axson [18].

Table 8

Type of frame		cotton	worsted
Number of spindles $z$		400	400
Ring diameter $D_r$ in mm		56	57
Type of ring		normal	lubricated
••			16.7 mm height
Type of traveller		$C ext{-flat}$	ear-round
Yarn count (metric)		34	28
Traveller weight G in mg		60.59	130
Spindle speed $n$ in r. p. m.	Ī	10,000	8,000
Twist per inch		18.92	10
Traveller speed $n_l$ in r. p. m.	( <i>u</i> )	9,820	7,730
rravener speed nt mr.p.m.	(l)	9,920	7,870
37 1 37% · 1 377	( <i>u</i> )	1.45	1.45
$N_{8t}$ and $N_{8t}^*$ in kW	(l)	1.89	1.91

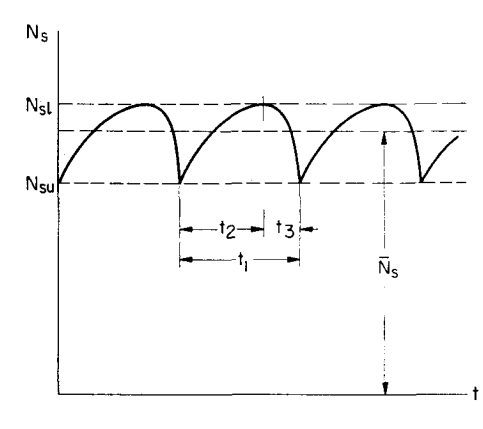


Fig. 63. Variation of the spinning power during one cycle of ring rail movement.

- $t_1$  time of one period of ring rail movement,  $t_2$  time of the downward stroke,
- t<sub>3</sub> time of the upward stroke.

For frames with fixed spindle rails, the spinning power at the beginning and end of the time of build of a bobbin was assumed to be  $\pm 10\%$  of its value at half this time respectively. The corresponding values for frames with movable spindle rails are  $\pm 5\%$ . These assumptions were found to agree with measurements recorded in industry (see chapter 15).

# 12. Power absorbed by the driving head

In this chapter we shall consider the power  $N_9$  absorbed by the driving head with the drafting systems uncoupled. This power is very small and practically independent of the number of spindles of normal frames.  $N_9$  depends

mainly on the speed of the front cylinder  $n_j$  of the drafting systems. This power was measured for three types of frames manufactured by Messrs. J. J. Rieter & Co., Winterthur, namely  $G_3$ ,  $G_4$  (cotton) and  $G_4$  (worsted). The input power of the driving motor was measured at no load and when loaded only by the driving head. The difference between the two readings gives  $N_9$ , neglecting the very small increase of the motor losses due to the small loading.

The tests covered a wide range of front cylinder speeds  $n_f$  (25 to 400 r. p. m.). The results of these tests are given in figure 64. The driving heads of the two

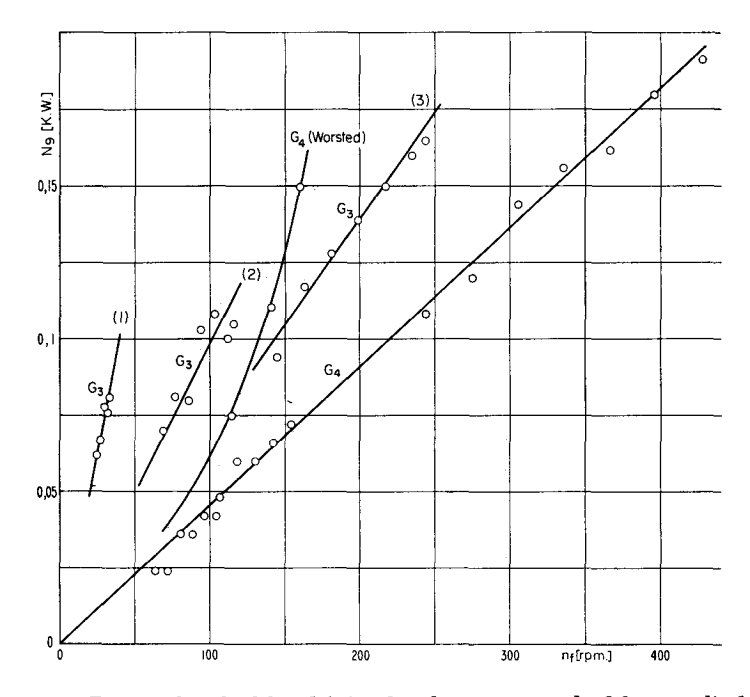


Fig. 64. Power absorbed by driving head versus speed of front cylinder.

cotton frames  $G_3$  and  $G_4$  were tested at different motor speeds. This was repeated with different twist wheels. These gears are in an intermediate position in the gear chain of the driving head of the frame  $G_3$ , while in  $G_4$  they are just after the driving shaft. Accordingly, all the results for  $G_4$  with different yarn twists (different twist wheels) lie on the same curve. For  $G_3$ , the curves (1), (2) and (3) correspond to twists of 50.5, 33.2 and 15.8 per inch respectively (1990, 1310 and 620 per meter).

However, with regard to the relatively small power requirement of the driving head, it can generally be stated that, for practical ranges of  $n_f$  (80 to 220 r.p.m.),  $N_9$  varies from 0.05 to 0.15 kW.

## 13. Power absorbed by drafting systems

#### 1. General considerations

Due to the low speeds of the drafting cylinders, the power absorbed by them is comparatively small. The power  $N_{10}$  required to drive the drafting systems must overcome the following resistances:

- Fibre-fibre friction when drafting,
- bearing friction of the drafting cylinders and of the upper rollers,
- rolling resistance of the upper rollers.
- the increase of gear losses of the driving head when loaded by the drafting systems.

The last one is small and is mainly a function of the others. The drafting force of cotton slivers measured by Wegener [19], was found to be higher for lower drafts and smaller main drafting field distances. Combed slivers show lower values of the drafting force. The drafting force depends also on the fibre length, material, yarn count and roving twist. It may depend on the type of the drafting system.

The bearing friction of the drafting cylinders and of the upper rollers depends on the loading of the upper rollers, which in turn depends on the material, draft and count to be spun.

The rolling resistance of the upper rollers is affected by their material and loading.

Accordingly, the power  $N_{10}$  required to overcome these resistances depends mainly on the speed of delivery  $v_d$ .

#### 2. Experiments and results

The power  $N_{10}$  was measured for several cotton and worsted wool frames in different mills. The output power of the driving motor was measured as will be described in a later chapter. The differences in motor output, when different parts of the ring frame are uncoupled, give the power consumption of each part. That of the drafting systems  $(N_{10})$  in kW is given in table 9 together with other important data.

Figure 65 represents a logarithmic plot of  $N_{10}$  in kW per 400 spindles versus  $v_d$ . The straight lines (1), (2) and (3) correspond to frames for cotton (medium and high counts), cotton (rather low counts) and worsted wool respectively. It is clear that  $N_{10}$  should be higher for heavy frames (for low counts) which have larger gauges and higher normal loads on the upper rollers.

 $N_{10}$  for worsted frames was found to be higher than that for cotton frames. This may be due to the higher drafting force of wool and the higher normal load on the rollers.

The results given in figure 65 can be expressed as follows:

$$N_{10} = C_{10} \cdot v_d^2 \cdot 10^{-3} \tag{43}$$

where  $N_{10}$  = the power required to drive the drafting systems in kW per 400 spindles,

 $v_d$  = the speed of delivery in m/min.,

 $C_{10}=2$ —3.5 for cotton frames (higher values correspond to heavy frames), and

= 4-5 for worsted wool frames (medium size).

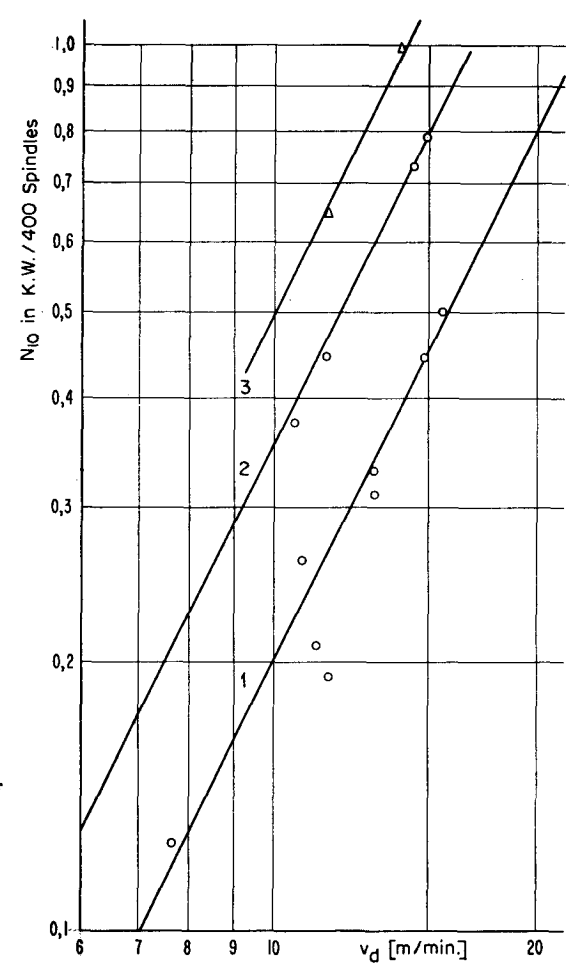


Fig. 65. Power absorbed by drafting systems against the speed of delivery.

- 1 cotton (fine and medium counts).
- 2 cotton (low counts).
- 3 worsted.

Table 9

$N_e$	draft	$v_d \ (\mathrm{m/min.})$	z	$N_{10} \  m (kW)$	$N'_{10} \ ({ m kW/400 \ sp.})$
30	15	11.5	396	0.19	0.192
20	10	13	400	0.33	0.33
40	32	14.8	480	0.53	0.44
16	8.9	15.6	312	0.39	0.5
60	48	11.2	480	0.25	0.21
50	40	7.6	480	0.15	0.125
24	10.3	10.7	360	0.235	0.26
24	19.2	10.6	400	0.375	0.375
14	11.2	14.5	400	0.73	0.73
12	8.6	14.9	304	0.6	0.79
30	18.7	13	416	0.32	0.31
40	25	11.5	448	0.5	0.45
*(52)	11.6	11.8	440	0.71	0.645
*(36)	14.4	14.0	400	1.02	1.02

<sup>\*</sup> Worsted frames, metric counts given in brackets.

## 14. Power absorbed by tin roller bearings and other losses

Up to this chapter, we have considered, all the parts of a conventional frame except the tin roller bearings. This chapter deals not only with the power absorbed by the bearing friction of the tin rollers, but also with all other miscellaneous losses. These losses, such as the power loss due to the tape junctions, are less important and rather more complicated to measure separately. The tape junctions, which have higher bending resistances, cause successive sudden increases in the tape tension when passing over each spindle wharve. The jerks caused by these junctions may increase the spindle power  $N_3$ . They also cause additional vibrations of the pendulum-supported tension rollers.

The power  $N_{11}$  considered in this chapter was determined for full-size frames as follows. The power output of the driving motor was measured (as will be described in the next chapter) for each frame with empty tubes, without balloon and with uncoupled drafting systems, i.e. only the spindles without load were driven. The power absorbed by the spindles, tapes, tension rollers, air friction of tin rollers and driving head was calculated using the equations

given above. This power was subtracted from the measured output power  $N_{\mathbf{0}}$  of the motor to find  $N_{\mathbf{11}}$ .

In the case of movable spindle rails, the tin rollers generally execute the same movement as the spindle rails. Six V-belts with a tension roller are used to transmit the power from the main frame axis (motor axis) to the movable axis of the tin rollers. These belts transmit practically the total power consumption of the frame, except that of the drafting systems and the driving head. The power loss of the V-belts and their tension roller was empirically estimated to be about 6% of the transmitted power at full load. This was also subtracted from the measured power  $N_{\theta}$ .

The power  $N_{11}$  was determined in this way for several frames in different mills. Data and results are given in table 10.

$d_t$ (mm)	$d_w \pmod{(\mathrm{mm})}$	gauge (mm)	$T_m$ (kg)	$L_t$ (m)	Z	$egin{array}{c} n_t \ {f r.p.m.} \end{array}$	N <sub>11</sub> (kW)	$N_{11}/Z$
230	32	82.5	1.42	12.9	8	1,200	0.72	0.09
254	27	70	0.63	16.8	10	1,250	1.1	0.11
254	27	70	0.63	16.8	10	1,210	1.2	0.12
254	27	70	0.62	16.8	10	1,100	1.05	0.10
254	27	65	0.77	13	7	995	0.48	0.07
230	27	65	0.75	13	7	1,180	0.43	0.06
254	32	82.5	0.65	16.5	10	1,130	0.4	0.04
254	42	110	1.36	16.7	11	1,150	0.45	0.04
254	27	75	0.85	16.5	11	910	0.72	0.06
254	32	82.5	0.85	16.5	10	917	0.44	0.04

Table 10

 $T_m$  = the mean tape tension =  $\frac{1}{2}(T_{max} + T_{min})$ , Z = the number of bearings of the tin rollers.

Figure 66 gives the values of  $N_{11}/Z$  in watts per bearing against the speed of tin rollers  $n_t$  plotted logarithmically. From this figure  $N_{11}$  can be expressed as follows:

$$N_{11} = 0.06 \, Z \, n_t^2 \tag{44}$$

where  $N_{11}$  = the power in kW required to overcome the bearing friction of the tin rollers and other losses,

Z = the number of tin roller bearings in the frame,

 $n_t$  = the speed of tin rollers in thousands of r. p. m.

With this chapter, the study of the power requirements of conventional cotton and worsted (wool) ring spinning frames is completed. The results are expressed by the equations for  $N_1$  to  $N_{11}$ .

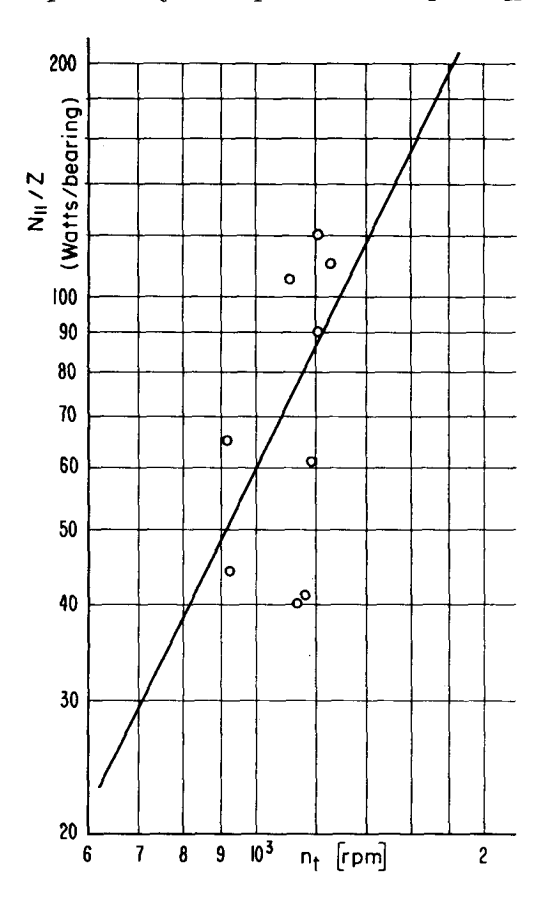


Fig. 66. Power absorbed by tin rollers against their speed.

# 15. Measurements in industry

#### 1. General

To check the agreement of the attained lab results with those of full-size frames in actual production, two types of measurements were carried out in several spinning mills.

In the first type of measurements, the output power of the driving motors was measured under normal spinning conditions during the total time of build (with empty bobbins, different partial fillings, and full bobbins). Different

Table 11

Type of Frame								Cotton	frame	a a								Wor	sted fra	ameg		]	Frames	with s	pecial s	sp. driv	ъ
Type of Frame										· · · · · · · · · · · · · · · · · · ·								WOI	stea ire				Gear	drive		Single	e drive
Frame no.	1	2	3	4	5	6	7	8	9	10	11	12	13	14	15	16	17	18	19	20	21	22	23	24	25	26	27
Year of installation	1957	42	59	58	57	25	14	45	59	25	57	45	45	42	52	59	55	57	55	57	57	56	54	53	53	59	59
Spindle rail	M	M	M	M	M	F	F	M	M	F	M	M	M	M	M	M	M	M	M	M	M	F	F	F	$\boldsymbol{F}$	M	M
Number of spindles z	304	312	480	480	480	400	396	384	480	632	304	384	384	312	400	480	400	440	400	440	440	448	416	360	360	400	400
Gauge $g \text{ (mm)}$	110	82.5	70	70	70	65	65	90	70	65	110	90	90	82.5	82.5	70	82.5	75	82.5	75	75	70	75	75	75	82.5	82.8
Ring diameter $D_r$ (mm)	75	51	45	45	45	45	45	56	45	38	75	56	56	51	51	45	57	51	57	51	51	42	50	48	48	51	51
Lift $h$ (mm)	280	230	215	215	215	210	210	225	215	175	280	225	225	230	250	215	225	215	225	215	215	210	230	210	210	250	250
Spindle speed $n (1000  \text{r.p.m.})$	6.8	8.35	10.94	11.3	9.95	9.0	9.65	10.2	13.6	11.1	3.16	9.35	10.0	9.05	8.8	11.3	7.05	8.25	7.66	7.78	7.97	10.7	10.25	7.37	6.48	8.05	8.05
$\tilde{N}_e$	12	16	40	50	60	20	30	20	44	78	3	20	20	12	24	60	36+	52+	28+	87+	64+	40	30	48+	40+	14	24
Yarn count tex	49.2	36.9	14.8	11.8	9.85	29.5	19.7	29.5	13.4	7.57	197	29.5	29.5	49.2	24.6	9.85	27.8	19.2	35.7	11.5	15.6	14.8	19.7	20.8	25	42.2	24.6
Draft	8.6	8.9	32	40	48	10	15	14.3	35.2	43.3	4.3	14.3	14.3	6.7	19.2	48	14.4	11.6	14	12.4	11.6	25	18.7	14.2	10.3	11.2	19.2
Twist per inch	11.2	13.8	19	38	23	17.6	21.2	18.9	33	31.3	5	18.9	18.9	16.7	21.5	29.8	12.7	17.4	10	16.9	14.7	23.9	19.7	17.2	15.2	13.8	21.8
Speed of delivery $v_d$ (m/min.)	14.9	15.6	14.8	7.6	11.2	13	11.5	13.6	10.6	9.0	14.9	12.6	13.6	14.2	10.6	9.6	14	11.8	19.1	11.7	13.6	11.5	13	10.8	10.7	14.5	9.6
Traveller no. 1	7	6	4/0	9/0	14/0	3	2/0	1	7/0	11/0	64	1	1	8	1/0	12/0	24	26	22	30	28	2/0	3	2	3	6	1/0
Traveller weight $G$ (mg)	116.6	103.7	37.3	23.3	15.9	77.8	47	60.6	27.9	19.8	907.2	60.6	60.6	129.6	53	18.3	92	60	130	29	39	47	77.8	68.4	77.8	103.7	53
Package diameter $d$ (mm)	69	48	40	42	42	42	42	51	42	34	70	51	51	48	47.5	42	45.5	38	46	40	41	39	45	42	42	48	45
Type of drafting systems	d.a.	s.a.	d.a.	d.a.	d.a.	s.a.	s.a.	s.a.	d.a.	d.a.	d.a.	s.a.	s.a.	s.a.	d.a.	d.a.	s.a.	s.a.	s.a.	s.a.	s.a.	d.a.	d.a.	s.a.	s.a.	d.a.	d.a
Balloon height at half the $(u)$	250	200	175	200	200	180	180	200	175	140	250	200	200	200	220	175	215	190	215	190	190	165	165	160	160	220	220
time of build $H$ (mm) $(l)$	315	245	225	255	255	210	210	250	225	170	315	250	250	245	270	225	265	230	265	230	230	215	215	195	195	270	270
Diameter of balloon control rings	60							0.5			60	0.5			00		0.5	20	0.~	60	0.0					60	60
(mm)	87	-	50	50	50	_		65	50	_	87	65	65	—	60	50	65	60	65	60	60	-		_		60	60
$\int d_w$	42	32	27	27	27	27	27	32	27	25	42	32	32	32	32	27	32	27	32	27	27	_				28	28
Dui	30	24	22	22	22	22	22	24	22	18.5	30	24	24	24	24	22	24	22	24	22	22	22	22	22	22	23.5	23.4
Spindle dimensions <sup>2</sup> (mm) $\{d_b\}$	12	8.8	7.8	8.8	8.8	8.8	8.8	8.8	7.8	7.8	12	8.8	8.8	8.8	8.8	7.8	8.8	8.8	8.8	8.8	8.8	7.8	7.8	7.8	7.8	8.8	8.8
B	300	250	230	230	230	230	230	250	230	190	300	250	250	250	250	230	210	220	210	220	220	230	250	230	230	260	260
igl( L	370	310	295	290	290	290	290	310	295	250	370	310	310	310	310	295	270	280	270	280	280	280	300	280	280	370	370
( material	C	C	C	C	C	C	C	N	C	N	C	N	C	C	N	C	C	C	C	C	C	_		_ '		N	N
width $w  (\text{mm})$	16	12	12	12	12	12	12	11	12	11	16	11	12	12	13	12	12	12	12	12	12	<u> </u>	_		_	6.5	6.5
Tapes $\begin{cases} thickness & t \text{ (mm)} \end{cases}$	1.2	1.2	1.2	1.2	1.2	1.2	1.2	0.6	1.2	0.6	1.2	0.6	1.2	1.2	0.6	1.2	1.2	1.2	1.2	1.2	1.2		_			0.6	0.6
min. tension (kg)	1.1	1.25	0.5	0.5	0.5	0.63	0.63	1.2	0.5	0.5	1.1	1.2	1.2	1.25	0.5	0.5	0.75	0.75	0.75	0.75	0.75				_	0.75	0.7
Diameter of tin tollers $d_t$ (mm)	254	230	254	254	254	254	230	230	254	230	254	230	230	230	254	254	254	254	254	254	254			_		70×	70×
No. of tin roller bearings	11	8	10	10	10	7	7	10	10	12	11	10	10	8	10	10	10	11	10	11	11		_				
Time of build (h)	8	4	$7\frac{1}{2}$	$18\frac{1}{2}$	$13\frac{1}{2}$	$5\frac{1}{2}$	7	$6\frac{1}{2}$	13	11	13/4	7	$6\frac{1}{2}$	$4\frac{1}{2}$	8	17	4	6	$3\frac{1}{3}$	$9\frac{1}{4}$	7	$8\frac{1}{2}$	$9\frac{1}{4}$	7	$5\frac{3}{4}$	$3\frac{1}{2}$	83
	<u> </u>		.1	1		I	<u>I.</u>	1	1	1	1	1	,   T	Ring he	ight (m	m)	16.7	10.3	16.7	10.3	10.3		<u> </u>		<u> </u>		,

<sup>&</sup>lt;sup>1</sup> C-flat spinning travellers for cotton frames except frames no. 22 to 25. Eleptical (Rieter-Bräcker) travellers for frames no. 22 and 23.

N.B. All measurements in industry were carried out in 1960 and part of 1961.

C-round travellers for frames no. 24 and 25.

Ear-travellers for worsted frames.

<sup>&</sup>lt;sup>2</sup> See figure 17.

<sup>+</sup> Metric counts.

<sup>×</sup>Diameter of driving pulleys.

M movable spindle rails. F fixed spindle rails.

d. a. double apron drafting systems.
s. a. single apron drafting systems.
C cotton tapes.
N nylon tapes.

<sup>(</sup>u) upper position of the ring rail.
(l) lower position of the ring rail.

parts of the frame were then uncoupled in turn and the power differences were noticed. This type of measurements was used to check the agreement of the spinning power  $N_s$  and the package power  $N_p$  calculated with the help of equations (23), (24), (36), (39) and (41), with those measured in industry. It was also used to find  $N_{10}$  and  $N_{11}$  (see chapter 13 and 14).

Another type of measurements was carried out to record the output power of the driving motors during the total time of build. This was used to compare the total power calculated by the formulas for  $N_1$  to  $N_{11}$  with that measured for full-size frames under normal mill conditions.

### 2. Experiments and results

Most of the frames tested were driven by variable speed commutator motors. The input power  $N_i$  of the motors, the primary current  $I_1$  and the terminal voltage V (from which the power factor  $\cos\varphi$  was found) were measured by a Gossen power measuring head. The secondary current  $I_2$  (stator current) was directly measured by an ammeter. The spindle speed n was kept constant during each test. The motor speed could be exactly adjusted by varying the angle of the motor brushes, which was also recorded. The motor efficiencies at partial loads were supplied by the manufacturing company, Messrs. Brown-Boveri & Co., Baden.

Some of the frames were driven by squirrel cage induction motors, in which cases the motor speed was not exactly constant owing to the variation of the motor slip with the load. These speed variations are however very small.

The measurements were carried out for the following range of frames conditions:

Ring diameter  $D_r$ : 38 to 75 mm Lift h: 175 to 280 mm

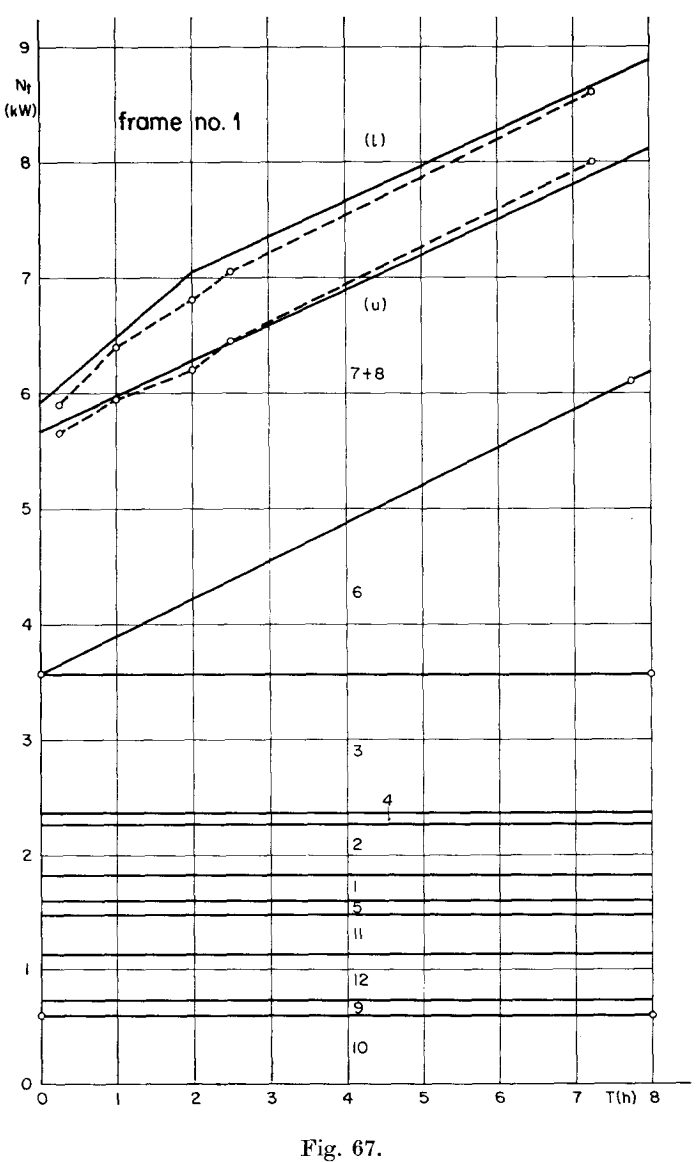
Yarn count  $N_e$ : 3 to 78s (tex 197 to 7.66)

Traveller weight G: 15.9 to 907.2 mg (no. 14/0 to 64)

Spindle speed n: 3,160 to 13,600 r. p. m.

The frames tested were mainly of the conventional cotton type with spindles driven by cotton or nylon tapes. Worsted frames with lubricated rings and ear travellers were also tested.

The specifications of the frames tested are given in table 11 and the results are illustrated by figures 67 to 79 and table 12. Figures 67 to 75, which relate to the first type of the measurements, show the variation of the total power consumption  $N_t$  (motor output) during the build of a bobbin and at spindle speeds as given in table 11 for each frame. The dotted lines join the measured



# Key to figs. 67 to 79, 84 and 90:

- 1 Power absorbed by air friction of tapes  $N_1$ .
- 2 Power required to overcome the bending resistance of tapes  $N_2$ .
- 3 Spindle power  $N_3$ .
- 4 Power absorbed by tension rollers  $N_4$ .

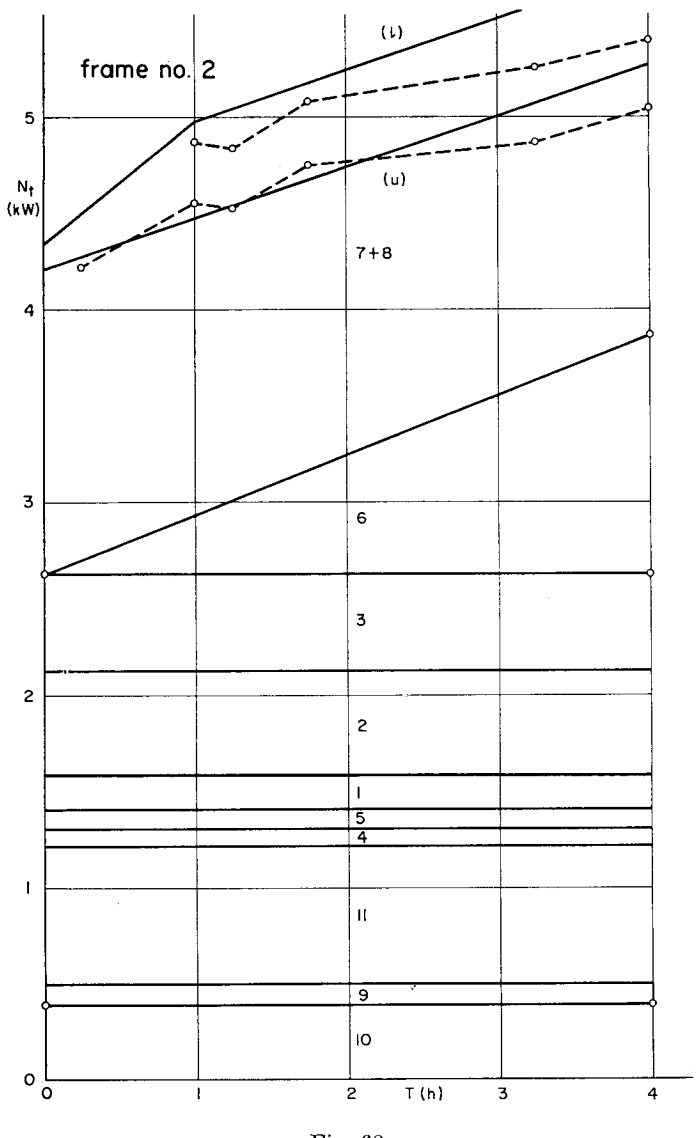
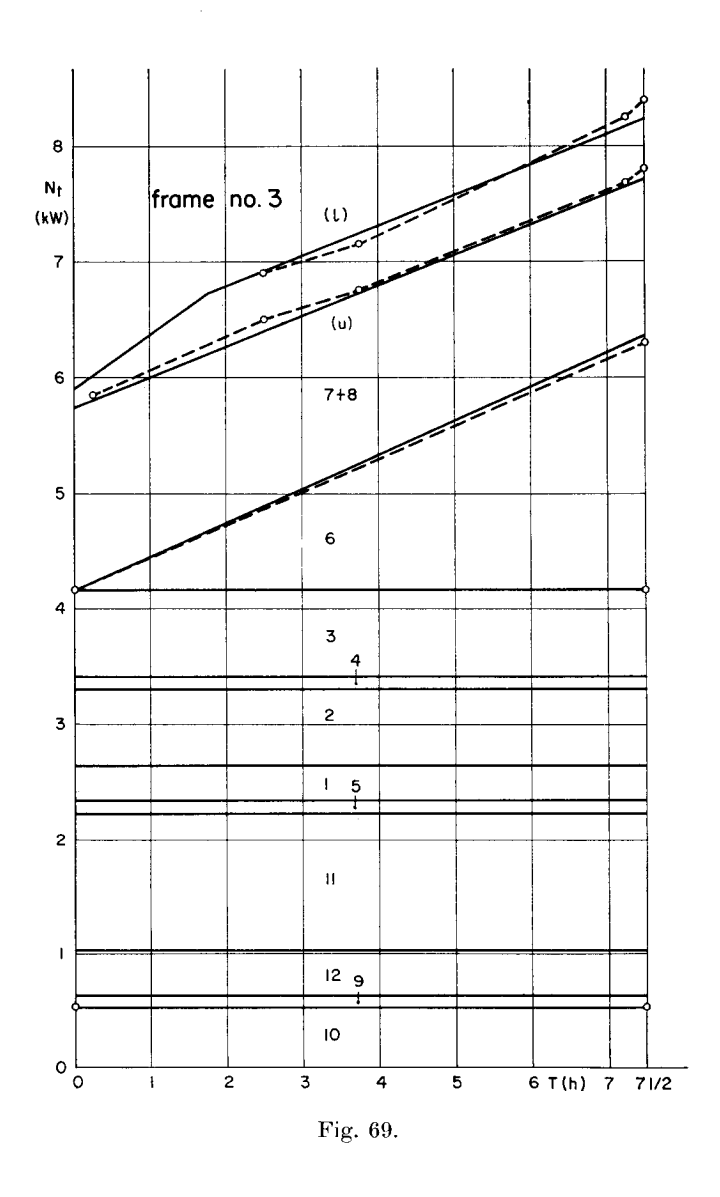
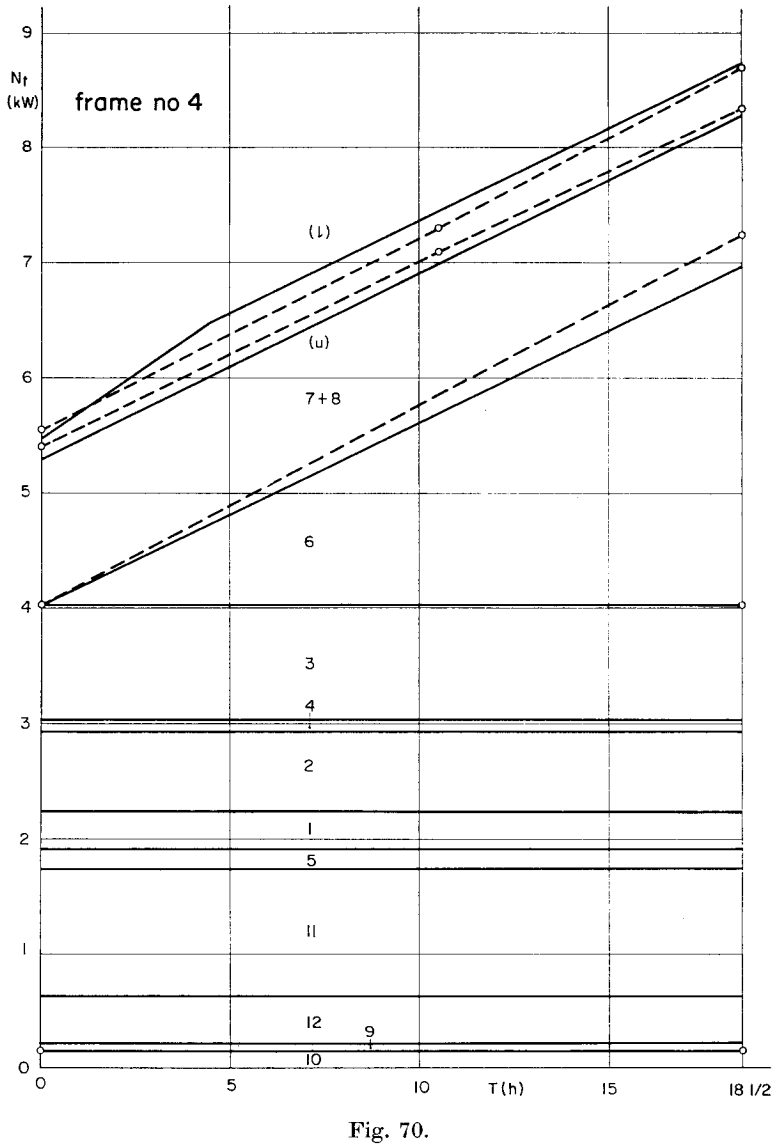


Fig. 68.

- 5 Power absorbed by air resistance of tin rollers  $N_5$ .
- 6 Package power  $N_6$ .
- 7 Power absorbed by air resistance of the spinning balloon  $N_7$ .
- 8 Power absorbed by traveller friction  $N_8$ .
- 9 Power absorbed by the driving head  $N_9$ .
- 10 Power absorbed by drafting systems  $N_{10}$ .



- 11 Power absorbed by tin roller bearings and other losses  $N_{11}$ .
- 12 Power absorbed by V-belts in the case of movable spindle rails  $N_{12}$ .
- 10 and 9 the ancillary power (drafting systems and driving head), constant.
- 11, 5, 1, 2, 4 and 3 the secondary power (tin rollers, tapes, tension rollers and spindles). approx. constant.
- 6, 7 and 8 the primary power (package, balloon and traveller), varying during spinning,



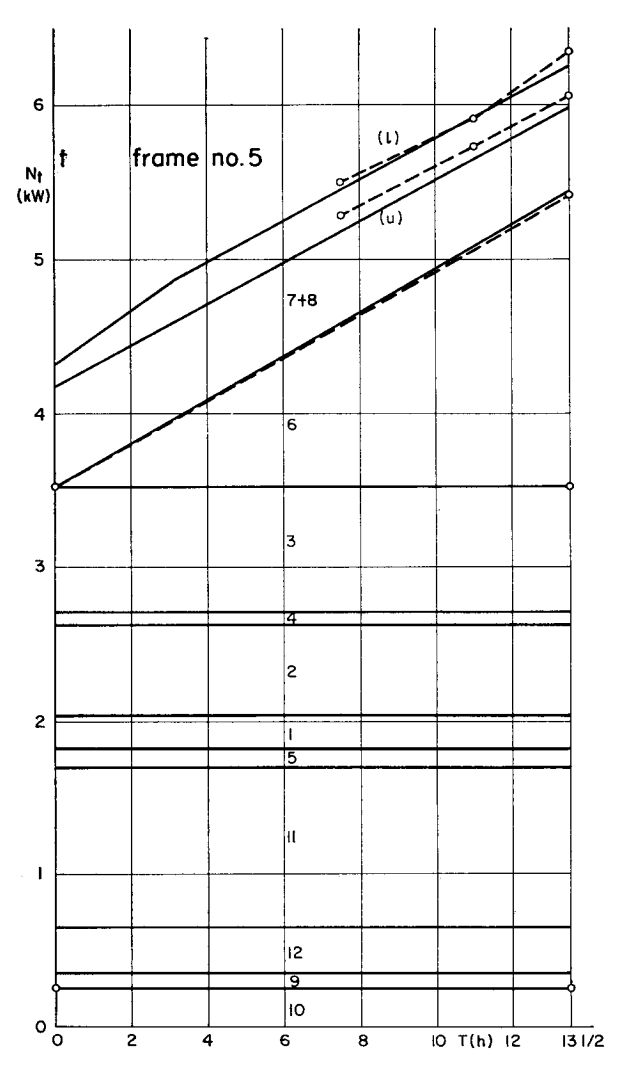


Fig. 71.

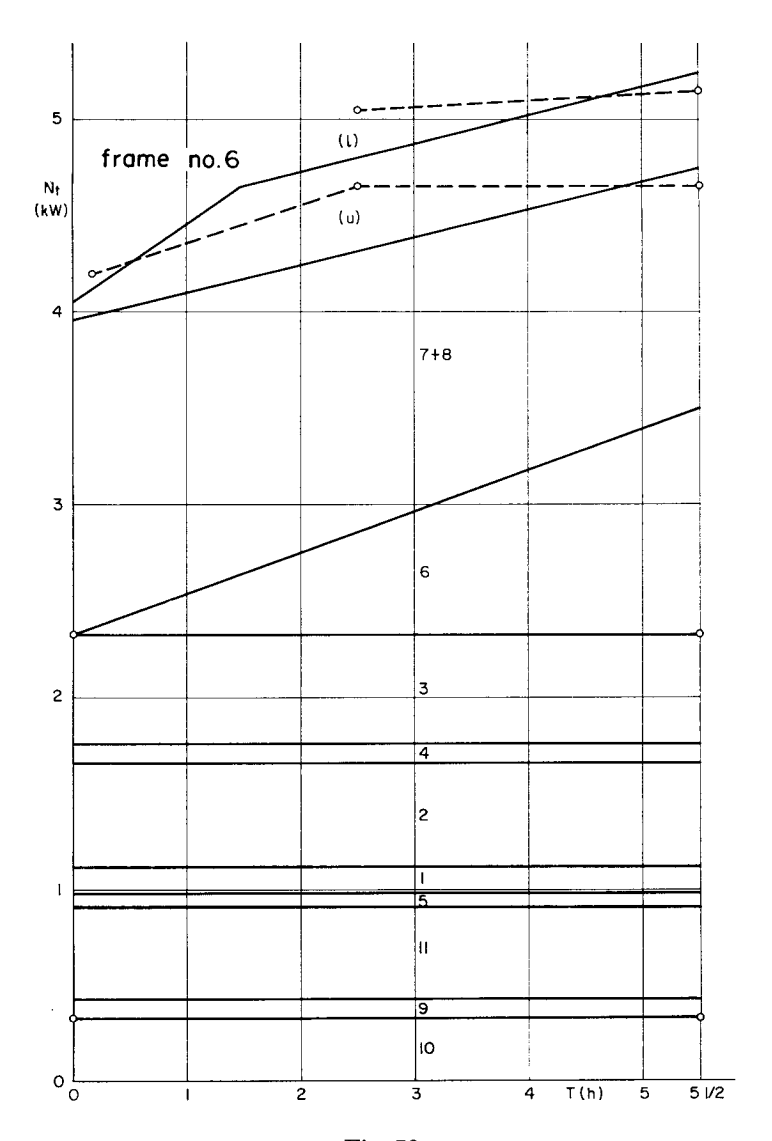


Fig. 72.

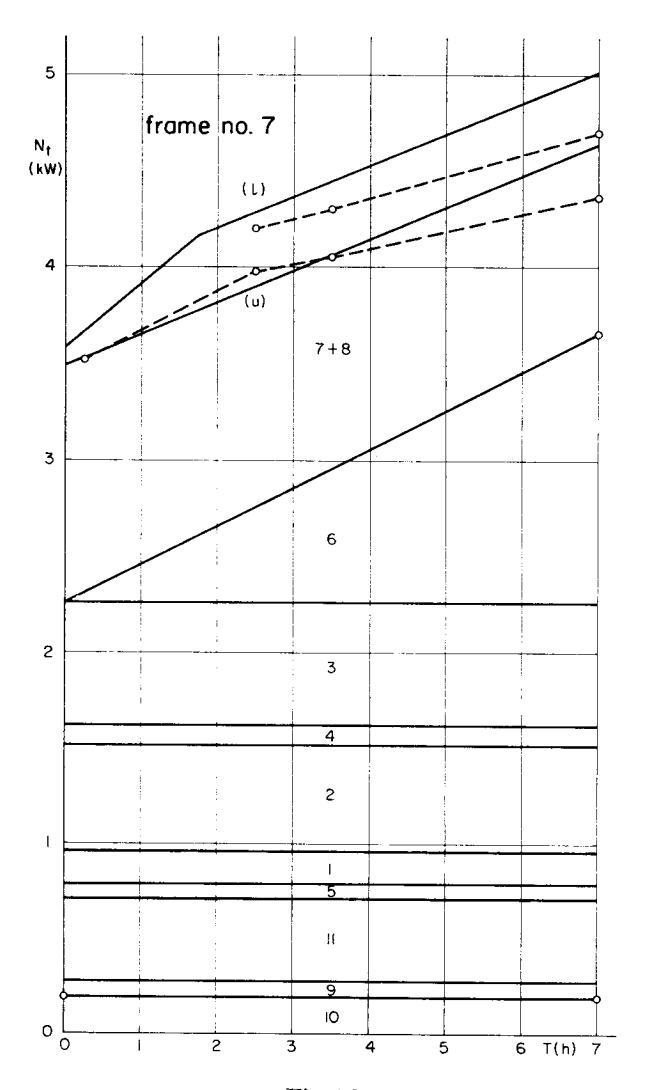


Fig. 73.

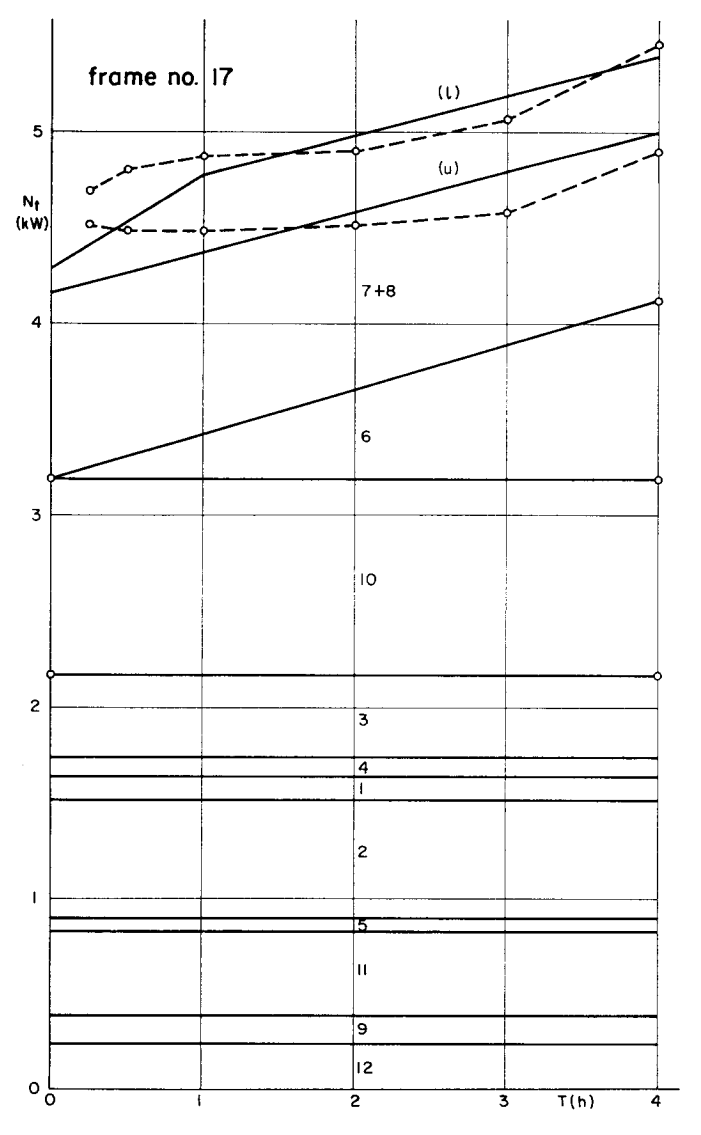


Fig. 74.

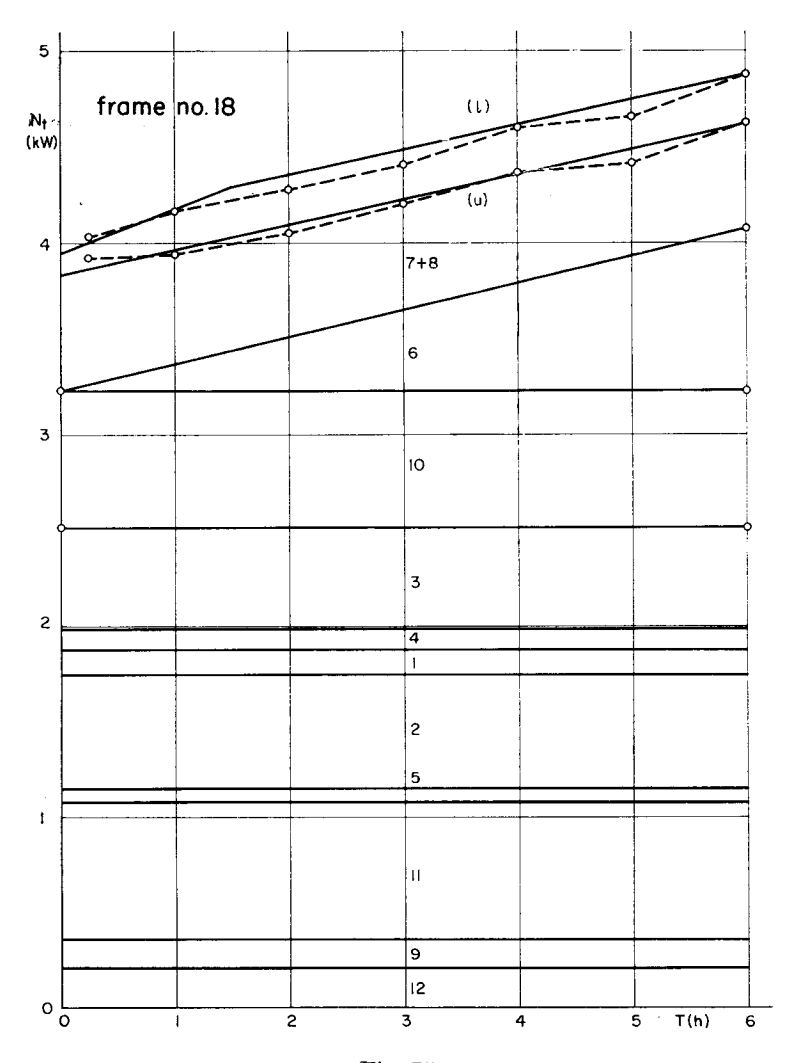


Fig. 75.

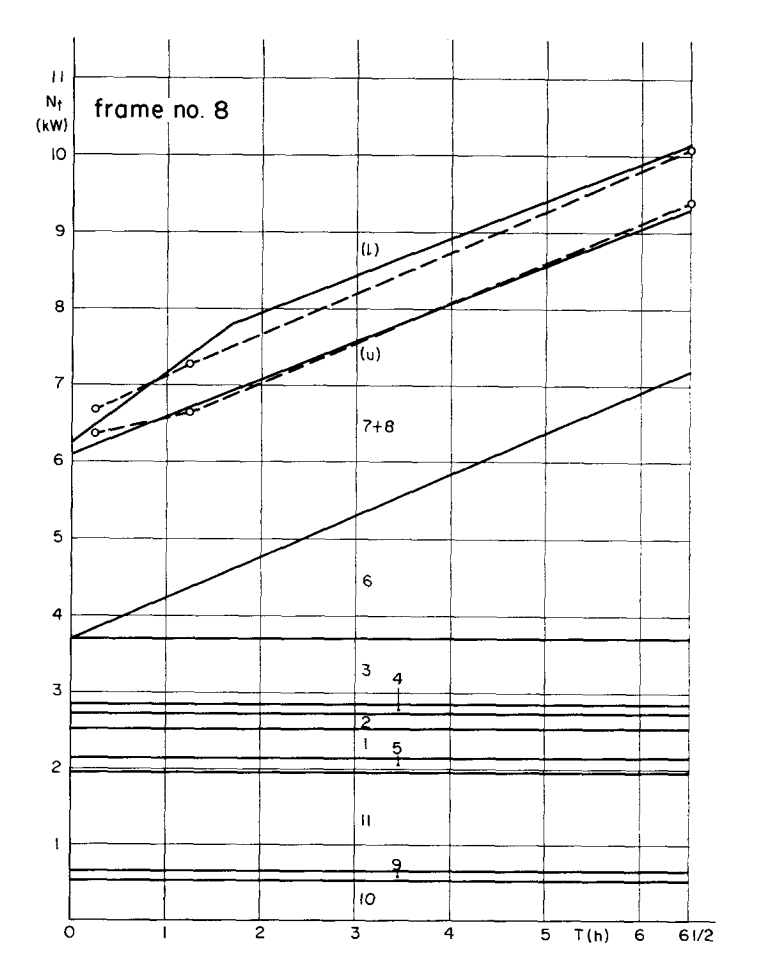


Fig. 76.

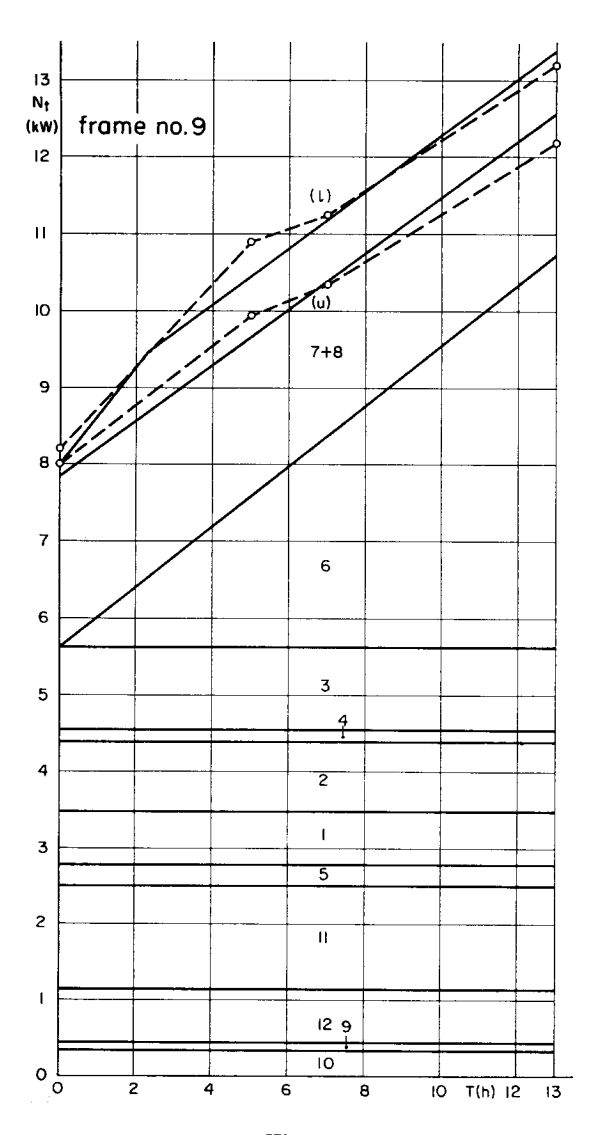
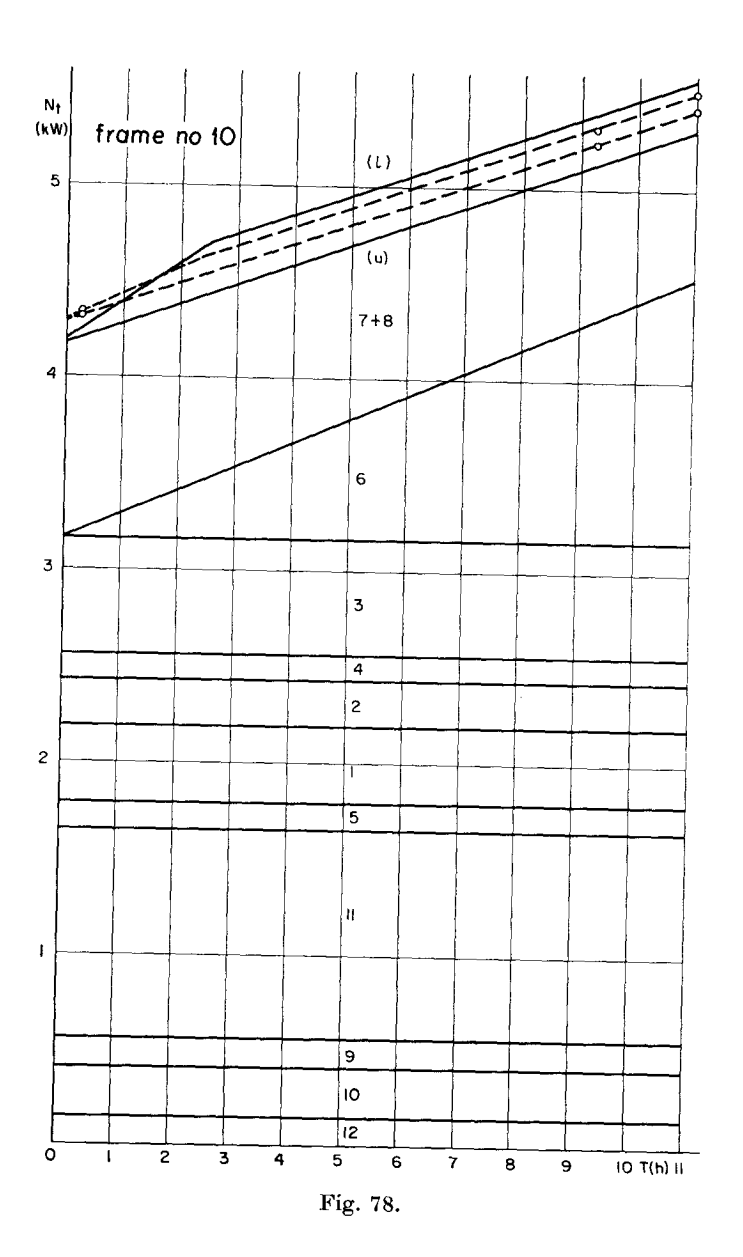
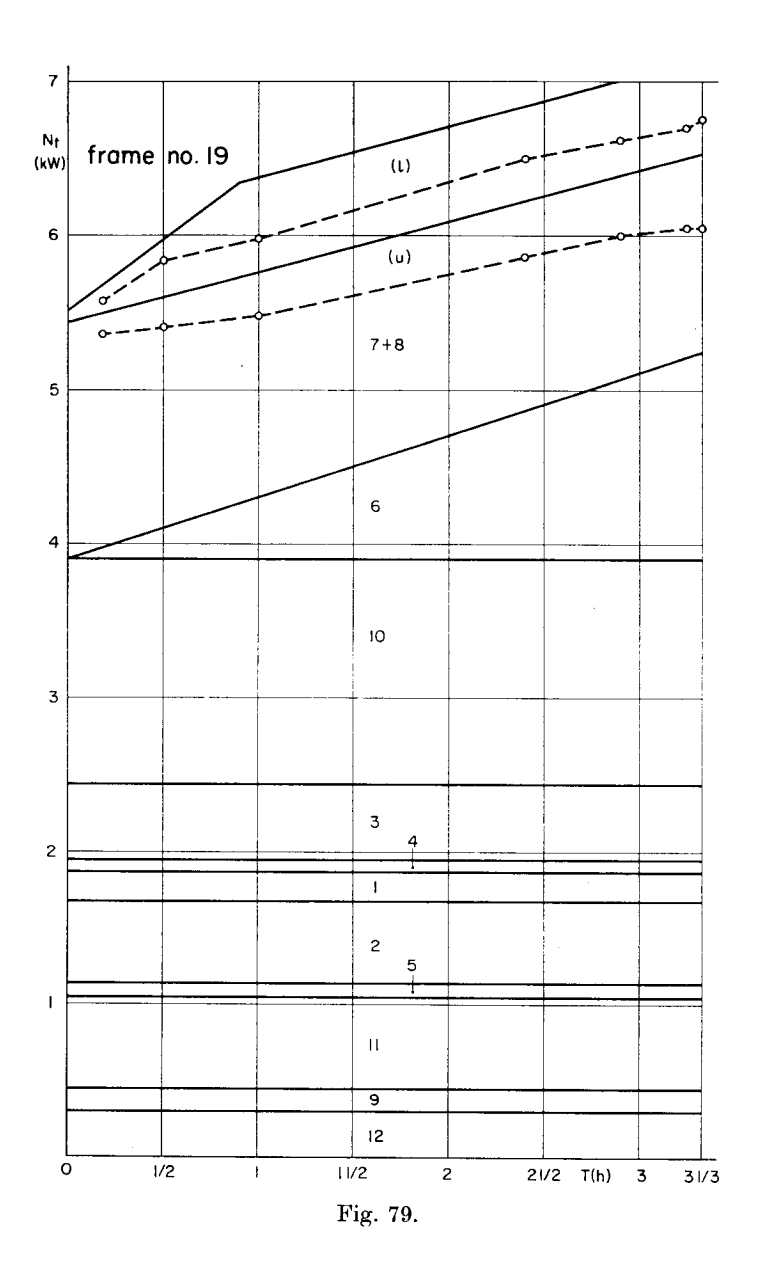


Fig. 77.





points, whereas the full lines give the calculated values obtained by the formulas derived in the preceding chapters. In all cases, good agreement of the calculated values for the spinning power  $N_s$  (approx. due to traveller friction + balloon air drag) and the package power  $N_p$  with those measured on full-size frames can be observed.  $N_{10}$  and  $N_{11}$  were determined from these figures (see chapter 13 and 14).

It should be noticed here that the secondary power (see fig. 1) — i.e. the power absorbed by the spindle bearings, tension rollers, tapes and tin rollers — was assumed to be constant during the time of build. Actually, it increases as the primary power increases. The increase is, however, very small and was considered to be a part of the primary power.

Figures 76 to 79 illustrate some results of the second series of the tests, in which the total power consumption  $N_t$  was measured.  $N_t$  was also calculated by the formulas for  $N_1$  to  $N_{11}$ . The calculated values are given in full lines. A satisfactory agreement between measured and calculated values of  $N_t$  can be seen.

Further results are given in table 12.

Frame	no. *)	11	12	13	14	15	16	20	21
N <sub>t</sub> **) (kW)	begin end	$\frac{3.7}{3.9}$	$5.4 \\ 8.2$	7.3 10.1	7.3 9.2	4.6 6.3	7.2 10.1	3.35 3.95	3.8 4.55

Table 12

# 16. Approximate estimation of the power consumption

In the prior chapters, the power analyses were studied separately and the results were expressed in several formulas. When these formulas are used to calculate the total power consumption, detailed knowledge of the frame specifications is necessary. Moreover, it takes time to apply these formulas.

In this chapter, an approximate but very swift method to estimate the power consumption is described. The total power  $N_t$  is divided into three main parts (see fig. 1):

- Spinning power  $N_{st}$ ,
- Package power  $N_{pt}$ ,
- No load power  $N_{nt}$ , which is the sum of the secondary and the ancillary powers.

<sup>\*)</sup> The specifications of these frames are given in table 12 under the corresponding frame number.

<sup>\*\*)</sup> The values of  $N_t$  are mean values over one cycle of the ring rail movement (see p. 80).

The major part of the spinning power is absorbed by the traveller friction. The balloon air drag was found to be, in all the cases considered, from 5 to 12% of the traveller friction at the upper position of the ring rail and from 10 to 25% at its lower one. Higher percentages correspond to finer counts. Assuming the air drag to be 8% and 18% of the traveller friction, the traveller speed  $n_l$  to be 98% and 99% of the spindle speed  $n_l$  at the upper and lower positions of the ring rail respectively, the mean spinning power can be written as follows:

$$N_{ct} = 4.25 z G^{0.87} D_{\pi}^{1.7} n^{2.4} \cdot 10^{-8}$$
(45)

where

 $N_{st}$  = the mean spinning power in kW,

z = no. of spindles,

G = traveller weight in mg,

 $D_r = \text{ring diameter in cm},$ 

n = spindle speed in thousands of r. p. m.

The package power for full bobbins  $N_{pl}$  is given by equation (23) and its mean value equals  $0.53 \cdot N_{pl}$ .

The no load power  $N_{nt}$  is mainly absorbed by the spindles and tapes. The chief variables which affect  $N_{nt}$  are therefore, the spindle speed n, lift h and the gauge g.  $N_{nt}$  was found to satisfy the following equation empirically:

$$N_{nt} = 3.33 z g^{1.9} h n^{1.4} \cdot 10^{-7}$$
 (46)

where

 $N_{nt}$  = the no load power of the total frame in kW,

z = no. of spindles,

g = gauge in cm,

h =lift in cm,

n =spindle speed in thousands of r. p. m.

Equations (45), (23) and (46) are represented graphically in figures 80 to 82 respectively. It should be noticed here that these figures are valid for cotton frames with cotton tapes. For frames with nylon tapes,  $N_{nt}$  is somewhat less than that given by equation (46) or figure 82.

To illustrate the practical use of these charts, a numerical example will be considered, for a cotton frame with the following specifications:

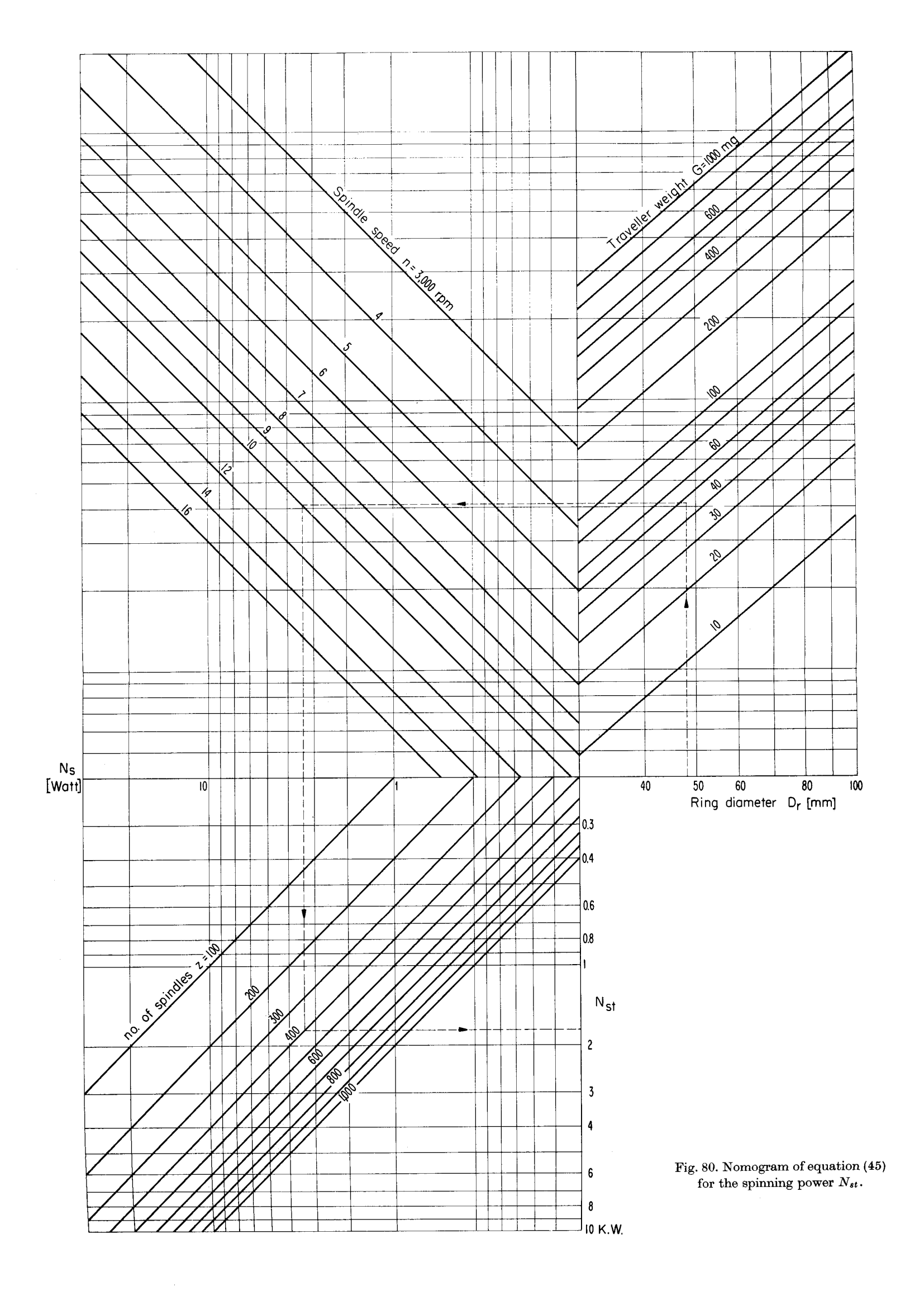
Ring diameter  $D_r = 48 \text{ mm}$ , Gauge g = 70 mm,

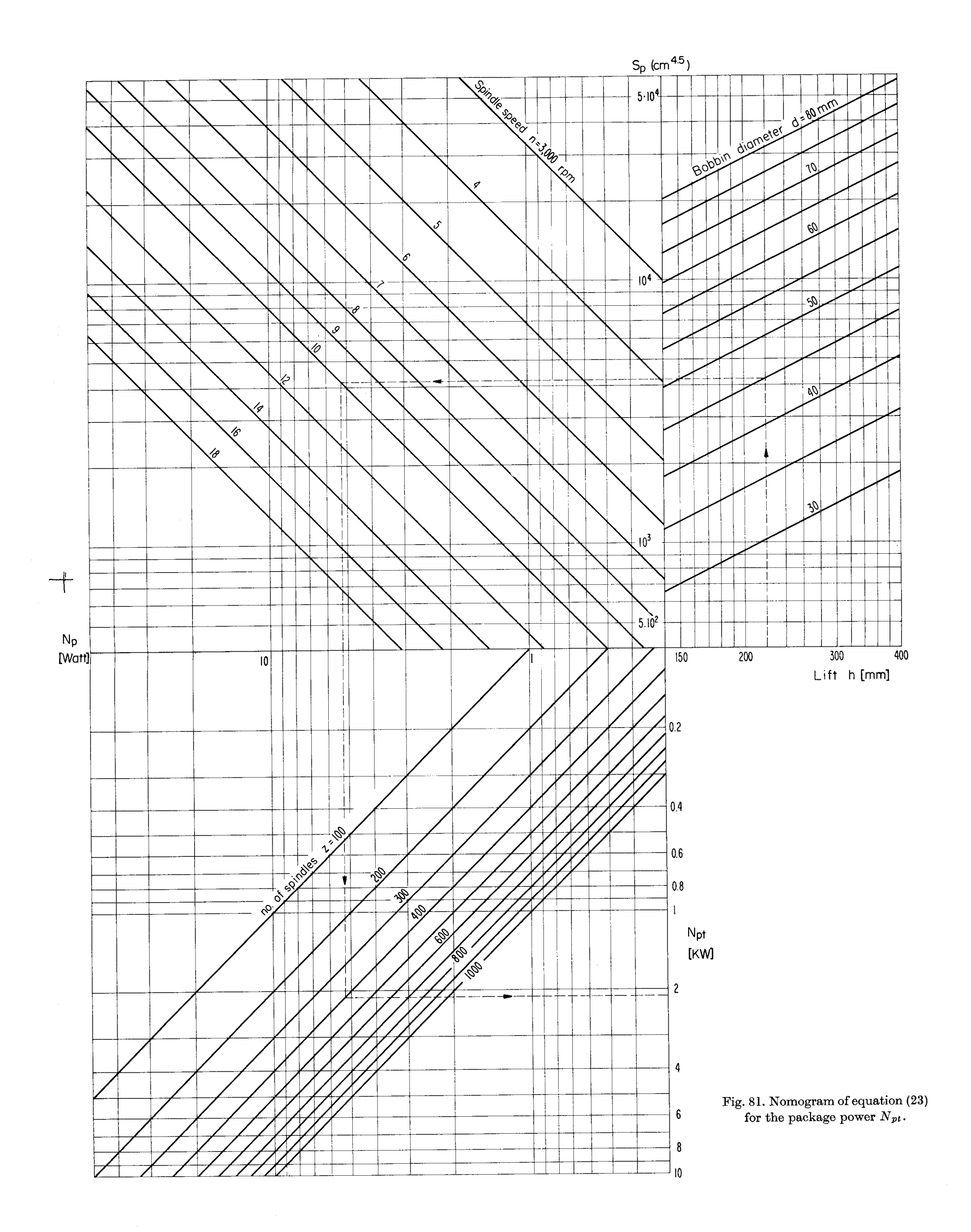
Lift h = 220 mm,

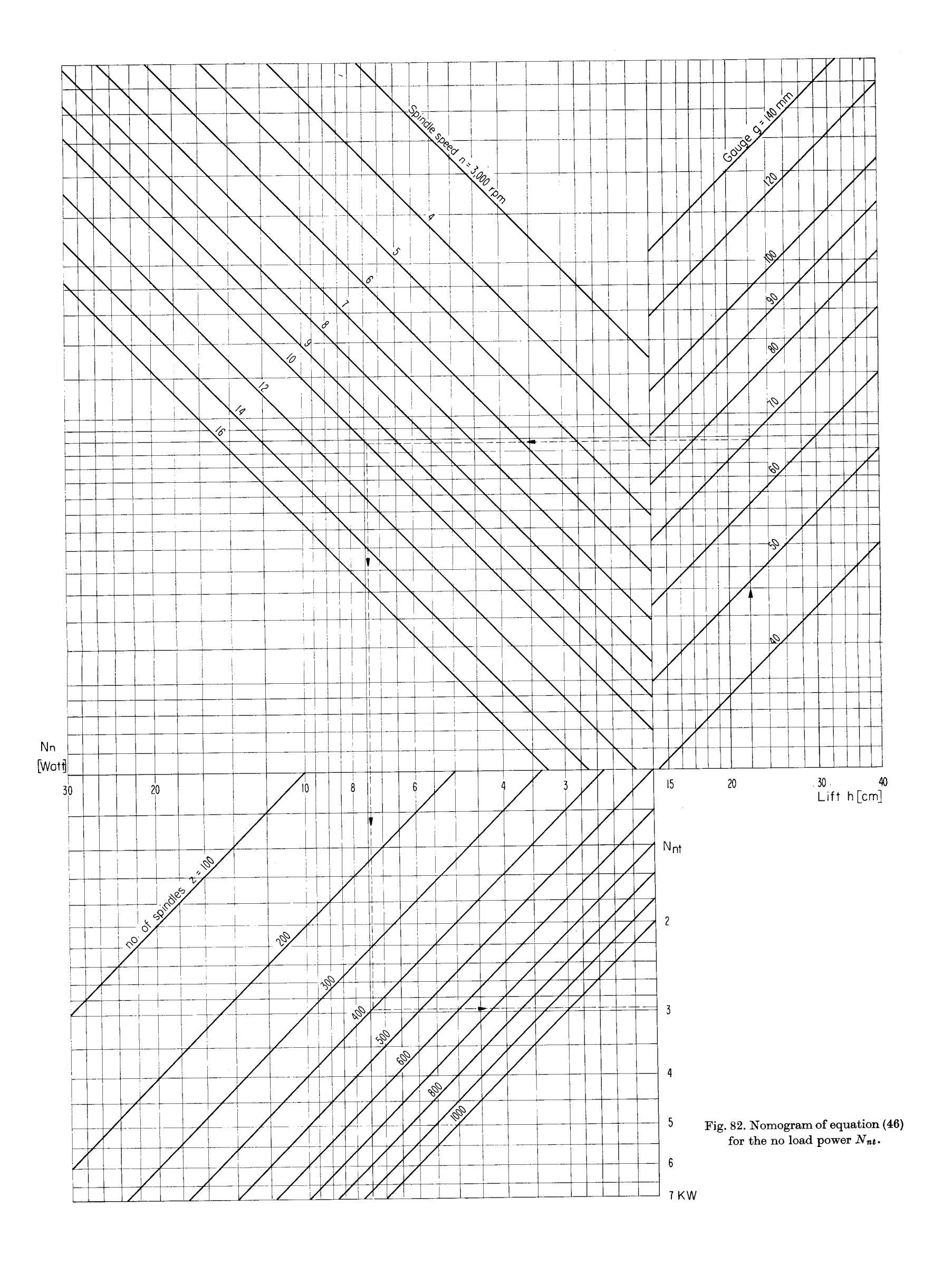
Spindle speed n = 10,000 r. p. m.,

No. of spindles z = 400,

Yarn count  $N_e = 30 \text{ s} (19.7 \text{ tex}),$ Traveller weight G = 47 mg (no. 2/0).







From figures 80 to 82, the following values were found:

$$N_{st} = 1.75 \text{ kW}, \ N_{nt} = 2.13 \text{ kW}, \ N_{nt} = 2.96 \text{ kW}.$$

Therefore, the total power consumption  $N_t$  with full bobbins equals  $6.85\,kW$ . The mean power consumption is:

$$\overline{N}_t = N_{st} + 0.53 N_{nt} + N_{nt} = 5.84 \text{ kW}.$$
<sup>7</sup>).

To illustrate the effect of higher spindle speeds on the total power consumption, the frame considered above was assumed to run at n=12,000 and 14,000 r. p. m. Suitable travellers were considered in each case. Table 13 shows the values of the power consumption in kW, taken from figures 80, 81 and 82.

n	10,000	12,000	14,000
G in mg	47.0 (2/0)	41.7 (3/0)	37.3 (4/0)
$N_{st}$	1.75	2.44	3.22
$N_{pt}$	2.13	3.75	6.06
$N_{nt}$	2.96	3.82	4.76
$N_t$	6.84	10.01	14.04
$\overline{N}_t$	5.84	8.25	11.20

Table 13

# 17. Modern trends in ring spinning

Apart from higher spindle speeds and larger packages, which have been thoroughly dealt with in this work, a new development of the ring spinning frame has been recently made. Roller-bearings are used now for the front cylinders of the drafting systems. This allows the construction of frames with 600 spindles or more, i.e. frame lengths of more than 25 m.

The power absorbed by the drafting systems of these frames may be less than that of the usual type with slide bearings for the front cylinders (naturally with equal number of spindles). But with regard to the relatively small power absorbed by the drafting systems (5–8% for cotton frames), no considerable effect on the total power might be expected. All the power components can be calculated by the formulas given in this work. Figures 80, 81 and 82, in which frames with up to 1000 spindles are considered, can also be used.

<sup>7)</sup> All powers considered in this work are output powers of driving motors.

## 18. Power requirements of frames with special spindle drive

In this chapter two types of frames having special spindle drives are considered, namely gear drive and single spindle drive. The primary and ancillary powers (see fig. 1) of these frames are evidently the same as those of a conventional one. The secondary power  $N_{sec}$  should be determined for each type of drive.

### 1. Gear drive (Hispano Suiza)

Gear-driven spindles are now being fitted to ring frames.  $N_{sec}$  in this case is the power absorbed by the spindle bearings, the driving gears and the bearings of the driving shafts at no load (with empty tubes and without yarn tension). This power depends naturally on the frame size, the quantity of lubricating oil in the gear casing, its viscosity, the assembly of the frame and the number of working hours.

 $N_{sec}$  was measured at different spindle speeds for several medium-size frames with gear-driven spindles. The datas of these frames are given in table 11. The values of  $N_{sec}$  measured, which show a considerable scatter, lie in the range given in figure 83. Comparing these results with those of conventional frames, it was found that the values of  $N_{sec}$  for conventional frames of approximately the same size, driven by cotton tapes, lie in the lower part of the range given in figure 83.

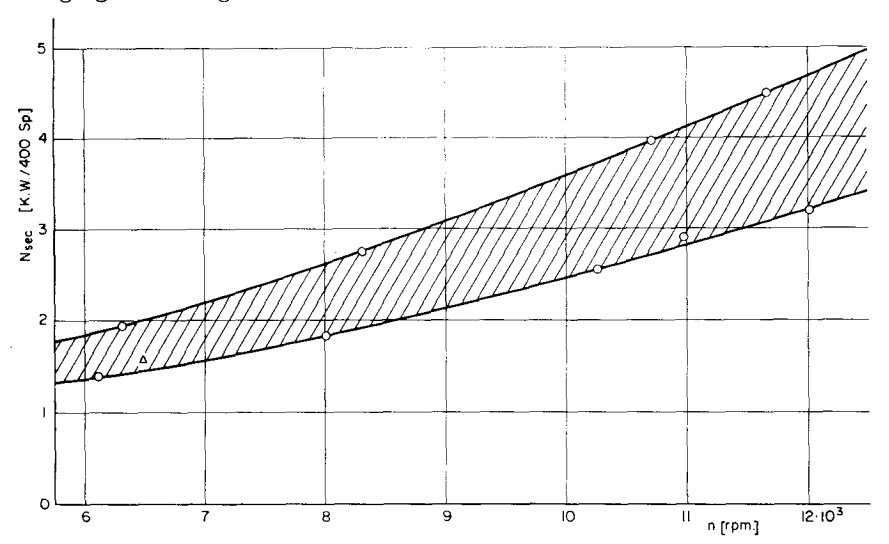


Fig. 83. The secondary power of frames with gear driven spindles against the spindle speed n.

Figure 84 shows the power analysis of frame no. (22). Here also, the agreement of the measured package power and spinning power with those calculated by equations (23), (36) and (39) can be observed. Further results are given in table 14.

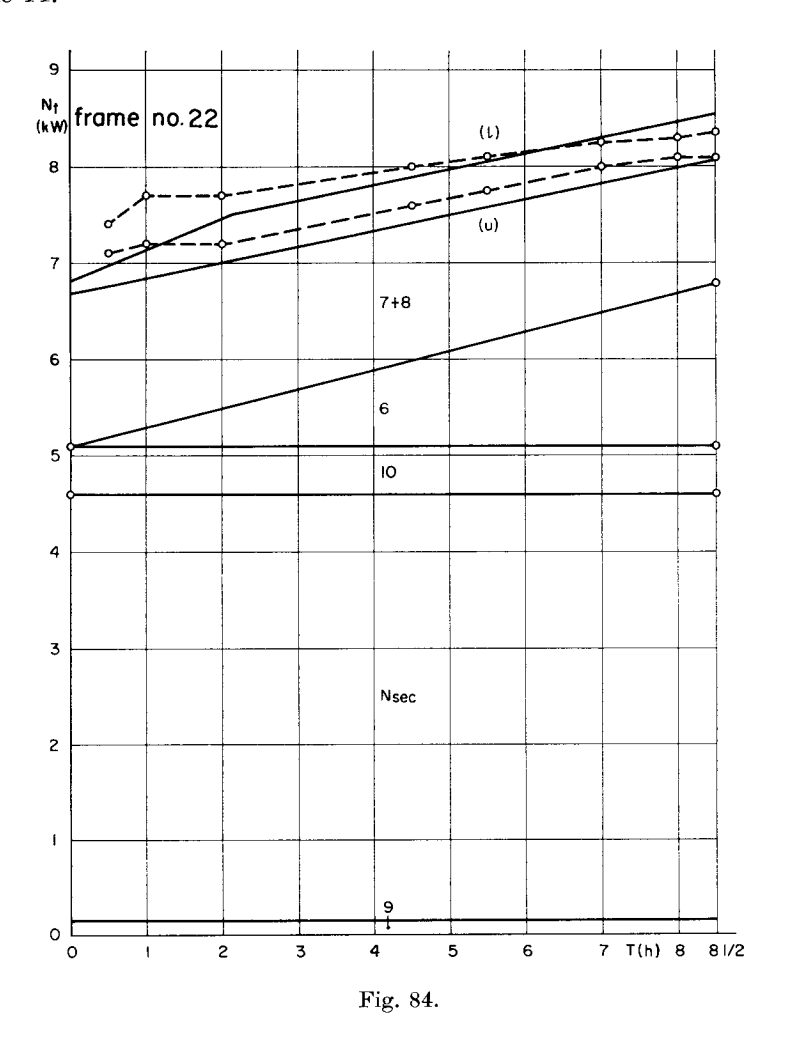


Table 14

Fram	e no.	23	24	25	27
$N_t$ (kW)	begin end	7.0 9.7	2.9 3.5	$\frac{2.3}{2.6}$	4.35 5.55

### 2. Single spindle drive (Süssen)

A new type of spindle drive has recently been fitted to ring frames, namely the single spindle drive. Referring to figure 85, each spindle (1) is driven by a narrow tape (2) over two tension and guide rollers (3) and (4). The secondary power  $N_{sec}$  of this frame will now be considered.

The spindle power  $N_3$  can also be calculated here by equation (14).

The power consumption of the tension rollers  $N_4$  was determined in the same way as described in chapter 7. In figure 86,  $N_4$  in watts for Süssen rollers having a diameter  $d_r$  of 28 mm is plotted versus  $n_r$  in r. p. m. and the tape speed  $v_t$  in m/sec., for different tension roller loads  $P_r = 1.0$  and 1.5 kg. From this figure, the values of  $C_4$  and a in equation (16) were found for these rollers to be as given in table 15.

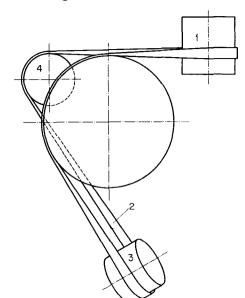


Table 15

P <sub>r</sub> (kg) *)	1.0	1.5
$egin{array}{c} C_{4} \ a \end{array}$	$0.021 \\ 1.65$	$0.023 \\ 1.65$

\*)  $P_r$  was found to be in the range considered.

Fig. 85. Diagrammatic sketch of the single pindle drive (Süssen).

Table 16

Type of frame	z	n r. p. m.	$d_w \atop  ext{mm}$	$d_r$ mm	$n_r$ r. p. m.	$P_r$ kg	$egin{array}{c c} N_4 \  ext{watt} \end{array}$	$egin{array}{c} N_{4t}  ^*) \ \mathrm{kW} \end{array}$
conventional	400	10,000	27	70	3,910	1.0	0.8	0.08
Süssen	400	10,000	28	28	10,000		0.88	0.70

<sup>\*)</sup>  $N_{4t}$  = the power in kW required to overcome the bearing friction of the tension rollers of the whole frame,

<sup>=</sup>  $z/4 \cdot N_4 \cdot 10^{-3}$  for conventional frames.

<sup>=</sup>  $2 z \cdot N_4 \cdot 10^{-3}$  for Süssen frames.

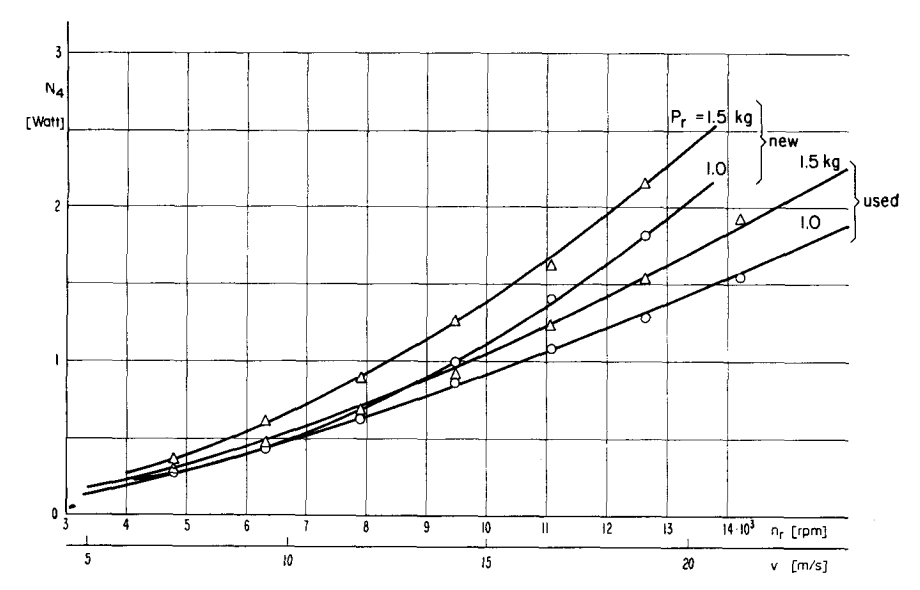


Fig. 86a. Power absorbed by Süssen rollers,  $d_r = 28$  mm.

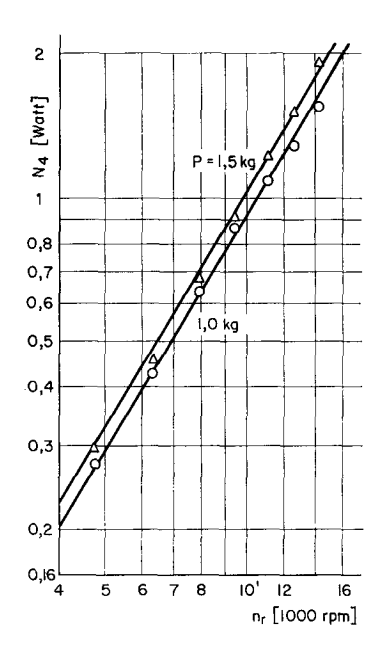
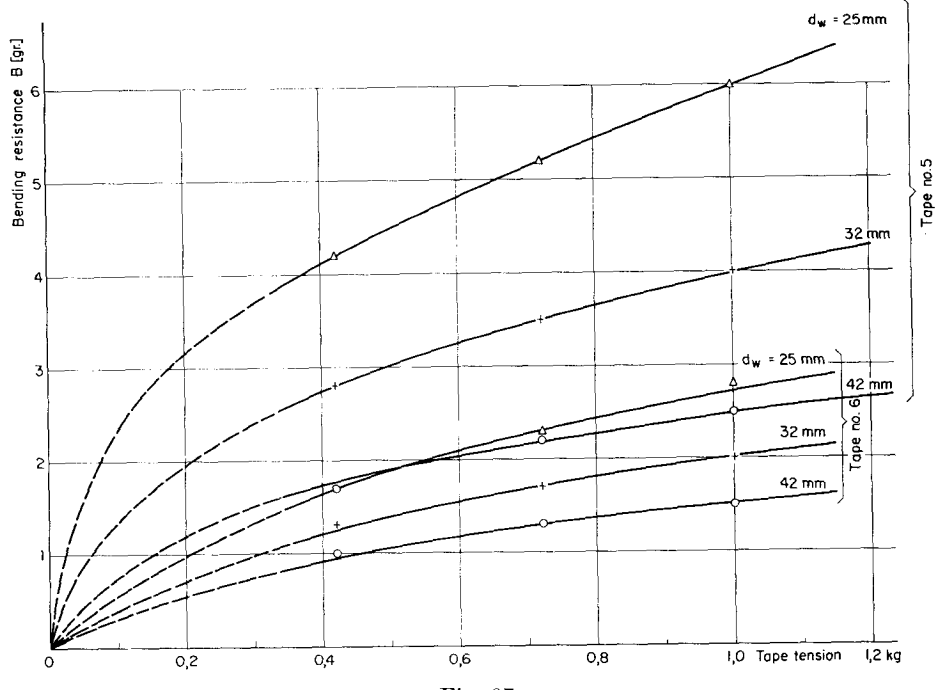


Fig. 86b.

To compare the power consumption of the tension rollers of a conventional frame with that of the considered one, equation (16) and tables 6 and 15 were used to calculate  $N_{4t}$  of both frames. The data and results on these frames are given in table 16.





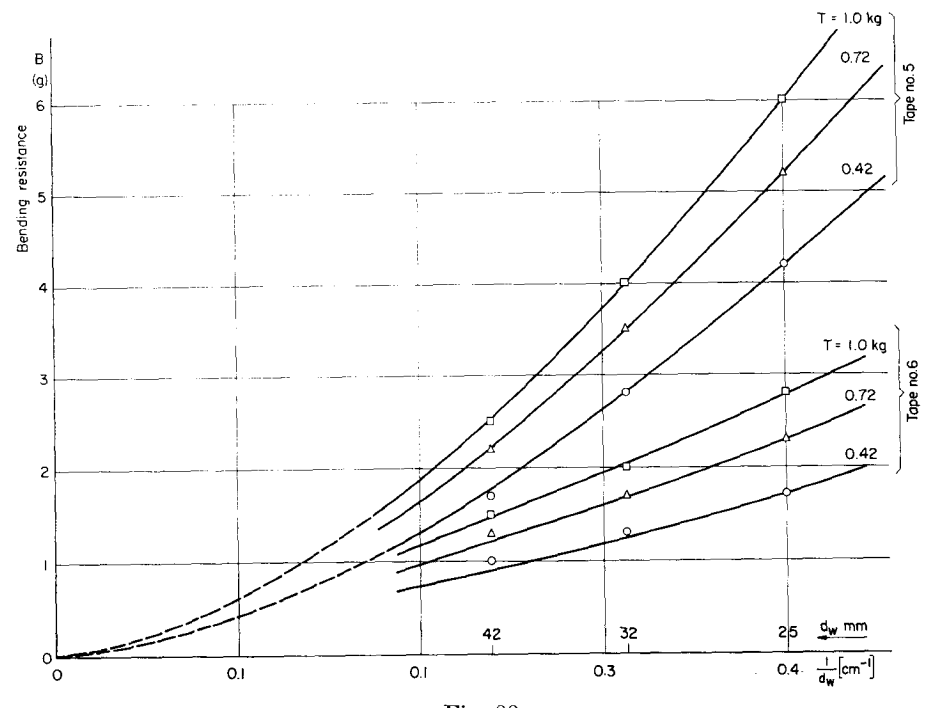


Fig. 88.

From the above table, it can be stated that for Süssen rollers, although they run at much higher speeds than the conventional ones (for the same n), the power consumption  $N_4$  is only slightly higher. But, as the Süssen frame contains eight times the number of rollers, the total power consumption  $N_{4t}$  is much higher.

The bending resistance of the tapes was also determined as described in chapter 5. The results for two types of tapes, whose data are given in table 17, are illustrated in figures 87 to 89 and 16. From these figures, the constants  $C_2$ , b and c in equation (7) were found. In this case, each spindle has a tension roller, a guide roller and a driving pulley. The tension and the guide rollers

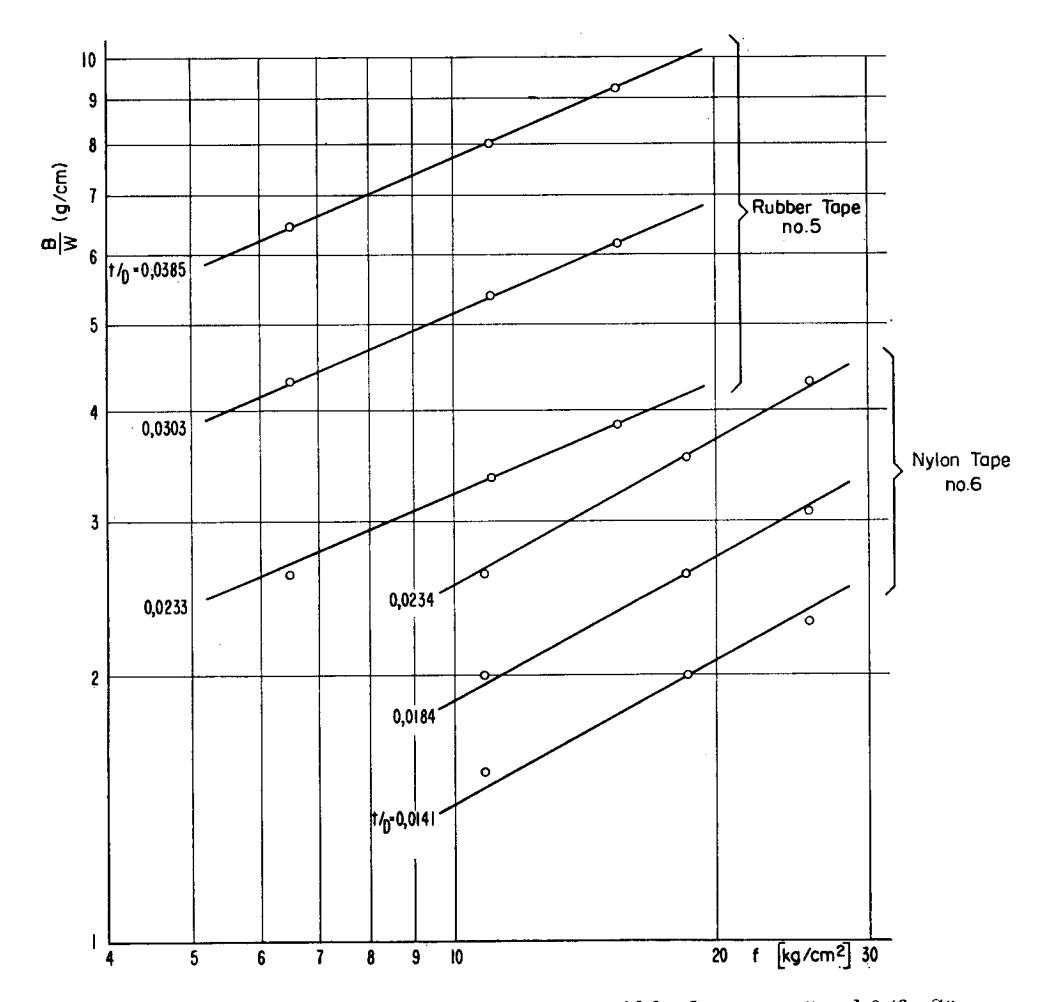


Fig. 89. The bending resistance B/W in gram per cm width of tapes no. 5 and 6 (for Süssen drive) against the tensile stress f.

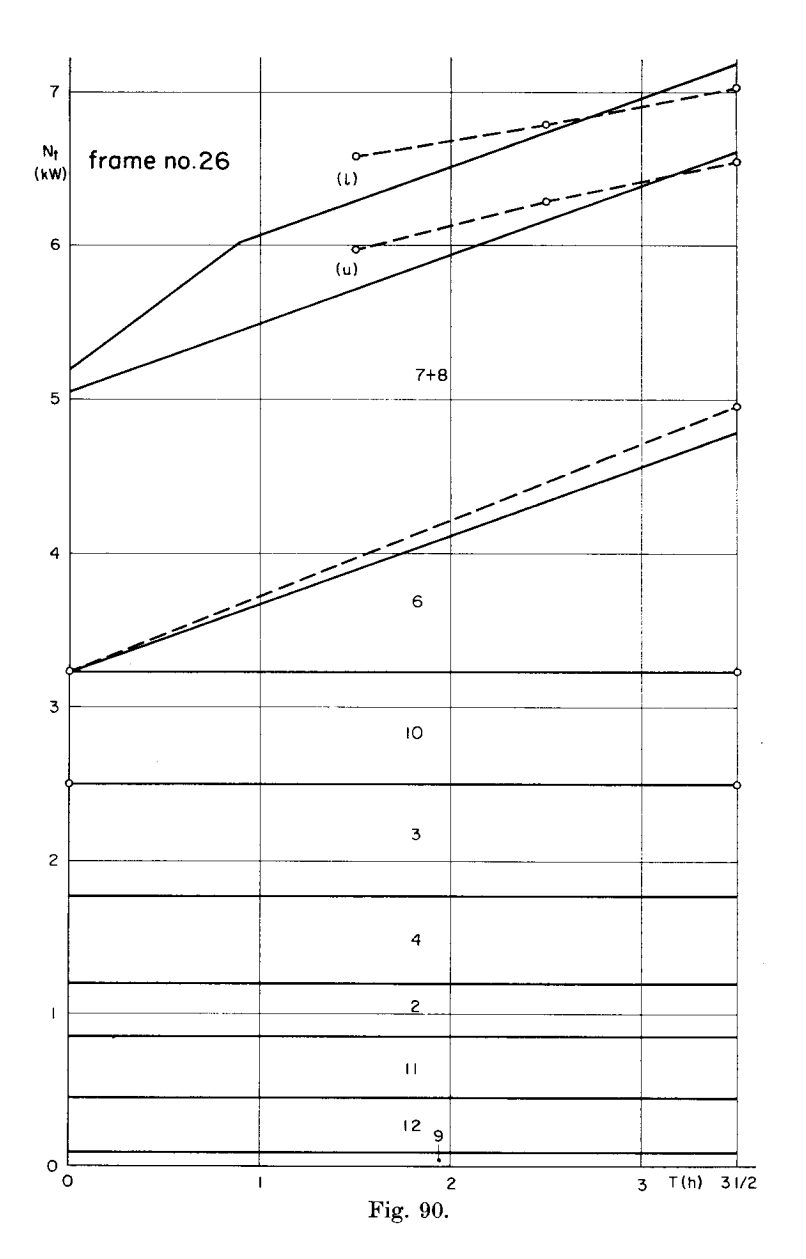


Table 17

Tape no.	material	W (mm)	t (mm)	wt. (g/m)	$C_2$	b	c
5	rubber (reinforced)	6.5	1.0	8.75	736	0.42	1.7
6	nylon	6.5	0.6	3.64	43.5	0.55	1.1

have normally the same diameter as the wharve. Therefore, the power required to overcome the bending resistance can be written as follows:

$$N_2' = 9.8 C_2 W v z f^b \left[ 3 \left( \frac{t}{D_1} \right)^c + \left( \frac{t}{D_4} \right)^c \right] \cdot 10^{-6}, \tag{47}$$

where  $N'_2$  = the power required to overcome the bending resistance of tapes in kW,

 $D_4 = d_p + t,$ 

 $d_p = \text{diameter of the driving pulley in cm.}$ 

The air friction of the tapes was found to be small because of their small surface area and relatively smooth surface.

The driving pulleys are mounted on two shafts, one at each side of the frame. These correspond to the tin rollers of a conventional frame. The air resistance of these pulleys is also negligible  $(d_p = 70 \text{ mm} \text{ and } n_p \text{ about } 4,000 \text{ r. p. m.})$ .

The power consumption of the driving shafts, which run in ball bearings, was determined for a frame of medium size (no. 26, table 12). Figure 90 shows the power analysis of this frame. The results for frame no. (27) are given in table 14. The power consumption of both frames tested was found to be higher than that of conventional frames of the same size.

## 19. Acknowledgements

It is a pleasure to acknowledge the help and interest of

Professor Dr. Emil Honegger

during the course of this work, which was in fact undertaken on his suggestion. His valuable guidance and encouragement enabled me to develop and complete my research programme.

I am also indebted to

#### Professor André Dutoit

for having consented to examine my thesis and for his recommendation of its acceptance.

The co-operation of Messrs. Rieter & Co., Winterthur, and Brown-Boveri & Co., Baden, is appreciated.

My best thanks are also due to Messrs.

Blumer & Co., Rorbas-Freienstein, Blumer & Co., Bülach, Trüb & Co., Uster, Weber & Co., Aarburg, Ed. Bühler & Co., Kollbrunn, Vereinigte Kammgarnspinnereien, Schaffhausen und Derendingen, Spinnereien Aegeri,

for having generously permitted me to carry out the power measurements on frames in actual production in their spinning mills.

### 20. References

- W. Stiel, Elektrobetrieb in der Textilindustrie, S. 223, Verlag von S. Hirzel, Leipzig 1930.
- H. Catling and A. E. De Barr, Journal of the Textile Institute 48, 11 (1957), T 440.
   "A Study of Power Requirements in Ring Spinning."
- 3. M. Nakamura, Journal of the Textile Machinery Society of Japan 6, 1 (1960), p. 51. "Vibrations and Horsepower Consumption of High-Speed Spinning Frames."
- 4. O. Johannsen, Handbuch der Baumwollspinnerei, 5. Band, S. 133, Verlag Bernh. Friedr. Voigt, Berlin.
- 5. Bollettino "Marzoli", Anno III, Giugno 1961, numero 4, pag. 4. "La Potenza Assorbita Delle Macchine Di Filatura" (S. G.).
- 6. Ergebnisse der Aerodynamischen Versuchsanstalt zu Göttingen, 1. Lieferung, S. 120, Verlag von R. Oldenbourg, München und Berlin 1921. "Untersuchungen über den Reibungswiderstand von stoffbespannten Flächen."
- A. E. Müller, Forschungsarbeiten auf dem Gebiete des Ingenieurwesens, H. 318, VDI-Verlag GmbH, Berlin 1929. "Verluste der Riementriebe bei Verwendung kleiner Scheiben unter besonderer Berücksichtigung des Biegewiderstandes."
- 8. J. Ackeret, Zeitschrift für angewandte Mathematik und Physik (ZAMP), Vol. IXa, 1958, S. 284, Birkhäuser-Verlag, Basel. "Über Reibung und Grenzschicht-Stabilität an rotierenden angeblasenen Zylindern."
- 9. A. Capello, Journal of the Textile Institute 49, 11 (1958), T 566 and T 579. "The Spinning Balloon", Part I and II.
- P. F. Grishin, Platts Bulletin, Vol. VIII, No. 6, p. 161. "Balloon Control", Part I and II.
- 11. G. Lindner, Leipziger Monatsschrift für Textil-Industrie 1910, S. 213. "Ballonform, Fadenspannung und Läuferstellung an Ringspinnmaschinen."
- C. Mack and E. Smart, Journal of the Textile Institute 45, 4 (1954), T 348. "Measurements of the Air-Drag of Textile Threads."
- S. Goldstein, Modern Developments in Fluid Dynamics, Oxford University Press, 1938.
- 14. E. Honegger, Melliand-Textilberichte, Heidelberg 1935, Nr. 5. "Experimentelle Untersuchung des Ringspinn-Prozesses."
- D. Brunnschweiler and I. S. Mohamadain, Textile Research Journal 29, 2 (1959),
   p. 119. "A Simple Ballooning Yarn Apparatus."
- 16. G. J. Morris, Dissertation, Eidg. Techn. Hochschule, Zürich 1959.
- E. Honegger and A. Fehr, Journal of the Textile Institute 38, 8 (1947), T 353. "Effects
  of Accessory Influences on Ring Spinning of Cotton and Spun Rayon."
- 18. M. Axson, Journal of the Textile Institute 52, 1 (1961), T 26. "An Instrument for the Measurement of Traveller Friction."
- 19. W. Wegener, Textil-Praxis 1960, H. 12, S. 1223. "Verzugskraftmessung an Streckenbändern aus Baumwolle."

#### Curriculum vitae

Hosny Ali Soliman, born in Alexandria, U.A.R., on 5th October 19	Hosny	Ali	Soliman.	born	in	Alexandria.	U.A.R.,	on	5th	October	1933
--	-------	-----	----------	------	----	-------------	---------	----	-----	---------	------

- 1940—1944 Ras El-Tin Primary School, Alexandria.
- 1944—1950 Ras El-Tin Secondary School, Alexandria. Final certificate of secondary education 1950 (section mathematics).
- 1950—1955 Faculty of Engineering, University of Alexandria. B. Sc. Mechanical Engineering 1955. Practical training in the workshops of the Ports and light-houses department (Alexandria), the Maintenance Workshops of the Egyptian Railways and "La Société Misr Pour La Soie Artificielle à Kafr El-Dawar".
- 1955—1957 Junior lecturer in the Mechanical Engineering Department, Faculty of Engineering, Alexandria.
- 1957—1959 Studying Textile Engineering and Textile Industries in the Swiss Federal Institute of Technology, Zurich. Admission Examination for research work, May 1959.
- 1959—1961 Working for the degree of Dr. sc. techn. under the supervision of Professor Dr. E. Honegger, Head of the Textile Department of the S.F.I.T., Zurich.

H. A. Soliman